Compaction of Soil by Repeated Loading

Rouzbeh Roudgari

A Thesis

in

The Department

of

Building, Civil, and Environmental Engineering

Presented in Partial Fulfillment of the Requirements
for the degree of Master of Applied Science (Civil Engineering) at
Concordia University
Montreal Quebec, Canada

February 2012

This is to certify that the thesis prepared

By: **Rouzbeh Roudgari**

Entitled: Compaction of Soil by Repeated Loading

and submitted in partial fulfillment of the requirements for the degree of

Master of Applied Science (Civil Engineering)

complies with the regulations of the University and meets the accepted standards with respect to originality and quality.

Signed by the final examining committee:

	Chair
Dr.M. Nokken	

	External Examiner
Dr.A.Agarwal	

	BCEE Examiner
Dr.L.Tirca	

	BCEE Examiner
Dr.M.Nokken	

	Supervisor
Dr. A.M. Hanna	

Approved by

Dr. M. Zaheeruddin
Chair, Department of Building, Civil, and Environmental Engineering

February 8th, 2012

Dr. Robin A.L. Drew
Dean, Faculty of Engineering and Computer Science

ABSTRACT

Construction of roads is usually made by stripping the top soil (600 to 1000 mm), which often contains organic materials, and replacing it with a layer of subgrade material (crushed stones, well-graded sand). One of the main design requirements is that the subgrade material must be compacted up to a minimum of 95% of the Proctor maximum dry density, as determined from laboratory test results (AASHTO T99). This requirement is usually specified as a norm in any contract document involving field compaction.

Soils can be compacted by repeated, systematic application of high energy using hammer. The imparted energy is transmitted from the ground surface to the deeper soil layer by propagating shear and compression waves types, which force the soil particles into a denser state (R. Massarsch, 1999)

Research in this field has been directed to establish relationships between the water content, the dry density and the compacting effort, the type of soils which allow a higher level of compaction, and to develop field equipment and techniques which would be more effective in performing field compaction. Nevertheless, there are reports to confirm that achieving 95 % of the Proctor maximum dry density in the field compaction is impossible in some cases. The role of the surrounding soils, in particular the underlying layer, in determining the level of compaction, is a paramount parameter in achieving high level of compaction.

This thesis presents a plane-strain numerical model using PLAXIS computer software to simulate shallow compaction of a subgrade layer underlain by a deep deposit of various stiffness levels. The compaction effort is applied by means of repeated loading on the ground and modeled as a static load applied to the soil through a rigid plate having similar properties of roller material. Based on the results obtained in this study, it can be stated that the level of compaction achieved in the field depends on the thickness of the subgrade layer, stiffness of the lower layer, the number of load cycles, and the magnitude of the load applied.

The results of this study are presented in the form of compression curves of the subgrade and lower layer, and accordingly, the level of compaction for a given soil/load/geometry conditions can be predicted. Design guidelines are presented for practitioners.

ACKNOWLEDGEMENTS

TABLE OF CONTENTS

LIST OF FIGURES

LIST OF TABLES

LIST OF ABBREVIATIONS

E_1:   Stiffness of top layer soil

E_2:   Stiffness of lower layer soil

L: Length of the imprinted area on soil by the roller

B: Width of the imprinted area on soil by the roller, and essentially width of load applied to the soil

H_1:   Top layer soil no.1

HS: Soil modeled as Hardening Soil Model Constitutive model

M_1:   Lower layer soil no.1

MC: Soil modeled as Mohr Coulomb Model Constitutive model

f: Number of loads

H: Thickness of top layer soil

q: Load applied to the top layer

CHAPTER 1

INTRODUCTION

1.1   General

Soil surface compaction is perhaps the simplest and the oldest method of ground improvement. Compaction improves the soils bearing capacity, decreases settlement and reduces water seepage. Compaction of soil is an essential component in building road and highways. The term "compaction" is known to explain the phenomena of increasing in the dry density of soil by reducing the void volumes over a very short period of time. The compaction process can be accomplished by rolling, tamping, vibration or by impact forces. Shallow compaction of soil can be done using different compaction machinery or techniques.

1.2   Problem Statement

In practice, shallow compaction of soil is achieved by applying repeated loading. The result depends on the magnitude of the load applied, type of the soil, number of loads passes, area of the load applied, depth of the soil layer, and the strength of the lower layers. This research is directed to develop a numerical model capable to simulate the case of compaction of a cohesionless thin layer overlying a deep weak deposit. The objective is to examine the effect of the lower layers strength and stiffness properties on the achieved compaction level achieved in the top layer.

1.3   Boundary Conditions

Often compaction parameters to be used on field are pre-determined using laboratory compaction test called Proctor. The Proctor compaction test is a laboratory method of experimentally determining the optimal moisture content at which a given soil type will become most dense and achieve its maximum dry density. Proctor (AASHTO T99) testing procedures can be followed to determine the moisture density relationship of soil for highway construction projects. Predicting the compaction is a major problem itself, and there has recently been a controversy in the soundness of prediction of compaction using laboratory proctors test due to boundary differences.

In Proctors compaction test the soil sample is generally assumed to be strained one dimensionally in the mold, and on the other hand in the field the soil is undoubtedly subjected to three dimensional strains caused by the dynamic loads from the compaction equipment. This is partly due to the scaling difference between a field compaction situation and its corresponding laboratory Proctors compaction test and mainly due to the boundary conditions (the bottom plate, and the radial wall) imposed from the Proctors mold. However, the radial or vertical restrains of proctors mold wall could be neglected because number of passes and coverages in the field can compensate for this effect, thus the main problem of concern herein is the query of compatibility of representation of a lower layers of soil with proctors 100% stiff bottom plate.

It is clear that there is a fundamental difference in the mechanism of boundary conditions of both the field and Proctors compaction test. This in turn would bring about different ways that energy waves would propagate through the soil and thus causes significant discrepancies in the results were they could be seemingly blamed on the

random behavior of the equipment and non-linearity of the soil, whereas the chief reason is believed to be the considerable difference between the field and the laboratory Proctors compaction test boundaries.

The differences in boundary condition between laboratory Proctor test and field compaction can be seen in the figure 1.1 below.
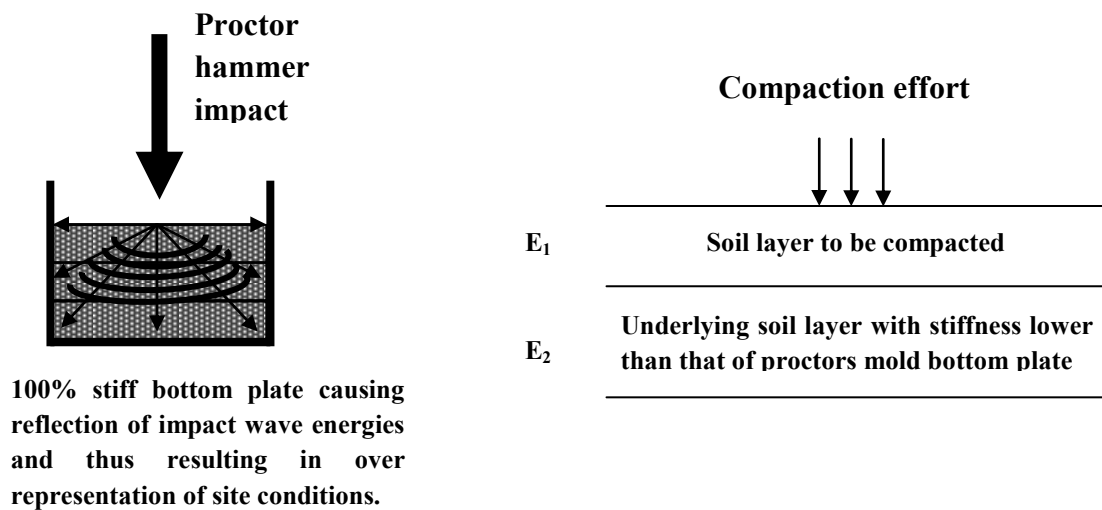
Figure 1.1 Boundary conditions of Proctor test and field compaction

1.3   Surface Compaction

Field compaction is usually achieved by applying mechanical energy by means of rolling and kneading and ramming. The types of field equipment employed for such process include rammers, rollers and vibrators. The rammers transfer the compaction energy to the ground by dropping weights. The rollers consist of smooth wheel, pneumatic, and sheep-foot. The vibrators consist of out-of-balance type or pulsating hydraulic type mounted on plate rollers.

1.3.1 Smooth Drum Rollers

A roller, figure 1.2, is a compacting device having a drum (roll or horizontal cylinder) used to dense/compact soil, asphalt or other materials through employing the effect of static force (weight of the drum) to increase the strength and thus the load-bearing capacity of the surface. Many factors contribute to the success of compaction using rollers, factors such as roller dimensions, roller weight, number of load passes, type of soil, and the depth of soil layers.
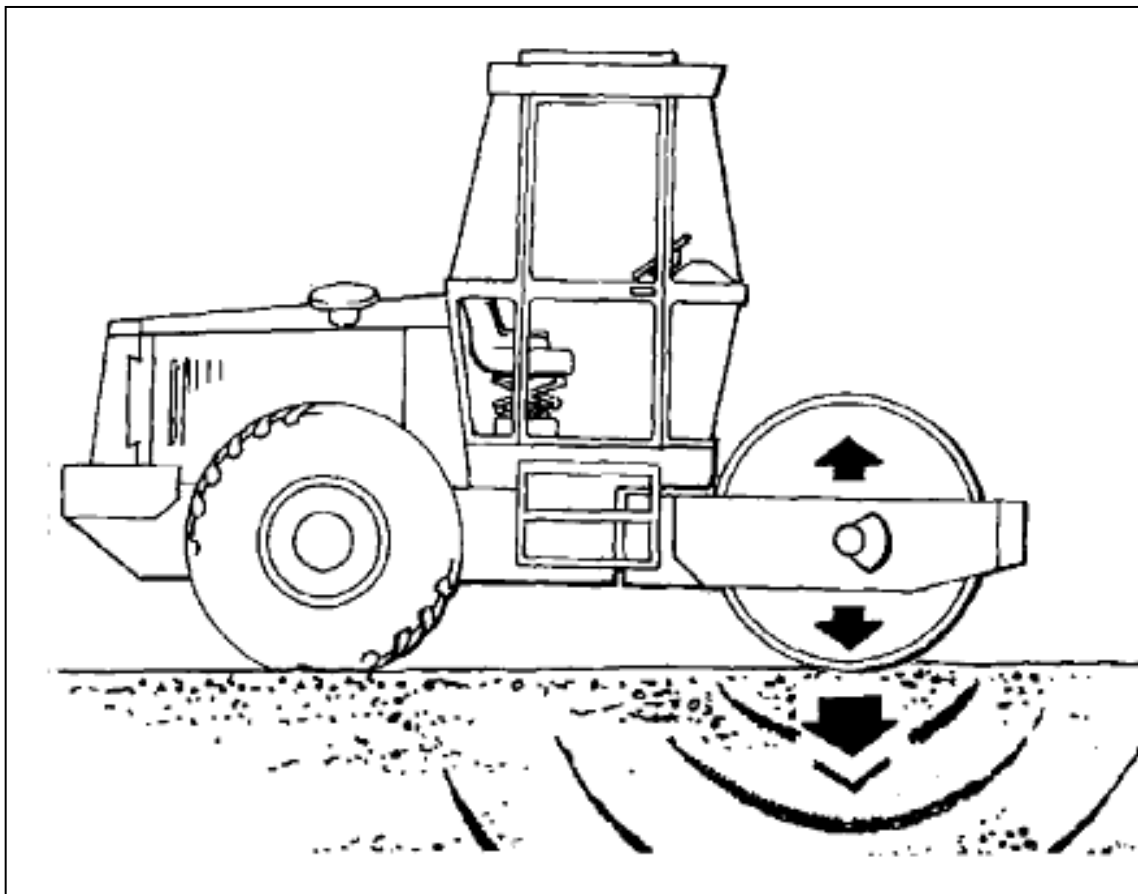
Figure 1.2: Smooth drum roller, static, and or vibratory (from Sandström, Å, 1994).

1.4   Research Motivation

The academic and experimental field of research on compaction are mostly studying on the mechanical characteristics of soil compaction. Research are conducted on controlling parameters such as moisture content, compaction energy, soil grain size characteristics, and other parameters related to the nature of the soil. There has been little or perhaps none research on the significant role that the surrounding material may play on the level of compaction that can be achieved. Often on construction sites involving compaction of a subgrade layer this phenomenon is neglected and it could lead into ill compacted foundation for road constructions. This is believed to be a major contributing factor for such conditions and thus it is the motive of this research to take into account the influence of an underlying layer on level of compaction that can be achieved on top layer subgrade.

1.5   Objective of this Thesis

1. To develop a numerical model capable to simulate the case of a thin soil layer overlying a deep weak deposit subjected to repeated loading

2. To conduct parametric study to examine the effect of the strength of the underlying layer, the thickness of the layer, load magnitude and number of passes on the level of compaction, which can be achieved for a given soil/geometry/loading conditions.

3. To develop design procedure to be recommended for predicting the level of compaction to be attained in a thin layer subjected to repeated loading.

CHAPTER 2

LITERATURE REVIEW

2.1   General

In the literature, studies are mainly focused on equipment development and laboratory testing. Furthermore, there are very few reports dealing with site-dependent factors such as the role of the underlying soil.

2.2   Effect of Lift Thickness

Howeedy et al. (1975) carried out field vibratory roller tests on a poorly graded medium to fine sand, the lift thicknesses varied from 0.14 to 0.3m, and it was observed that the final relative density of this type of soil did not vary as the lift thickness varied in their field test range. Henrich (1987) gives recommendations for lift thickness for surface compaction using vibratory rollers. He suggested lift thicknesses of less than 400mm.

2.3   Effect of Number of Passes or Coverage

Howeedy et al. (1975) showed through their field experiments that the final relative density of a poorly graded medium to fine sand, compacted by vibratory roller, has a direct relationship with the number of coverages, however they also observed that the rate of increase beyond six coverages was smaller than that from three to six coverages. Sleig et al. (1977) realized through their study that as the number of roller passes increase then compaction effort per pass can increase. They further explain that progressive passes of roller increase the soil stiffness, and also by employing same frequency above resonance for a scenario with more passes will result in greater roll vertical displacement

(comparing to one with less number of passes) and thus a greater dynamic component of compaction will be generated while the static component (generally the weight of the drum) will remain unchanged. Sleig et al. (1980) conducted laboratory experiments to see the effects of number of passes while the generated dynamic force from the drum either remained constant, decreased, or increased progressively after each pass. They observed that decreasing dynamic force resulted in highest rate of compaction for the first four passes, but only a small increase after that. They further detected that employing a constant dynamic force results in smaller amount of compaction however it continues to increase up to 12 passes. And for the increasing dynamic force per pass they realized that the amount of compaction achieved was well below that of the other two cases. Their results indicated that the amount of compactive effort subjected to the ground during the first few passes is a dictating factor in determining the total amount of compaction that will be achieved after appropriate number of passes.

2.4   Effect of Rolling Speed

Howeedy et al. (1975) showed through their field experiments that the final relative density of a poorly graded medium to fine sand, compacted by vibratory roller, decreases as the rolling speed increases. The author employed rolling speeds of 1.5 to 4.5 mph.

Sleig et al. (1977) illustrated in their research, through field experiments, that an increase in roller speed will cause decrease in compaction per pass. They explain that an increase in speed will not noticeably affect the soil stiffness, and as a result the roll vertical displacement will not change. As the speed increases, the oscillation per distance will decrease provided that frequency is kept constant, and thus the dynamic component

of compaction will also decrease, and since the static component of compaction is unchanged, then the net effect is decreased in total. The authors suggest that in general any increase in roller speed, when using vibratory compactors, will cause a decrease in the amount of compaction. They further recommend that in order to offset this decrease in compaction, additional coverages will be required. Moreover the authors believe that the best productivity will be obtained at the slowest practical speed which normally ranges between 1 and 4 mph.

Henrich (1978) explains by the figure 2.1 below that speed of the machine affects the action and the layout of the impact of drum on the material.
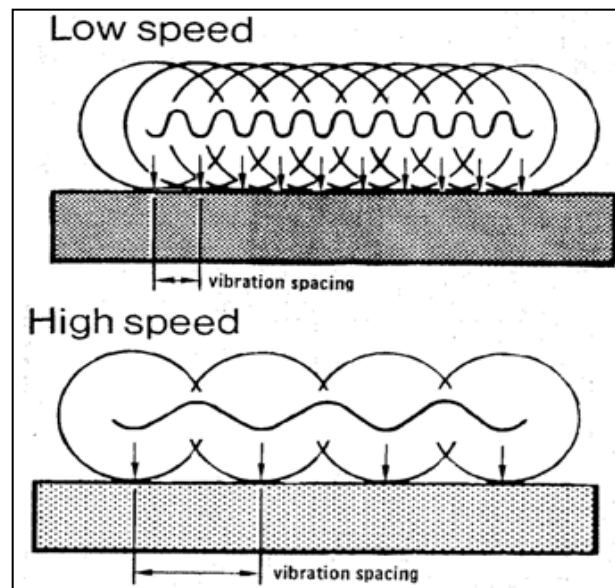
Figure 2.1: Difference in compaction when
speed is different (from Henrich, 1978)

As the authors further suggest, the slower the speed, the higher the number of vibrations per unit area, and where the speed is too high relative to the vibration

frequency, the intervals between the individual vibrations are too great and thus the entry of the compaction energy into the material is diminished, so that more passes would be necessary. The author recommends speeds of 3 km/h to 4 km/h for surface compaction using vibratory rollers.

2.5   Effect of the Drum Static Weight

Howeedy et al. (1975) conducted field tests on poorly graded medium to fine sand and suggest that the compaction using a vibratory roller increases as the total force per unit width of the roller also increases. Their data show an increase in relative density for a total force of 156 to 207 kN, and additional increase in the total force up to 285 kN did not cause any further change in the soils relative density. Sleig et al. (1977) consider the total compaction achieved under a vibratory roller the product of two components, namely the static component and the dynamic component (additional compaction achieved when vibration of drum is turned on), and static component represents that part of compaction produced by the roller when operated with no vibration, thus as the weight of the drum increases so does the static force on ground under roll, and in turn this increases the static component of the compaction which simply means partially increasing the net amount of compaction. Henrich (1987) recommends the use of lighter vibratory compactors for the purpose of surface compaction, and he suggests rollers with weights less than 9 tones.

2.6   Effect of Frequency

Lewis (1961) suggests that for well graded sand, dry density increases as frequency increases up to 2,400 cycles per minute and then it decreases as frequency is further

increased. Howeedy et al. (1975) used frequencies in the range of 1,200 to 1,800 cycles per minute in their investigation of vibratory roller compaction on poorly graded medium to fine sand at numerous test fills. Each lift in these fills received six coverages from compactors rolled at speed of 2.4 km/h. It was observed that the final relative density increases as the frequency of the compactor increases. They further confirmed their results by comparing to previous research data by D'Appolonia et al. (1969) which indicates that the increase in operating frequency up to 1,200 cycles per minute causes an increase in relative density for medium to fine sand. Henrich (1987) also gives recommendations for surface compaction of cohesionless soils employing vibratory rollers. He suggests using high vibration frequencies in the range of 35 to 45 Hz.

Sleig et al. (1977) conducted field and laboratory tests together with analytical and numerical analysis to provide a unified theory for multiple lift compaction. The authors explain that at resonant frequency the efficiency and compaction increases, since maximum energy would be utilized. And their research together with past experience shows that values of resonant frequency are affected by both the soil and machine properties. Moreover they explain that an increase in frequency above the resonance may produce a decrease in compaction, and this is because the generated dynamic force would increase but not the transmitted force to the soil. The authors recommend that if in such a case the operator is not getting enough compaction, he should decrease frequency to get better results. They also found out that if the operating frequency is far enough beyond resonance, then any further increase in frequency will cause decrease in compaction. And when the operating frequency is well below resonance, an increase in frequency will

result in compaction increase simply because both frequency and oscillation per unit length increase.

2.7 Roll Vertical Displacement Calculation

Sleig et al. (1977) conducted mathematical modeling for roll vertical displacement calculation based on the linear two-degree of freedom system of representation of the problem. Using such a model they represented the behavior of the mechanical system by the following figure 2.2.
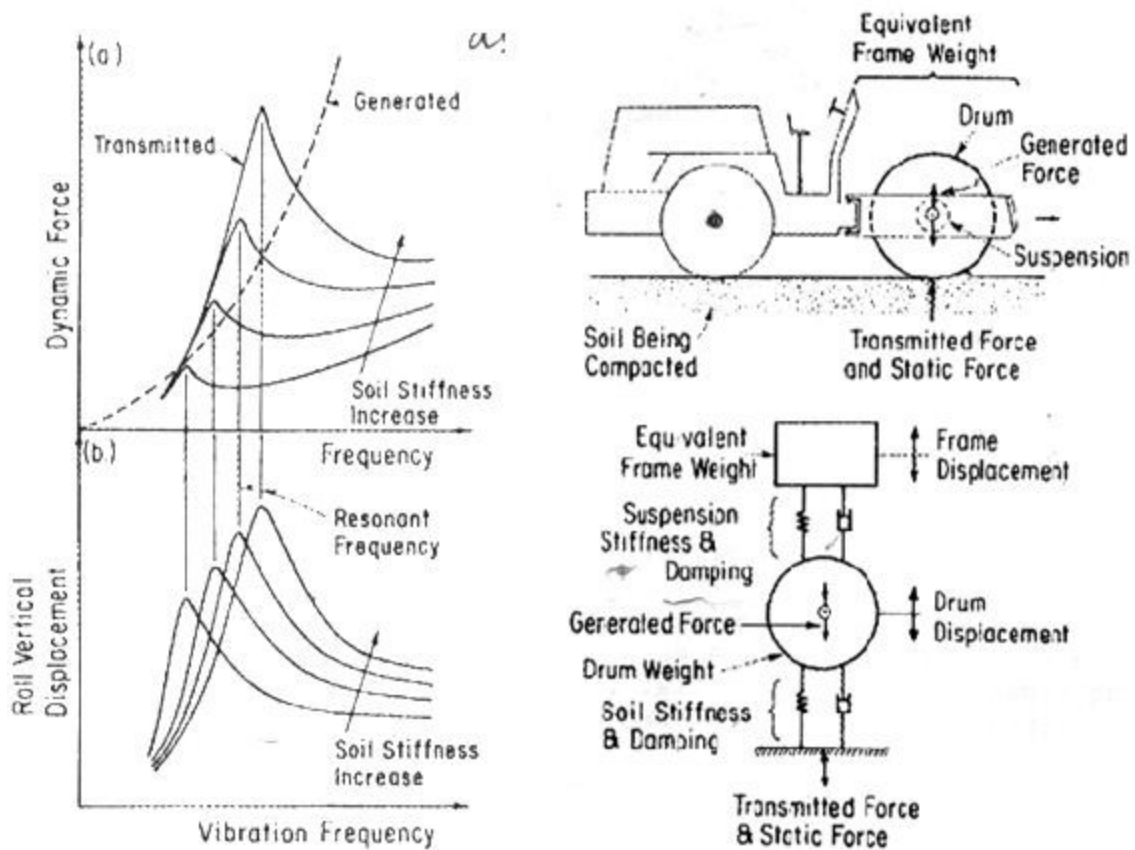
Figure 2.2: Linear two-degree of freedom system representing soil-roller problem (from Sleig et al. 1977)

They further used their mathematical model data and showed graphically (figure 2.3) the trends of roll vertical displacement when system parameters were varied one at a time. They showed that an increase in the mass of the roll, the suspension system damping, and the soil damping, decreases the roll displacement. In contrast, an increase in suspension system stiffness, soil stiffness, and generated dynamic force increases the roll displacement. And change in frame weight has no effect as long as the suspension system stiffness is constant.
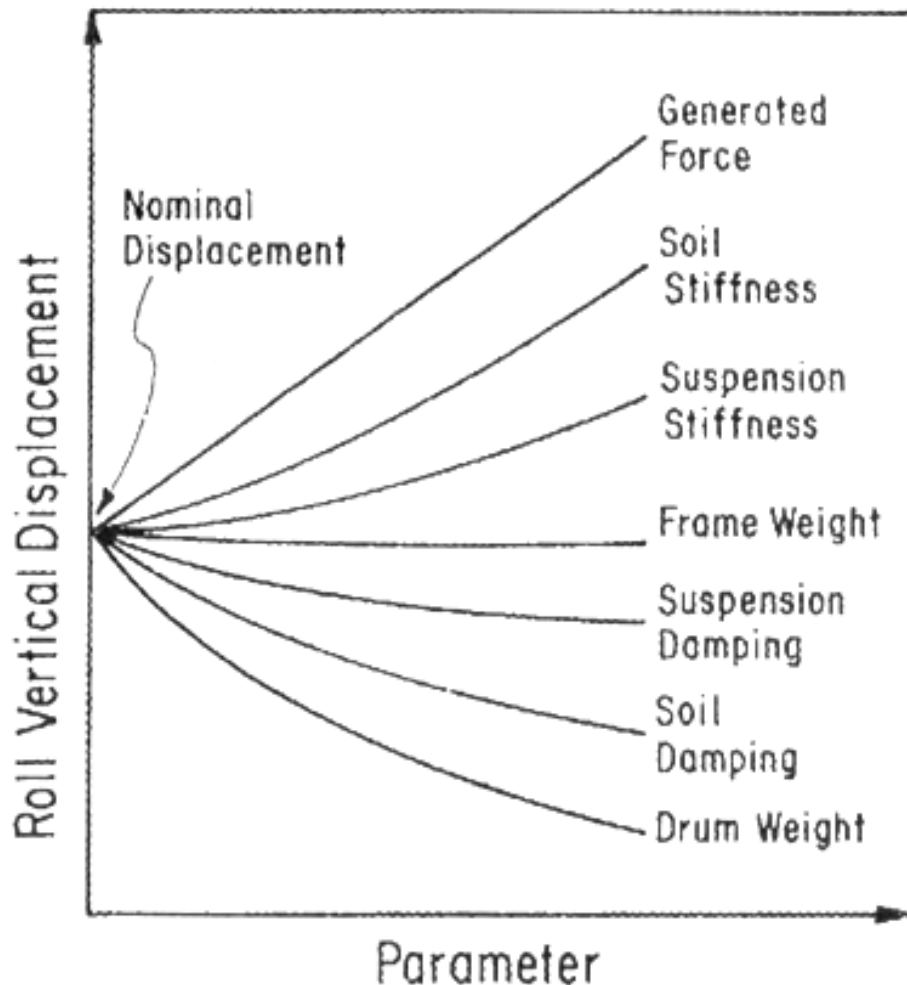
Figure 2.3: parametric study by E.T. Sleig et al. (1977), showing trends of roll vertical displacement

2.8   Parametrical Relationships

Howeedy et al. (1975) carried out field tests at Ludington, Michigan, a site consisting of poorly graded medium to fine sand. Test were carried out to obtain data to evaluate variables that affect the final relative density of the compacted sand, variables such as lift thickness, number of coverage, total force applied by the compactor, frequency, and rolling speed. Furthermore relationships between the final relative density and one factor expressing variations in compaction procedure, compactor characteristics, and properties of soil are established. Total number of 663 tests was performed in the test fills. Lift thickness varied from 0.14 to 0.3m, towed vibratory rollers of heavy to very heavy static weight with speeds from 1.5 to 4.5 mph and up to six coverages were used in this study. The operating frequency of the compactors use varied between 1100 and 2500 vibrations/min. They performed statistical analysis to come up with a dimensionless relationship between D_r and these variables, and they plotted these variations on a log-log scale, and came up with the following general relationship:

$$D_r = K\alpha^a$$

Where 'K' and 'a' are constants, with values 50 and 0.07 respectively, obtained from the log-log scale curve of D_r and α, where

$$\alpha = \frac{F_{total} \times number\ of\ coverages \times frequency}{rolling\ speed \times lift\ thickness \times \gamma_{dry,final} \times drum\ width}$$

Yoo, et al. (1979) carried a parametric study to investigate the effects of different system parameters and also the effects of parameter interactions on the system response. They concluded that a heavier frame and lighter drum will convey more compactive effort to the soil for the same static weight, so they believe that a frame heavier than the drum should be utilized if it is desired to produce a heavier compactor without losing the dynamic capability of the vibratory roller. Authors, through studying the effect of variation in suspension damping, recognized that the increase in suspension damping causes decrease in displacement amplitudes and the transmitted force, occurring mainly around the two resonant frequencies, and in most of the other frequency ranges the effect of suspension damping was seen to be negligible.

2.9   Compaction of Sands by Repeated Shear Straining

Youd (1972) reports that shear strain is the primary factor resulting compaction of granular materials. He explains that in order to increase the density of granular system, the particles have to be rearranged into denser states, and for this to happen, the particulate structure of the granular system must be distorted. He further points out that except if the system is distorted, particle rearrangements are not possible without them crushing. Furthermore, he states that because distortions are composed of strain components, consequently the primary factors directing compaction would be volumetric and shear strains; however the author further explains that published data show that the function of shear strain on compaction is governing over that of volumetric strain.

The author further sheds light on vibratory compaction, and presents the phenomenon from a qualitative and not quantitative point of view. The author through studying previous literature considers the case of a 12.5 kip (55.6 kN) vibratory roller

compacting a dune sand, and explains that appreciable amount of stress and acceleration fluctuations are propagated throughout a region that extends to several feet deep down below the roller, and further reports that within this depth the following three distinct compactive zones should exist:

1) A zone of over-vibration in which the soil is loosened by chaotic motion.

2) A zone of compaction due to repetition of free-fall followed by an impact

3) A zone of compaction due to stress fluctuations without the soil ever experiencing free-fall

As suggested by the author, these zones are better understood if one looked at the distinctly different shear strain conditions found in each zone as depicted in following figure 2.4
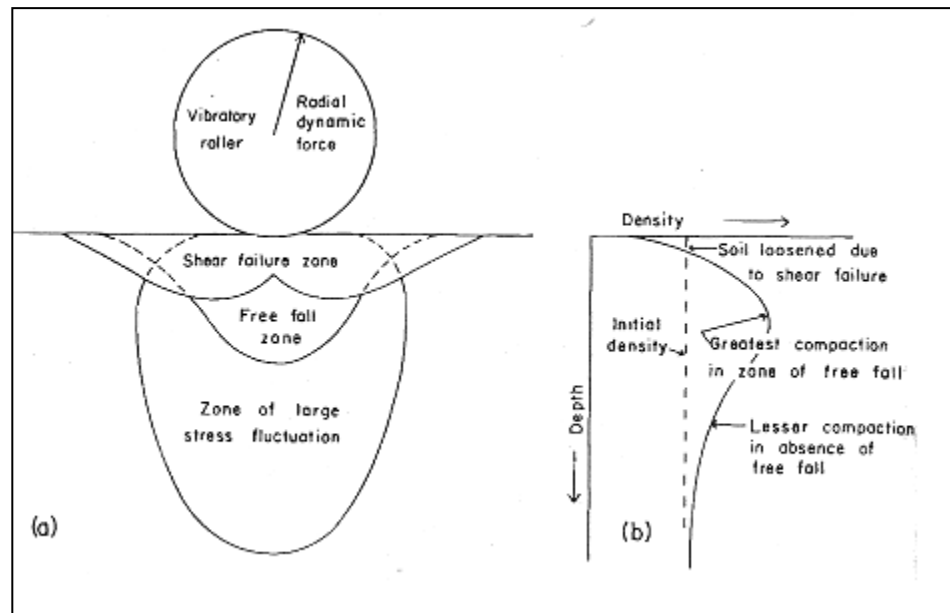
Figure 2.4: (a) Diagrammatic illustration of zones under vibratory roller;
(b) Qualitatively predicted density profile (from Youd, 1979)

2.10 Laboratory compaction of a subgrade layer overlaying a deep soil deposit

Hanna (2003) emphasizes on the lack of consideration and/or room to account for the effect the underlying soil has on the compaction of a subgrade layer. The author explains that depending on the stiffness of the underlying soil layer, some portion of the applied compaction energy is dissipated due to its transmission to the deeper compressible layers. The remaining energy is not always sufficient enough to produce the desirable density.

The author has demonstrated the significance of this matter by conducting an experimental investigation. Laboratory tests were carried out on a prototype set-up which consisted of a steel tank (1x1x1.25m3) filled with first layer (at minimum of four times the thickness of the upper layer) representing the weak underlying soil deposit, and the upper layer (150 or 250mm) representing the subgrade layer. Material used was well-graded silica with specific gravity of 2.70. By conducting modified proctor test, the OMC and maximum dry density of the soil was found to be 4.6% and 19.89 kN/m^3. The water content of the upper layer remained at the optimum value obtained from the modified proctor test. The upper layer was subjected to a uniform surface compaction by means of a hand-held air compactor. The compaction energy was equivalent to modified proctor test, which is 600kJ/m^3. Using three density cans placed at predetermined location in the tank, the moist unit weight was taken and the value of dry density was calculated (experimental results). The vertical displacement of the upper and lower layers was measured by using linear variable displacement transducers (LVDT). The developed prototype test was carried out using 3 different stiffness criteria (loos, medium, and dense). The results from this experiment show that the compression of the upper layer increases simultaneously if the lower layer's stiffness increases.

In order to integrate the influence of the lower layer stiffness on the level of compaction achieved in the upper layer, the author has conducted a laboratory test set-up. In this test the upper layer of silty clay representing the thin subgrade layer, and a spring to represent the lower layer (figure 2.5) with an equivalent coefficient of stiffness of k was employed. The surface of the upper layer was subjected to a compaction effort equivalent to modified proctor test. The dry unit weight and the vertical displacement of soil and spring were measured in the same manner done in the experimental investigation. In total this test was carried out three times using three different k values for the spring in order to accommodate the effect of changes in lower layer stiffness. The results show the same trend as of the experimental investigation (steel tank and silica sand)
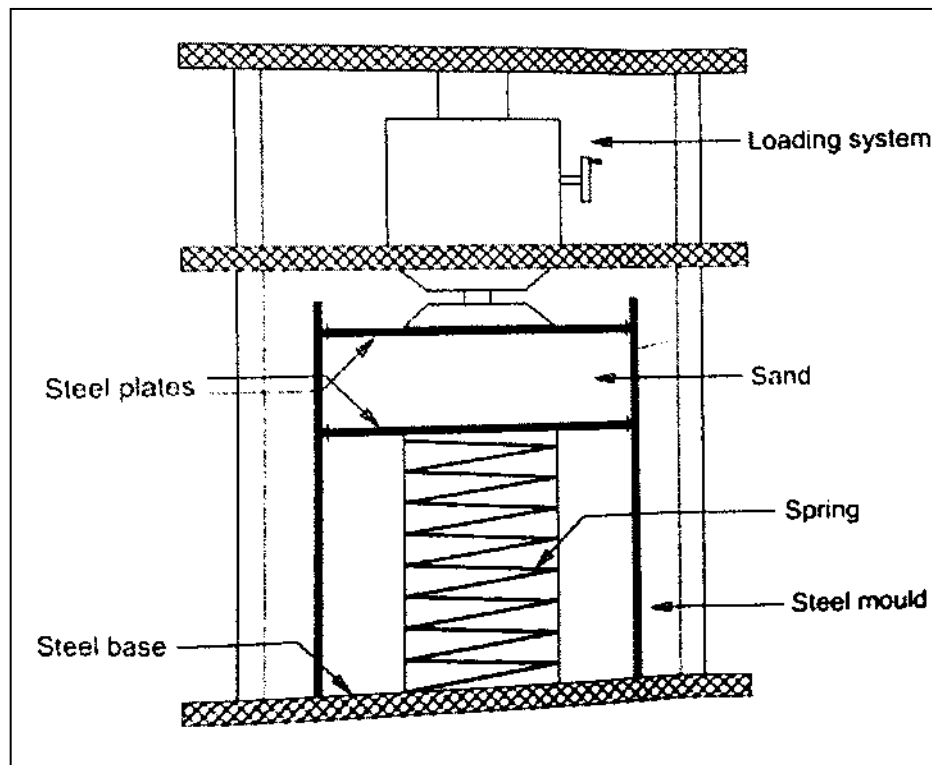
Figure 2.5: Experimental set-up (from Hanna, 2003)

Furthermore, numerical model was developed using finite element program CRISP in order to duplicate the experimental set-up. In this model, the soil was modeled as a non-linear elasto-plastic, with stress-and moisture-dependent properties, with strain softening, and irreversible load compression response. The constitutive law used to model the soil was Mohr-Coulomb. The surface of the upper layer was subjected to harmonic loading (500-2100kPa) through the nodal points in order to simulate the field compaction. The results of this numerical model compared well with the experimental results. The author provided a guideline in the form of a figure. Provided that the initial stiffness of the lower layer is known and the top layer is relatively thin and kept at its optimum moisture content, then the maximum compaction of the top layer can be determined using the following figure 2.6:
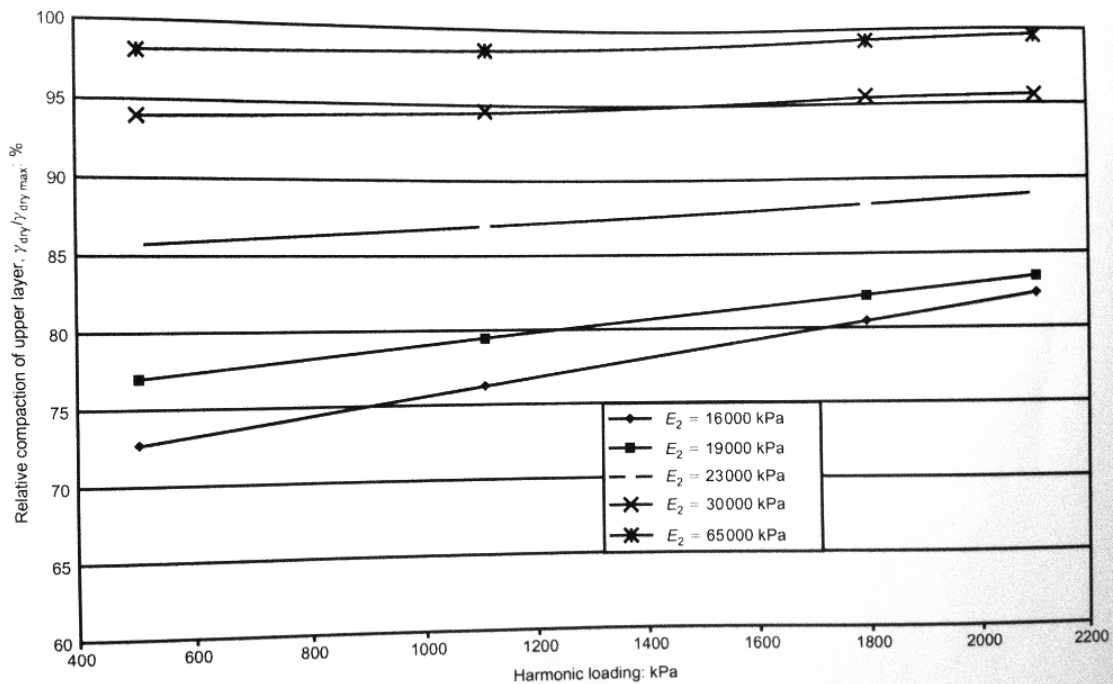
Figure 2.6: determination of maximum compaction given lower layer stiffness and the load applied, (from Hanna 2003).

2.11 Analytical Models

Generally vibration of an object on a medium can be represented by the lumped parameter vibrating system, in which the mass of the object is represented by a lumped mass, and   stiffness and damping characteristics of the medium are presented by a string and a dashpot respectively. In such systems, however, depending on the degrees of freedom, and the nature of vibration (free or forced), the equation of motion would be formed differently and as the consequence the system would behave differently.

The problem of vibratory roller on soil surface can also be represented by lumped parameter system. Many authors have simulated the vibratory roller compacting granular soils by employing a simple system of representation of linear, two degree of freedom of lumped masses, springs and dashpots. Furthermore, some authors (R. Sanejouand et al, 1980) believe that the behavior of a vibratory roller-soil response is not as simple as that represented by a linear-two degree of freedom, lumped-parameter, and spring-dashpot model representation of the problem.

Yoo et al (1979) represented the motion of vibratory roller-soil system via a simple two degree of freedom model. They further carried out a series of field tests under different operational and test conditions with several rollers and further announced the validity of their theoretical model. They explain that soil stiffness and damping values are ought to be determined indirectly from back calculations using their model. They show that the key roller characteristic is the magnitude of drum displacement during vibration. They also recommend that intuition and experience with a particular type of roller should not be used as a reliable basis of predicting the expected effects if any parameters are changed.

Following figure 2.7 is the analytical representation of the roller-soil system employing linear lumped parameters as depicted by Yoo et al (1979):
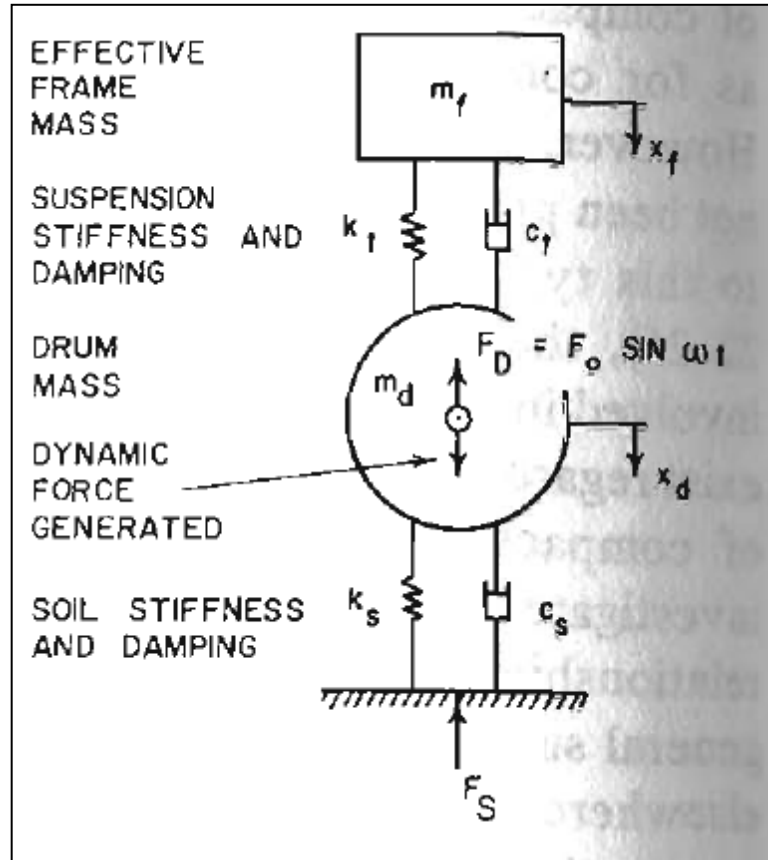
Figure 2.7: Analytical representation of the roller-soil system (from Yoo et al, 1979)

The generated dynamic force F_D, applied to the drum is represented by $F_0 sin\omega t$, in which $F_0=M_e\omega^2$, and M_e is the eccentric moment of the unbalanced mass which is the product of calculated unbalanced rotating mass m_e, and the moment arm e. the authors simplify their vibration model by considering only vertical motion, even though the motion of compactors with single rotating mass usually has an elliptical drum orbit

consisting of also horizontal movement component. They further simplify their model by assuming that stiffness and damping parameters of the suspension are to be constant for a given eccentric moment, and independent of frequency. Moreover their model also presumes that the drum remains in contact with the ground during vibration. The authors express the equations of motions for both drum and frame respectively as following:

$$m_d \ddot{x}_d + (c_t + c_s)\dot{x}_d + (k_t + k_s)x_d - c_t \dot{x}_f - k_t x_f = F_0 sin\omega t$$

and

$$m_f \ddot{x}_f + c_t \dot{x}_f + k_t x_f - c_t \dot{x}_d - k_t x_d = 0$$

In the above equations x_d and x_f are the drum and frame displacements, respectively, and the dot notations imply differentiation with respect to time. The solution for these equations, with the initial displacement and velocities zero, is expressed in terms of the drum and frame displacement amplitudes and phase angles, and is as following:

$$x_d = F_0 \left[\frac{(A_1^2 + B_1^2)}{(C^2 + D^2)} \right]^{1/2}$$

$$x_f = F_0 \left[\frac{(A_2^2 + B_2^2)}{(C^2 + D^2)} \right]^{1/2}$$

$$\emptyset_d = \tan^{-1}\left(\frac{B_1}{A_1}\right) - \tan^{-1}\left(\frac{D}{C}\right)$$

$$\emptyset_f = \tan^{-1}\left(\frac{B_2}{A_2}\right) - \tan^{-1}\left(\frac{D}{C}\right)$$

$\emptyset_d$ and $\emptyset_f$ are phase lags between the generated dynamic force and the drum displacement and generated dynamic force and the frame displacement, respectively.

33

$$A_1 = k_t - m_f \omega^2$$

$$B_1 = c_t \omega$$

$$A_2 = k_t$$

$$B_2 = c_t \omega$$

$$C = m_a m_f \omega^4 - m_a k_t \omega^2 - m_f k_s \omega^2 - m_f k_t \omega^2 - c_t c_s \omega^2 + k_s k_t$$

$$D = k_s c_t \omega + k_t c_s \omega - m_a c_t \omega^3 - m_f c_s \omega^3 - m_f c_t \omega^3$$

The model has 2 degrees of freedom so it also has two natural frequencies and thus two undamped natural frequencies given by:

$$\omega_{n1} = \left[\frac{(m_a k_t + m_f k_s + m_f k_t) - \sqrt{(m_a k_t + m_f k_s + m_f k_t)^2 - 4(m_a m_f)(k_t k_s)}}{2 m_a m_f} \right]^{1/2}$$

$$\omega_{n2} = \left[\frac{(m_a k_t + m_f k_s + m_f k_t) + \sqrt{(m_a k_t + m_f k_s + m_f k_t)^2 - 4(m_a m_f)(k_t k_s)}}{2 m_a m_f} \right]^{1/2}$$

The authors explain that when damping is relatively small so that stiffness would be the primary resistance to the system motion, then these undamped natural frequencies would be a good representation of the system resonant frequencies. The authors further introduce the notion of transmission ratio R_T, and they express it as the ratio of the transmitted force F_s to the generated dynamic force F_D, in the form of the following expression:

$$R_T = \frac{F_S}{F_D}$$

In which the transmitted force, F_S, by the compactor to the soil is the vector sum of the soil spring (stiffness) and damping forces, and is expressed by the authors as the following:

$$F_S = [(k_s x_d)^2 + (c_s \dot{x}_d)^2]^{1/2}$$

The authors further suggest that the value of this transmission ratio is an indication of how efficiently the compactor generated dynamic force is transmitted to the soil.

2.12 Issues Related to Analytical Modeling

The problem with analytical modeling is that the simulation would either become too simplified or very sophisticated and complicated to solve. The reason is that the behavior of the soil skeleton is oversimplified and assigned a linear elastic solution, assuming that all the soil compression is recoverable upon removal of the roller, and also the current analytical models do not consider the effect of any underlying layer. The problem at the soil part is assumed to be a single finite layer. For this reason the solutions for the soil part would not be appropriate and accurate enough to represent the soil behavior under such circumstances. Another approach, a more sophisticated one, is to use combination of elastic springs and dampers to represent this dynamic problem. Two layers can be modeled, with the first layer having both elastic and plastic properties. Elastic property represented by an elastic spring, and the plastic property represented by an elastic spring restrained by horizontal clicks to mimic a portion of subjected energy every time the

elastic spring is deformed. Thus in the next cycle of loading the elastic spring can only be deformed so far that the plastic spring was on the previous cycle. A good example of this approach can be pointed out by looking at the work done by D. Pietzsch and W. Poppy (1993).

    a. As the authors explain, solving the mechanics behind vibratory roller-soil interaction requires a mathematical description of the interdepencies of the state of roller operation and the state of compaction of the building material. They further point out that the mathematical model of this interaction requires analytical model comprising:

    b. An analytical model for the roller;

    c. A mathematical model describing the qualities of the soil, relevant to compaction.

The primary demand of their model is to describe the plastic and elasto-plastic compressions inherent in the system. They suggest that an increase in plastic compression (compaction) of the soil can only be achieved by increasing the effective force, and that this force must depend on the displacement of the soil and, in order to transform energy, counteract the effect of the loading velocity. The authors justify this law by introducing a spring model consisting of three springs as shown in the figure 2.8 below:
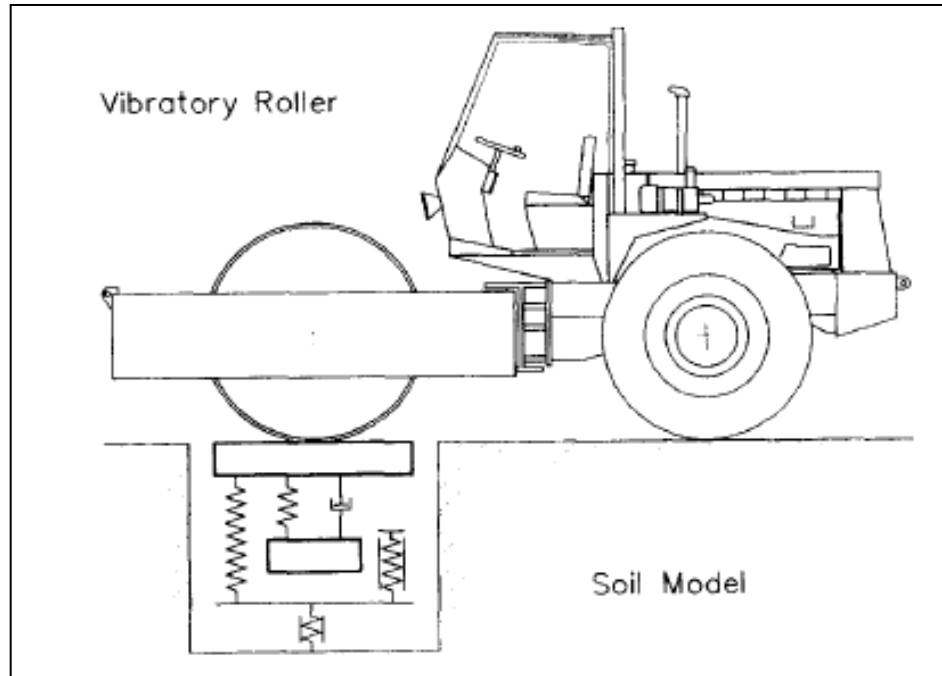
Figure 2.8: Soil-roller system (from D. Pietzsch and W. Poppy , 1993)
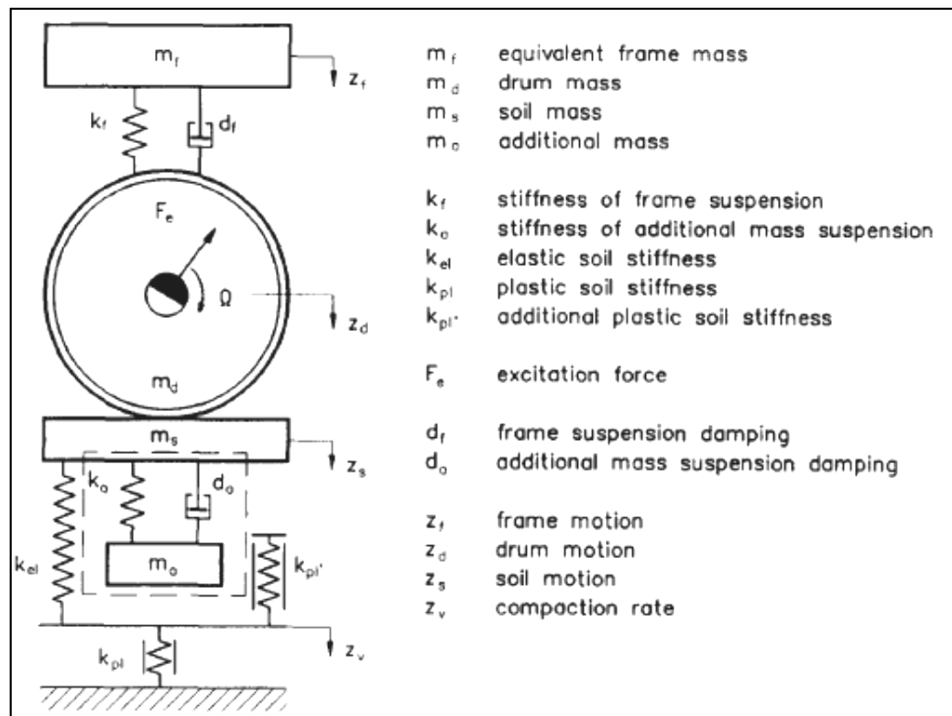
Figure 2.9: Analytical soil-roller interaction model (from D. Pietzsch and W. Poppy, 1993)

As it can be seen in the above figure 2.9, two springs k_{pl} and $k_{pl'}$ click into place at the points of maximum compression at each cycle of loading. For this reason any further plastic compression or compaction can only occur if the elastic spring k_{el} is deformed to the point that the maximum displacement of the previous loading is reached again. Consequently, a continually increasing portion of the kinetic energy of the drum is attained only by the elastic spring because after progression of each cycle the plastic spring is being incrementally deformed and it stays at its position, thus causing the elastic spring also to deform more and also return back a continually increasing portion of the received kinetic energy to the drum during relieving or unloading.

The plastic springs which click into place can be defined as having lateral guides allowing irreversible motion in only one direction. If these springs are compressed, the guides cause the springs to be kept in position, which would be the maximum compression of that cycle. The energy compressing the springs is thus stored therein.

During compaction, the state of roller motion is differentiated into three modes; a downward moving contact position, an upward moving contact position, and a bounced off position because the drum leave the ground when the vibrations exceed a certain intensity. Authors further explain that the state of drum motion at a certain time is dependent on the compaction force, which is the transmitted force to the contact area between the drum and the soil. The division of drum motion into the three different modes is depicted in figure 2.10 as illustrated by the authors.
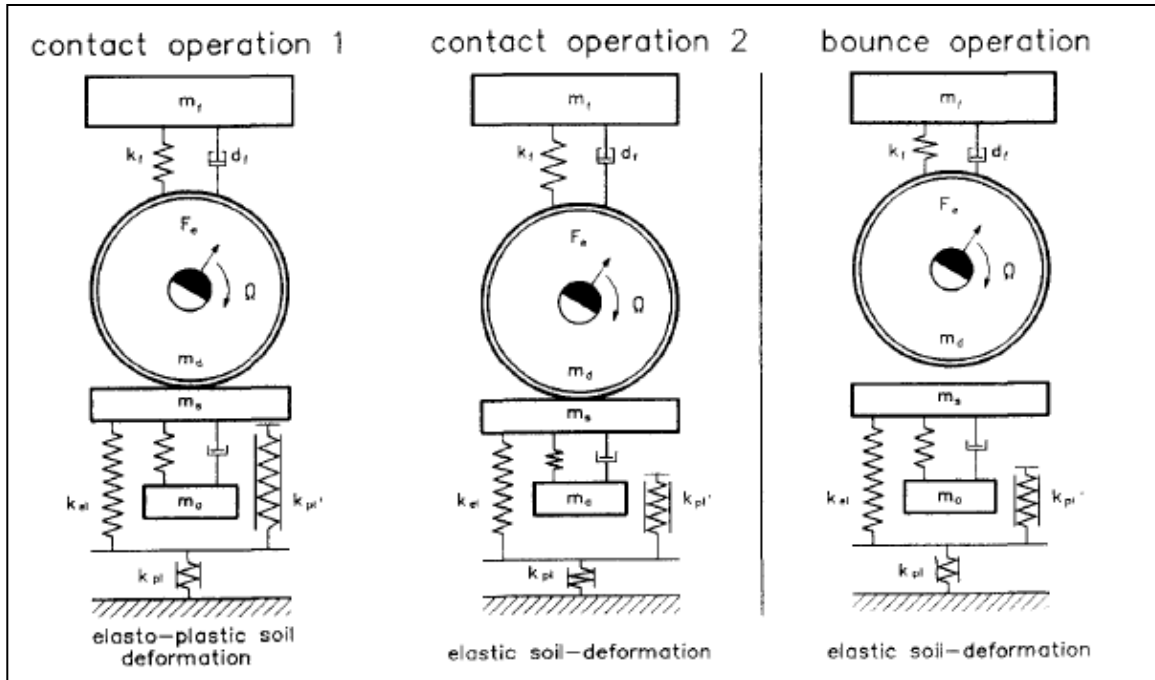
Figure 2.10: The division of drum motion into three different modes (from
D. Pietzsch and W. Poppy ,1993)

As shown above in figure 2.10, during contact mode two different states of soil

compression exist:

1. Contact operation 1: Elasto-plastic compression is present, during which
   all springs of the soil model are under load. The springs k_{pl} and $k_{pl'}$ are
   irreversibly and spring k_{el} is reversibly deformed.

2. Contact operation 2: elastic compression is present, during which the
   spring k_{el} is deformed, while springs k_{pl} and $k_{pl'}$ have already reached their
   maximum compression at the previous stage, the downward moving
   contact mode.

In the contact operation 2 the soil plastic springs are shown to be shortened, well this is simply because the soil has been deformed in the operation 1, which some of the compression is plastic and some is elastic, and also at operation 1 the kinetic energy subjected to elastic spring is partly consumed by the lateral guides of the plastic springs and stored within, and at operation 2 the remaining kinetic energy in elastic spring is send back to the drum.

During bounce operation following contact operation 2, the drum is lifted off the soil. The masses of drum and soil are no more in contact and therefore no more compaction is achieved at this level of motion. Then the next contact operation which is operation 1 would begin with an impact between drum and soil which again causes further compression of plastic springs. This is repeated until no more space is left for the lateral guides of plastic springs to be compressed.

The authors explain that the defined modes of drum motion and the types of soil compression associated with each contact operation are present during vibratory roller compaction, each with different duration and frequency. Furthermore they state that in order to calculate the non-linear drum motion and soil compression for the duration of compaction it is necessary to skip mathematically between the equations of motion of operation modes. And at the same time the transfer and the boundary conditions between the equations of motion has to be taken into account. The authors have solved this mathematical problem using calculation programs such as FORTRAN.

The authors have described the equations of motion in the form of matrix as written below:

Contact operation 1:

$$\begin{bmatrix} m_f & 0 & 0 \\ 0 & (m_d + m_s) & 0 \\ 0 & 0 & m_a \end{bmatrix} \times \begin{bmatrix} \ddot{z}_f \\ \ddot{z}_d \\ \ddot{z}_a \end{bmatrix} + \begin{bmatrix} d_f & -d_f & 0 \\ -d_f & (d_f + d_a) & -d_a \\ 0 & -d_a & d_a \end{bmatrix} \times \begin{bmatrix} \dot{z}_f \\ \dot{z}_d \\ \dot{z}_a \end{bmatrix}$$
$$+ \begin{bmatrix} k_f & -k_f & 0 \\ -k_f & k^* & -k_a \\ 0 & -k_a & k_a \end{bmatrix} \times \begin{bmatrix} z_f \\ z_d \\ z_a \end{bmatrix} = \begin{bmatrix} m_g \\ (m_d + m_s)g \\ m_a g \end{bmatrix} + \begin{bmatrix} 0 \\ F_e \\ 0 \end{bmatrix}$$

$$F_e = m_u r_u (f_e)^2 \sin(f_e t)$$

$$k^* = \left[(k_{el} + k_{pl}{}')k_{pl} / (k_{el} + k_{pl}{}' + k_{pl}) \right] + k_a + k_f$$

In the above equation, the inputs are the masses, spring stiffness, damping, and the excitation force, and the outputs are the displacement, velocity and acceleration. It has to be noted that $z_s = z_d$, but only in the downward motion, since whatever the drum travels down the soil also does the same, and z_s is the total displacement and it includes both elastic and plastic compression, thus in the next matrix solution the actual plastic compression has to be defined which would be a function of this total displacement.

41

Contact operation 2:

$$\begin{bmatrix} m_f & 0 & 0 \\ 0 & (m_d + m_s) & 0 \\ 0 & 0 & m_a \end{bmatrix} \times \begin{bmatrix} \ddot{z}_f \\ \ddot{z}_d \\ \ddot{z}_a \end{bmatrix} + \begin{bmatrix} d_f & -d_f & 0 \\ -d_f & (d_f + d_a) & -d_a \\ 0 & -d_a & d_a \end{bmatrix} \times \begin{bmatrix} \dot{z}_f \\ \dot{z}_d \\ \dot{z}_a \end{bmatrix}$$

$$+ \begin{bmatrix} k_f & -k_f & 0 \\ -k_f & k^* & -k_a \\ 0 & -k_a & k_a \end{bmatrix} \times \begin{bmatrix} z_f \\ z_d \\ z_a \end{bmatrix} = \begin{bmatrix} m_f g \\ (m_d + m_s)g + F_e + k_{el} z_v \\ m_a g \end{bmatrix}$$

$$k^* = k_{el} + k_f + k_a$$

In the above matrix, the inputs are again the masses, springs and dampers, and the excitation force, and a new parameter which is z_v , and is an indication of soil plastic compression of compaction. But it has to calculate through the obtained outputs of the operation 1.

$$z_v = \frac{k_{pl} z_s}{k_{pl} + k_1}$$

Where $\boldsymbol{k_1 = k_{pl} + k_{pl}{}' + k_a + k_f}$

Bounce operation (roller):

$$\begin{bmatrix} m_f & 0 \\ 0 & m_d \end{bmatrix} \times \begin{bmatrix} \ddot{z}_f \\ \ddot{z}_d \end{bmatrix} + \begin{bmatrix} d_f & -d_f \\ -d_f & d_f \end{bmatrix} \times \begin{bmatrix} \dot{z}_f \\ \dot{z}_d \end{bmatrix} + \begin{bmatrix} k_f & -k_f \\ -k_f & k_f \end{bmatrix} \times \begin{bmatrix} z_f \\ z_d \end{bmatrix} = \begin{bmatrix} m_f g \\ m_d g \end{bmatrix} + \begin{bmatrix} 0 \\ F_e \end{bmatrix}$$

Bounce operation (soil):

$$\begin{bmatrix} m_s & 0 \\ 0 & m_a \end{bmatrix} \times \begin{bmatrix} \ddot{z}_s \\ \ddot{z}_a \end{bmatrix} + \begin{bmatrix} d_a & -d_a \\ -d_a & d_a \end{bmatrix} \times \begin{bmatrix} \dot{z}_s \\ \dot{z}_a \end{bmatrix} + \begin{bmatrix} k^* & -k_a \\ -k_a & k_a \end{bmatrix} \times \begin{bmatrix} z_s \\ z_a \end{bmatrix} = \begin{bmatrix} m_s g + k_{el} z_v \\ m_a g \end{bmatrix}$$

Where $k^* = k_{el} + k_a$

As mentioned by the authors, a closed form solution for these equations is not possible simply because of the variable changes in the dynamic behavior of the soil/drum system. They further explain that such dynamic behavior can be solved numerically by skipping between the equation systems by introducing transfer conditions using computer programs. The input parameters of the machine could be easily obtained from roller technical data of a specific machine or, if a new machine is designed, the parameters can be chosen freely. On the other hand, since the soil parameters related to model parameters are hard to determine from known soil properties, thus the soil model parameters must instead be calculated from measurable characteristics of roller/soil system, such as static soil compression, natural frequency or time responses of the drum and frame acceleration.

The authors show the trend of drum motion in the figure 2.11 below, and it is evident that there is contact and bounce present in the system behavior.
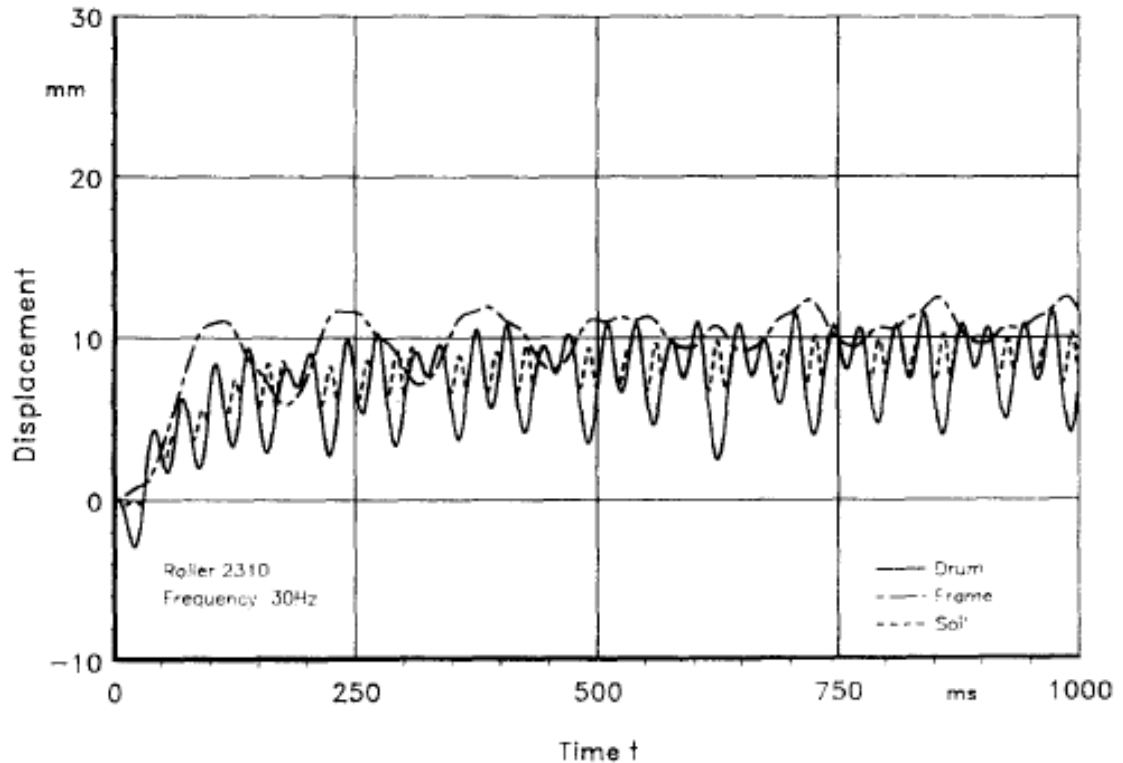
Figure 2.11: Simulated displacements of drum, frame and soil (f = 30 HZ, f ratio= 3.0, natural f of roller/soil = 15 Hz), from D. Pietzsch and W. Poppy ,1993

The problem with this approach is that it requires a whole lot of assumptions and mathematical formulations and it overpasses the limits of this study. However it would be interesting to see if the same trends can be realized if an underlying layer is also present, and to see the influence of the stiffness of underlying layer on the behavior of system through such formulations.

2.13 Differences between Laboratory compaction and field Compaction

Ping et al, (2002) undertook an experimental study to assess field and laboratory compaction characteristics and also studied various laboratory techniques for laboratory simulation of field compaction of A-3 sandy soil. They carried out experiments in two roadway construction projects, namely; Thomasville road project and Sun Coast Parkway project. The authors point out the primary goal of their field tests was to develop field compaction curves and to further compare these curves with those obtained in the laboratory. The authors evaluated and compared the field and laboratory results from both of the projects, employing 4 methods of laboratory simulation of field compaction, namely; standard proctor, modified proctor, vibratory compaction, and gyratory compaction. The authors present their results in figures 2.12, and it can be concluded that using modified proctor test the maximum dry density achieved was quite similar to that at the Sun Coast Parkway project, however this density was achieved in the field after 4 to 6 passes of compactor at a much lower water content than suggested by the modified proctor test. Also they observed that much higher densities of magnitude $17.3kN/m^3$ could be achieved in the field after few more passes (10 to 12 passes) of the compactor, whereas 98% of the modified proctor density would $16.3 \ kN/m^3$. Furthermore, their results obtained from the Thomasville road project indicate that the field densities were much higher than those obtained employing modified proctor test. As the authors suggest that based on the detected inconsistencies between field and laboratory compaction curve results the laboratory impact compaction technique is not a representative way of specifying field water content-density requirements for sandy soils. The authors so far have shown the limitation of such impact tests on determining field density requirements

for A-3 sandy soils, thus there are spaces left for skepticism on the same trends for different types of cohesionless soils. Moreover, they fail to depict in any manner the importance of the underlying layers in achieving density figures.
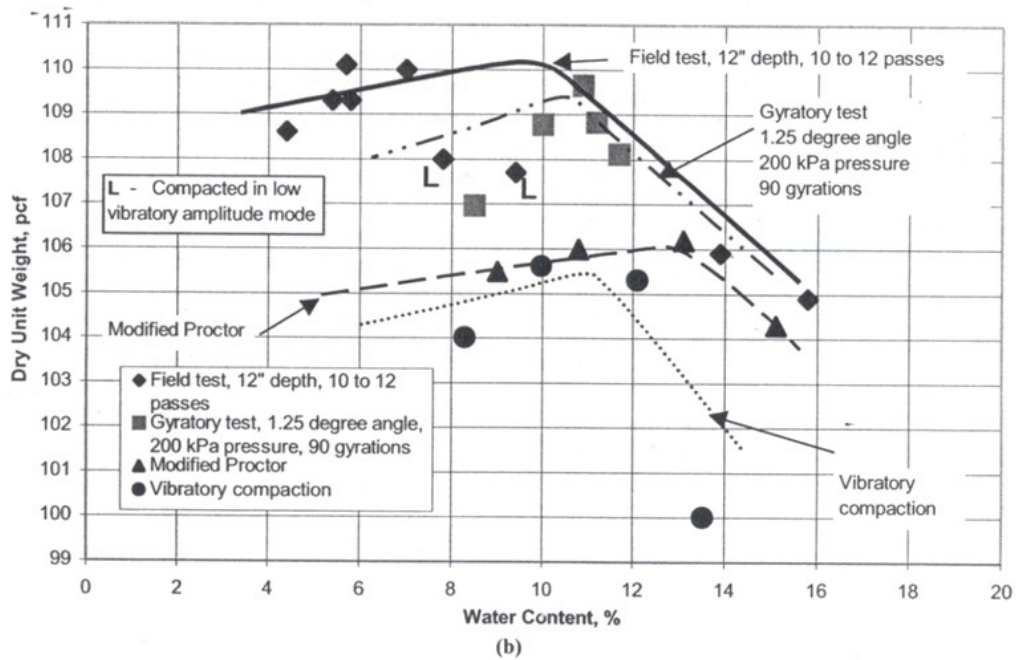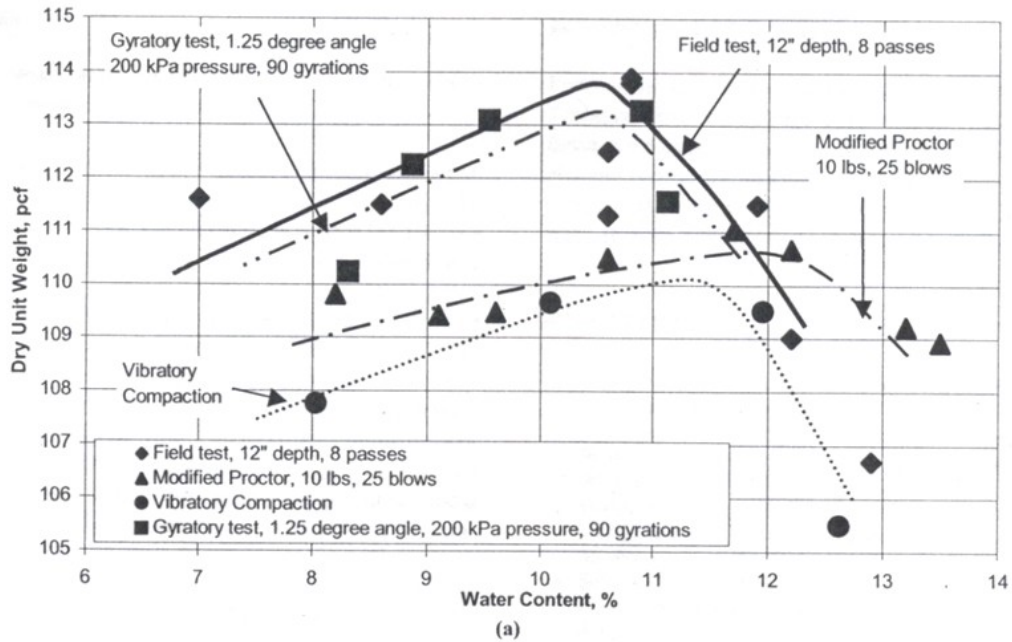
Figure 2.12 Comparison of field and laboratory test results: a) Thomasville
b) Sun Coast, (from Ping et al, 2002)

Martinez (2008), in University of Concordia, conducted laboratory Proctor test and intended to duplicate the laboratory results by numerical modeling. The following tables 2.1 -2.5 present the results from both laboratory and numerical modeling. Tables 2.1, 2.2 and 2.3 show deformation results, and tables 2.4 and 2.5 show percentage difference between proctor test and two numerical models, a model confined laterally but free to deform downwards, and a model for field compaction simulation.

Table 2.1 Vertical deformation of Proctor model, (Martinez (2008)

Sample number	Δy (m)
1	-1.839303
2	-1.839303
3	-0.398113
4	-1.60907
5	-1.418887
6	-1.267666
7	-0.624409
8	-0.812061

Table 2.2 Vertical deformation at point of impact for laterally confined model, (Martinez (2008)

Sample	Actual vertical deformation at point of impact (m)		
number	E2 = 2500 kPa	E2 = 20 000 kPa	E2 = 65 000
1	-1.92469	-1.842322	-1.807
2	-1.92469	-1.842322	-1.807
3	-0.69231	-0.62121	-0.551361
4	-1.705745	-1.627722	-1.713111
5	-1.630763	-1.556164	-1.516206
6	-1.470809	-1.399763	-1.359067
7	-0.766667	-0.676981	-0.638863
8	-0.961852	-0.861827	-0.826986

Table 2.3 Vertical deformation at point of impact for field model, (Martinez (2008)

Sample	Actual vertical deformation at point of impact (m)		
number	E2 = 2500 kPa	E2 = 20 000 kPa	E2 = 65 000
1	-5.42913	-4.87965	-4.42127
2	-5.42913	-4.87965	-4.42127
3	-2.2516	-2.46928	-1.86346
4	-4.88398	-4.91481	-4.57871
5	-4.40959	-4.67312	-4.07844
6	-4.02187	-4.00268	-3.67037
7	-2.54893	-2.57392	-2.02508
8	-3.11149	-3.18666	-2.60884

Table 2.4 Percentage difference between Proctor and laterally confined model

Sample number	% difference between Proctor and laterally confined model vertical deformation results		
	E2 = 2500 kPa	E2 = 20 000 kPa	E2 = 65 000
1	4.6	0.2	-1.8
2	4.6	0.2	-1.8
3	29.9	16.6	3.5
4	6.0	1.2	6.5
5	14.9	9.7	6.9
6	16.0	10.4	7.2
7	22.8	8.4	2.3
8	18.4	6.1	1.8

Table 2.5 Percentage difference between Proctor and field model

Sample number	% difference between Proctor and laterally confined model vertical deformation results		
	E2 = 2500 kPa	E2 = 20 000 kPa	E2 = 65 000
1	195.2	165.3	140.4
2	195.2	165.3	140.4
3	322.6	363.4	249.7
4	203.5	205.4	184.6
5	210.8	229.4	187.4
6	217.3	215.8	189.5
7	308.2	312.2	224.3
8	283.2	292.4	221.3

Table 2.4 shows that in a model confined laterally, but free to move downwards, with varying lower layer stiffness for different cases, the compaction results using the same energy as in Proctor brings about different compaction levels. This is because the lower layer is allowing the top layer to sink into it and thus some of the compaction energy is wasted to the lower layer, but in Proctor the lower layer is a stiff steel plate and does not allow any deformation at the interface between the soil and the plate, and thus all the energy is reflected back into the soil.

Table 2.5 also show the same trend as in table 2.4, with the only difference that the differences are more significant and the reason being that comparing to laterally confined model the field model does not impose any confinement for lateral movement of soil particles due to stresses subjected from compactive forces. Hence less compaction is achieved comparing with Proctor where the soil is restrained by radial wall and the bottom plate of the Proctor mold.

By looking at these findings it can be concluded that the predictions of Proctor laboratory test is not always satisfactory and recommended for field compaction situations specially in conditions where the lower layers would govern the compaction that can be achieved in a top layer. What Proctor test is predicting is that given the same boundary conditions, one can simply reach to maximum dry density of a given soil using the optimum moister content and compaction energy used in Proctor test.

CHAPTER 3

NUMERICAL MODELING

3.1 General

In this research, a numerical model simulating a static roller compacting a thin sand layer overlaying a deep deposit is developed using the commercial finite element software PLAXIS 2D 2010. The soil layer will be subjected to repeated loading.

3.2 Numerical Model

The model developed uses a plane-strain with 4th order triangular elements of 15 nodes for accuracy purposes. The Plane-strain mode is chosen to simulate the strains in the direction of the roller track. (Figure 3.1)
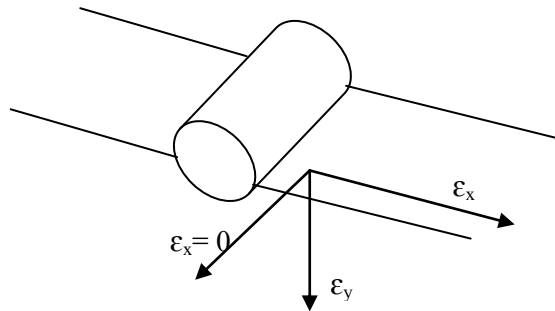
Figure 3.1: Rigid drum rolling on soil surface.

3.3   Boundary Conditions

In this model, the thickness of the upper layer varies between the two limits of the upper and lower homogenous layer of finite depth. The results obtained for these limits were used or serve as validation of the current model.

3.3.1   Mesh Generation

Appropriate type of the finite element mesh is necessary to produce accurate behavior and responses to the loading condition. "PLAXIS" has a built-in finite element mesh generator, which allows choosing the coarseness of a mesh. The individual clusters of a global geometry can be separately meshed with different coarseness in order to investigate the behavior of the soil in a selected zone. Furthermore, local coarseness should also be used in cases where large compressions are expected in a particular area of a problem.

Type of mesh used in this research was obtained via comparison of results of same cases with different mesh accuracy, if the refined mesh yielded similar results to the coarser mesh then the coarser mesh was chosen, and if not the process of refining was done until the results were similar to the coarser mesh.

3.3.2   Models Geometry

The model consist of a thin layer on top of a deep deposit (half space) and has dimensions of 25m x 25m for the lower layer, and for the top layer with width of 25m and with thickness ranging from half the load width (0.5x0.4m) to 5 times the load width (5x0.4m). The effect of variation of top layer thickness on the amount of compaction of top layer are presented with respect to either an increasing combination of parameters or increase in standalone parameters of underlying layer stiffness and strength parameters ,

load and load cycles. The stiffness of the lower layer for different cases varies from loose to dense (5000, 15000, 20000, and 40000 kN/m^2), and the load applied varies from 10, 20, 25, and 35 kN/m^2. The effect of load cycle is taken into account by using cycles ranging from 1 to 10. It is generally expected that when the lower layer is loose or soft, a great portion of compaction energy would be wasted by this layer to get compressed. However this does not always follow a general trend and it depends on many variables, such as material variables, boundary conditions variables and loading variables.

Following figures 3.2 and 3.3 show the model boundary condition and generated mesh.
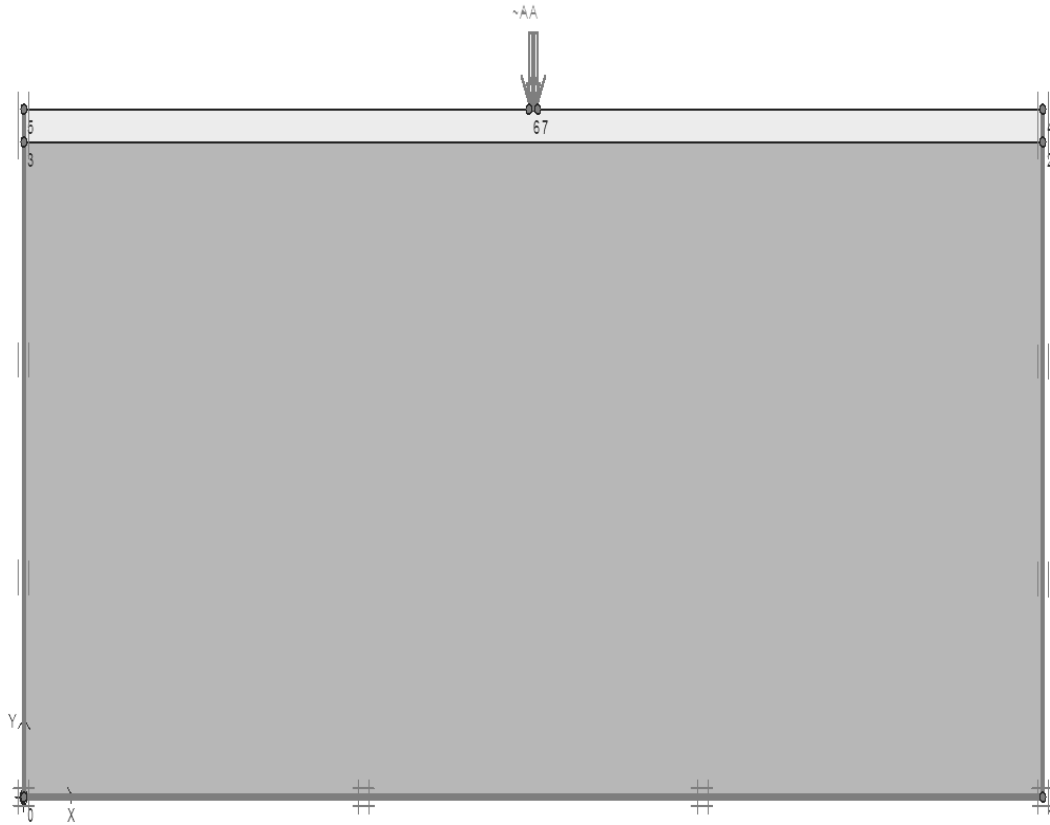
Figure 3.2: Boundary condition of model.
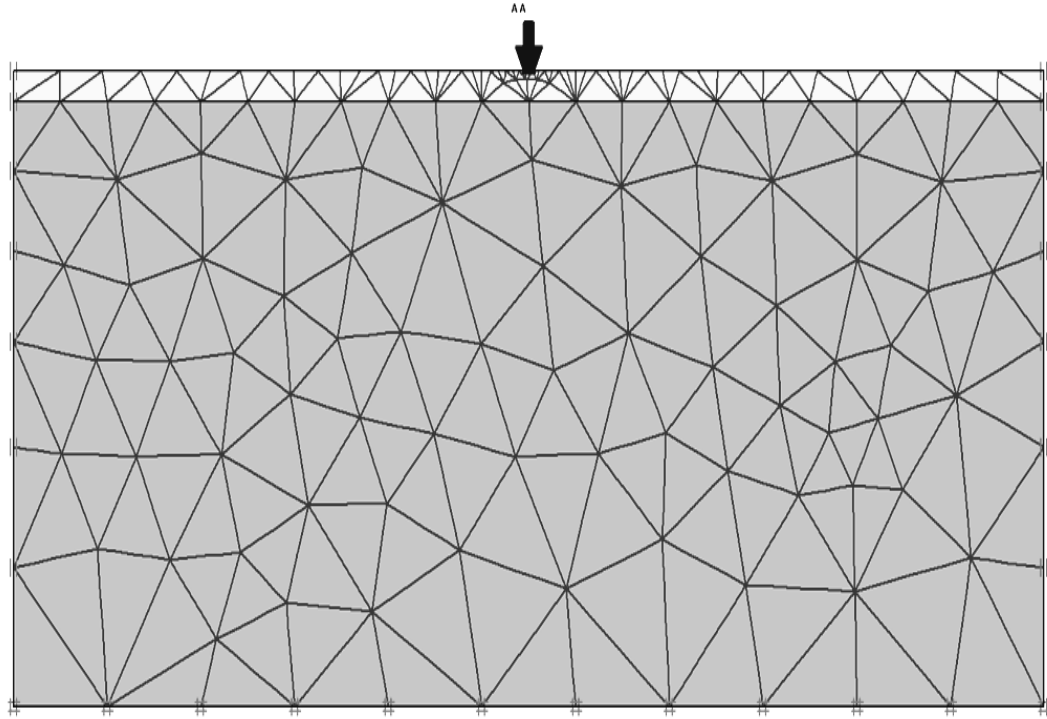
Figure 3.3: Mesh generation

3.4 Material Models

In this investigation the upper layer soil was modeled by the Stress Hardening model, which is suitable for the cases of repeated loading, where the mechanical properties of soil and the compression characteristics are continuously changing during each application of load and further will allow for the stiffness matrix of the soil to be updated progressively following each application of loading.

The magnitude of compaction energy and compression significantly reduces with depth in the underlying layer, and accordingly, the lower layer was modeled by the Mohr Coulomb constitutive law, which has a fixed yield surface, and it requires more simple soil input parameters.

Description of the models input parameters required by PLAXIS for both models are summarized in the following table 3.1.

Table 3.1: Mohr Coulomb and Hardening Soil model input parameters by Plaxis.

Parameter	Model	Name	Unit
Soil unit weight above phreatic level	MC/HS	γ_{unsat}	kN/m³
Soil unit weight below phreatic level	MC/HS	γ_{sat}	kN/m³
Permeability in horizontal direction	MC/HS	K_x	m/day
Permeability in vertical direction	MC/HS	k_y	m/day
Young's modulus of elasticity	MC	E_{ref}	kN/m²
Possion's ratio	MC	v	-
Cohesion	MC/HS	C_{ref}	kN/m²
Angle of internal friction	MC/HS	φ	degrees
Dilatancy angle	MC/HS	ψ	degrees
Secant stiffness in standard drained triaxial test	HS	E_{50}^{ref}	kN/m²
Tangent stiffness for primary oedometer	HS	E_{oed}^{ref}	kN/m²
Unloading/reloading stiffness	HS	E_{ur}^{ref}	kN/m²
Power for stress-level dependency of stiffness	HS	m	-
Poisson's ratio for unloading-reloading	HS	v_{ur}	-
Reference stress for stiffness	HS	p^{ref}	kN/m²
Value for normal consolidation-k_0	HS	k_0^{nc}	-
Failure ratio q_f/q_a	HS	R_f	-
Tensile strength	HS	$\sigma_{tension}$	kN/m²

3.5 Loading Type

The loading system used in this investigation is uniformly distributed load as shown in figure 3.4. This loading system is applied on the soil through a stiff weightless plate. The loading is activated and deactivated in calculation phases in order to simulate the amount of load cycles or passes by a static roller.

Uniformly distributed
load system A

Plate through
which the load
system A is
applied to the soil
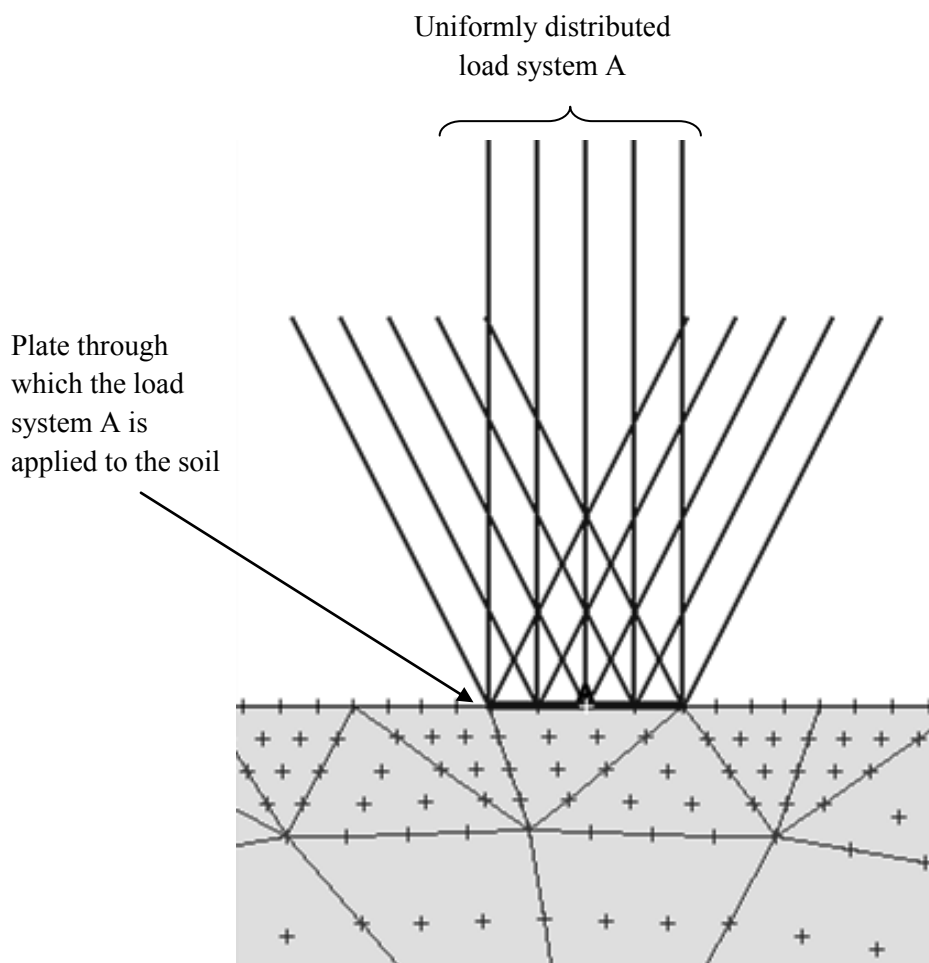
Figure 3.4: Load application

3.6 Materials Actual Parameters

In this investigation, the material parameters for the soil models were chosen to represent a wide range of practical cases. These values are given in tables 3.2 and 3.3 for the upper and lower layer soils respectively. The values represent wide range of soil properties encounter in field. Values are taken from Das (2003) and elasticity modulus of soils are obtained. The strength for the lower layer materials, used were ranging from very loose to very dense, while top layer was kept constant.

Table 3.2: Top layer material model parameters

No.	model	y_{unsat}	y_{sat}	E_{50}	E_{oed}	E_{ur}	m	c	φ	ψ	υ	k_x, k_y (m/day)
H_1	HS	17.5	19.0	9856	1000	1111	0.5	0.2	30	0	0.3	1.0

Table 3.3: Lower layer material model

No.	model	y_{unsat}	y_{sat}	E_{50}	c	φ	ψ	υ	k_x, k_y (m/day)
M_1	MC	15.5	17.0	5000	0.2	27	0	0.2	1.0
M_2	MC	19.0	20.0	1500	0.2	32	0	0.35	1.0
M_3	MC	19.5	20.5	20000	0.2	35	0	0.35	1.0
M_5	MC	20.0	21.0	40000	0.2	45	0	0.45	1.0

3.7   Simulating the Roller

In this investigation, a constant value for roller indentation into soil (a function of soil and roller properties) had to be chosen, even though for each type of load a different indentation exists. The indentation and essentially the roller-soil contact area, and thus loading area, depends on the diameter and the length of the roller, modulus of soil, and the Drum-Soil contact force. In Figure 3.5, the analogy of progression of roller-soil indentation area into a larger area is shown, and the definition of indentation area including indentation length and width of roller-soil system is shown as L and B, respectively.
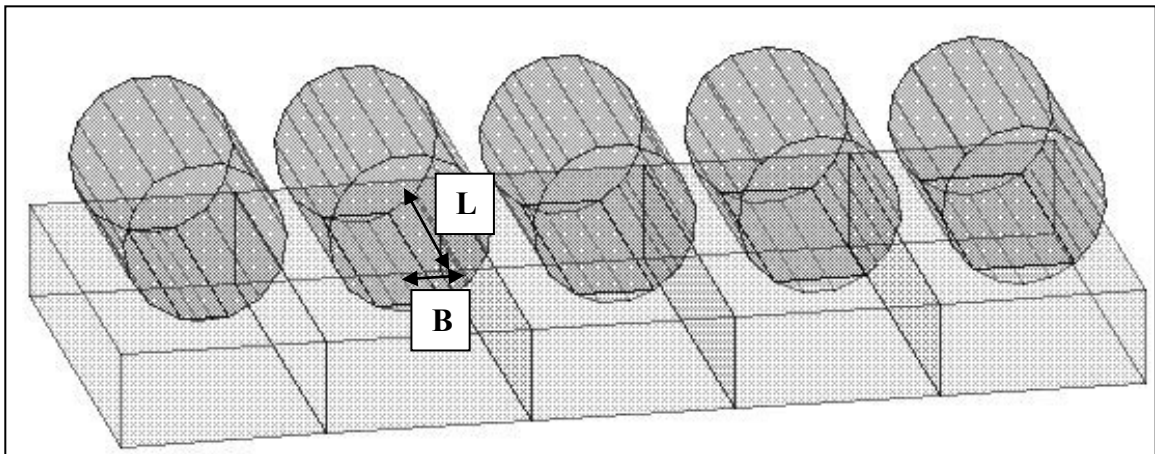
Figure 3.5: Imprinted area by the roller on soil

Due to complications in determining an appropriate value for contact width imprinted by a roller, an average value of 0.4m, based on experience, was chosen.

3.8   Variables Considered and Scheme of Analysis

In this investigation, the compaction of top layer was examined with regards to variation of applied loads, number of load applications, thickness of the top layer and underlying layer stiffness.

The effect of load cycles was studied by ranging the load cycles from 1 to 10 times. That means in the software there are in total 20 phases, 10 of which are activated and the other 10 are deactivated to simulated cycles of load. So one cycle of load consists of an active phase and a de-active phase, which means the load and the plate are applied to the soil, and in next phase they are not.

The effect of underlying layer was studied by ranging the lower material from loose to very dense. That means the stiffness and strength parameters is different for each material. In total 5 different lower layer soil has been used. The effect of these lower layer material are shown by their stiffness value even though many other parameters of the material are also changing (such as density, poisson's ratio, stiffness, internal angle of friction , shear modulus, shear wave velocities etc).

CHAPTER 4

RESULTS AND ANALYSIS

4.1   General

In this section the results produced by the present numerical model are presented in Figures and Tables. Sensitivity and parametric study was carried out in order to determine the effect of each governing parameter, and further to develop a design theory for practicing use.

4.2   Test Results

Each simulation is run in Plaxis software .Results of the analysis are first generated with curves and then translated into tabulated data in order to produce required curves and expressions for further analysis. As it can be seen in figure 4.1 the required points are first selected in order to extract data for curve generation. Point A is at soil and applied load contact, and point B is at the interface between the top layer and lower layer. This way it is possible to observe the behavior at interface and top layer separately. Since there are two points selected on the model geometry, thus two separate curves have to be plotted. These curves present the compression at each of these points against a load multiplier used in Plaxis.
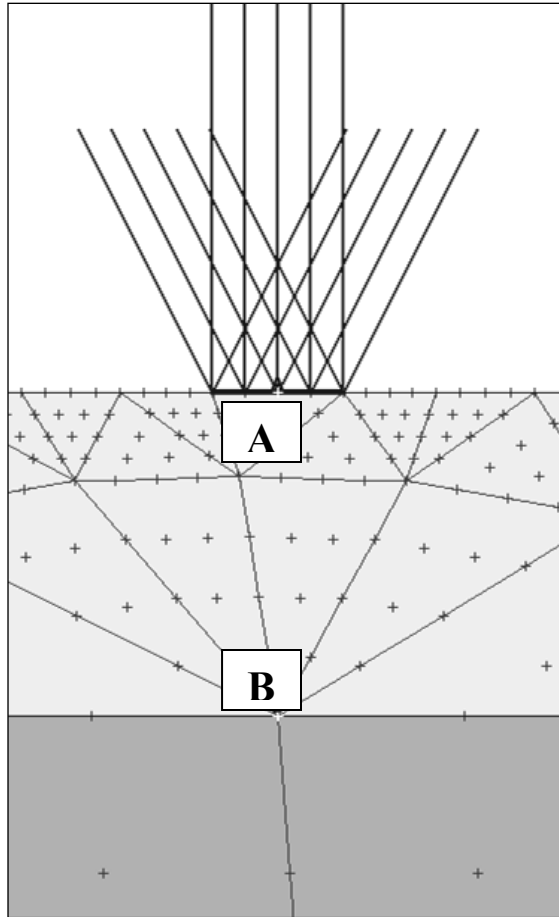
Figure 4.1: Points from which load-
displacement curves are plotted.

4.3   Results

Tables 4.1 to 4.4 summarize the results obtained in this investigation. Table 4.1 presents

the compression measured at top layer and at interface for different loading and lower

layer stiffness, number of load applications, and top layer thickness. It can be noted from

this table that there is a clear trend, where the compressions of top layer increases due to

an increase of the top layer thickness.

Table 4.1: Present test results for varying top layer thickness for
different lower layer stiffness and load combinations

H (m)	H/B	E_2 (kN/m²)	f	Load, q (kN/m2)	Δuy Total (cm)	Δuy interface (cm)	Δuy top layer (cm)
0.2	0.5	5000	10	10	0.371	0.242	0.078
		15000	10	20	0.41	0.15	0.263
		20000	10	25	0.51	0.15	0.361
		40000	10	35	0.77	0.09	0.683
0.4	1	5000	10	10	0.44	0.21	0.227
		15000	10	20	0.66	0.14	0.522
		20000	10	25	0.83	0.13	0.7
		40000	10	35	1.4	0.08	1.316
0.8	2	5000	10	10	0.49	0.16	0.336
		15000	10	20	0.86	0.1	0.761
		20000	10	25	1.1	0.1	0.998
		40000	10	35	1.7	0.07	1.631
2	5	5000	10	10	0.56	0.107	0.454
		15000	10	20	1	0.055	0.945
		20000	10	25	1.3	0.051	1.249
		40000	10	35	2	0.025	1.997

Table 4.2 presents the compression at top layer and at interface with respect to variation

of top layer thickness and lower layer stiffness for different loading magnitudes. It can be

noted from this table that there is a clear trend, where the compressions increases due to

an increase in load.

Table 4.2 Present test results for varying load for different lower layer stiffness and top layer thickness combinations

q kN/m^2	E$_2$ (kN/m^2)	f	H (m)	H/B	Δuy Total (cm)	Δuy interface (cm)	Δuy top layer (cm)
10	5000	10	0.2	0.5	0.371	0.242	0.078
	15000	10	0.4	1	0.41	0.15	0.263
	20000	10	0.8	2	0.51	0.15	0.361
	40000	10	2	5	0.77	0.09	0.683
20	5000	10	0.2	0.5	0.44	0.21	0.227
	15000	10	0.4	1	0.66	0.14	0.522
	20000	10	0.8	2	0.83	0.13	0.7
	40000	10	2	5	1.4	0.08	1.316
25	5000	10	0.2	0.5	0.49	0.16	0.336
	15000	10	0.4	1	0.86	0.1	0.761
	20000	10	0.8	2	1.1	0.1	0.998
	40000	10	2	5	1.7	0.07	1.631
35	5000	10	0.2	0.5	0.56	0.107	0.454
	15000	10	0.4	1	1	0.055	0.945
	20000	10	0.8	2	1.3	0.051	1.249
	40000	10	2	5	2	0.025	1.997

Table 4.3 illustrates the changes in the compression of both layers due to an increase of load cycles up to 10 cycles. It is evident that the compression of both layers increases up to a limited number of load cycles after which both layers come into equilibrium and no

more compression is apparent. This is more realized in cases with more shallow depth for top layer.

Table 4.3: Present test results for varying number of load cycles

f	load (kN/m2)	E_2 (kN/m^2)	H (m)	H/B	Δuy Total (cm)	Δuy interface (cm)	Δuy top layer (cm)
1	10	5000	0.2	0.5	0.346	0.242	0.103
	20	15000	0.4	1	0.562	0.139	0.424
	25	20000	0.8	2	0.94	0.099	0.841
	35	40000	2	5	1.7	0.026	1.674
2	10	5000	0.2	0.5	0.361	0.246	0.116
	20	15000	0.4	1	0.581	0.139	0.442
	25	20000	0.8	2	0.974	0.101	0.872
	35	40000	2	5	1.8	0.026	1.774
3	10	5000	0.2	0.5	0.37	0.25	0.12
	20	15000	0.4	1	0.59	0.14	0.455
	25	20000	0.8	2	0.99	0.1	0.887
	35	40000	2	5	1.8	0.03	1.775
4	10	5000	0.2	0.5	0.37	0.24	0.123
	20	15000	0.4	1	0.6	0.14	0.465
	25	20000	0.8	2	1	0.1	0.899
	35	40000	2	5	1.9	0.03	1.875
5	10	5000	0.2	0.5	0.37	0.244	0.125
	20	15000	0.4	1	0.61	0.139	0.474
	25	20000	0.8	2	1	0.101	0.899
	35	40000	2	5	1.9	0.025	1.875

Table 4.3: Present test results for varying number of load cycles (continue)

f	load (kN/m2)	E_2 (kN/m^2)	H (m)	H/B	Δuy Total (cm)	Δuy interface (cm)	Δuy top layer (cm)
6	10	5000	0.2	0.5	0.37	0.244	0.126
	20	15000	0.4	1	0.63	0.14	0.493
	25	20000	0.8	2	1	0.102	0.899
	35	40000	2	5	1.9	0.025	1.875
7	10	5000	0.2	0.5	0.37	0.243	0.127
	20	15000	0.4	1	0.64	0.139	0.499
	25	20000	0.8	2	1	0.102	0.898
	35	40000	2	5	1.9	0.025	1.875
8	10	5000	0.2	0.5	0.37	0.243	0.127
	20	15000	0.4	1	0.65	0.139	0.507
	25	20000	0.8	2	1.1	0.102	0.998
	35	40000	2	5	1.9	0.025	1.875
9	10	5000	0.2	0.5	0.37	0.243	0.128
	20	15000	0.4	1	0.65	0.139	0.515
	25	20000	0.8	2	1.1	0.102	0.998
	35	40000	2	5	2	0.025	1.975
10	10	5000	0.2	0.5	0.37	0.242	0.128
	20	15000	0.4	1	0.66	0.139	0.52
	25	20000	0.8	2	1.1	0.102	0.998
	35	40000	2	5	2	0.025	1.997

Table 4.4 presents the results for the system as the stiffness of the lower layer increases. It can be observed that as the lower layer stiffness is increased, the compression at interface decreases, and thus less compaction is lost to the lower layer. This means the top layer subgrade has achieved more compaction.

Table 4.4: Present test results for varying lower layer stiffness for different load and top layer thickness combinations

E_2 (kN/m^2)	load (kN/m2)	f	H (m)	H/B	Δuy Total (cm)	Δuy interface (cm)	Δuy top layer (cm)
5000	10	1-10	0.2	0.5	0.371	0.242	0.078
	20	1-10	0.4	1	1.000	0.485	0.515
	25	1-10	0.8	2	1.500	0.468	1.032
	35	1-10	2	5	2.600	0.357	2.244
15000	10	1-10	0.2	0.5	0.205	0.070	0.135
	20	1-10	0.4	1	0.661	0.139	0.522
	25	1-10	0.8	2	1.100	0.135	0.965
	35	1-10	2	5	2.200	0.094	2.106
20000	10	1-10	0.2	0.5	0.19	0.05	0.134
	20	1-10	0.4	1	0.61	0.10	0.504
	25	1-10	0.8	2	1.10	0.10	0.998
	35	1-10	2	5	2.20	0.07	2.130
40000	10	1-10	0.2	0.5	0.15	0.021	0.131
	20	1-10	0.4	1	0.54	0.042	0.496
	25	1-10	0.8	2	1.00	0.043	0.957
	35	1-10	2	5	2.000	0.025	1.997

4.4   Effect of Top Layer Thickness

Figure 4.2 presents the results for the case of lower layer stiffness of 5000 kN/m^2 and applied load of 10 kN/m^2. It can be seen from this figure that the compression of the top layer increases due to the increase of the thickness of the upper layer up to a thickness of 1.2 m, at which any further increase does not have any significant influence on the behavior on the top layer, as it starts to behave as a homogenous layer. Also it is noticeable that the compression at the interface is decreasing as the top layer thickness is increasing, which is due to the fact that stresses are contained throughout the depth of the top layer. The same trends can be observed in figure 4.3 to 4.5. Furthermore, it can be also noted from these figures that the compression of the top layer increases due to the increase of the applied load.
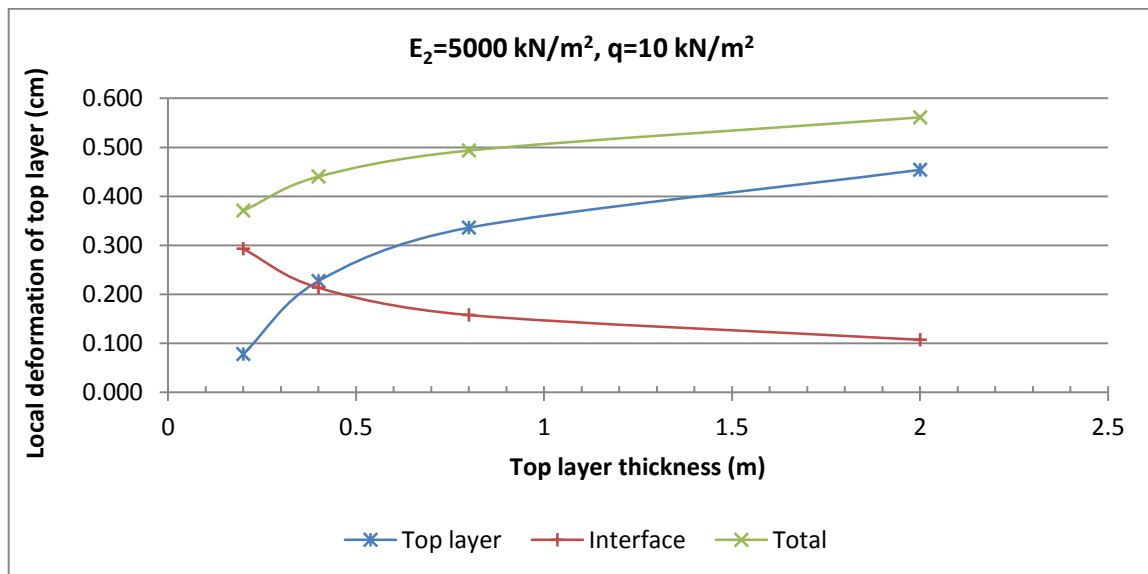

Figure 4.2: Results for increasing top layer thickness (lower layer stiffness of 5000 kN/m^2 and load of 10kN/m^2)
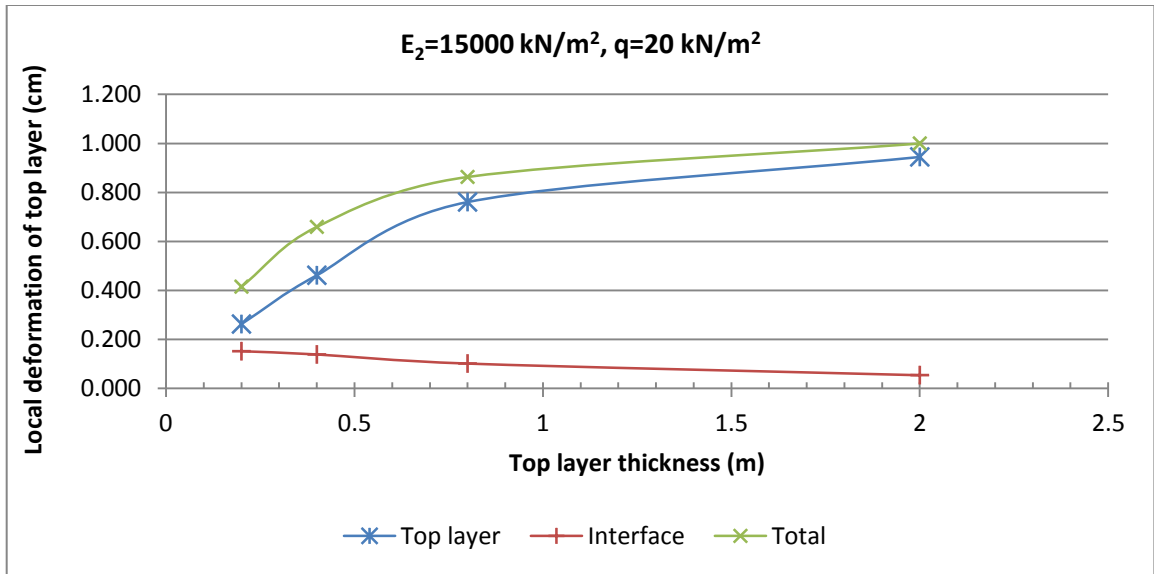
Figure 4.3: Results for increasing top layer thickness (lower layer stiffness of 15000 kN/m^2 and load of 20kN/m^2)
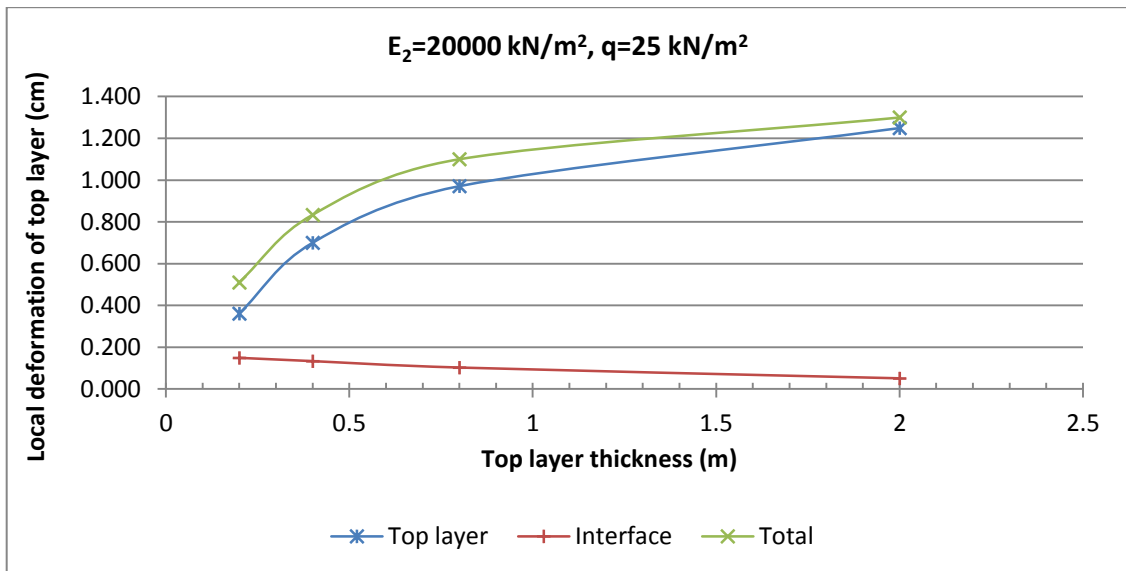

Figure 4.4: Results for increasing top layer thickness (lower layer stiffness of 20000 kN/m^2 and load of 25kN/m^2)
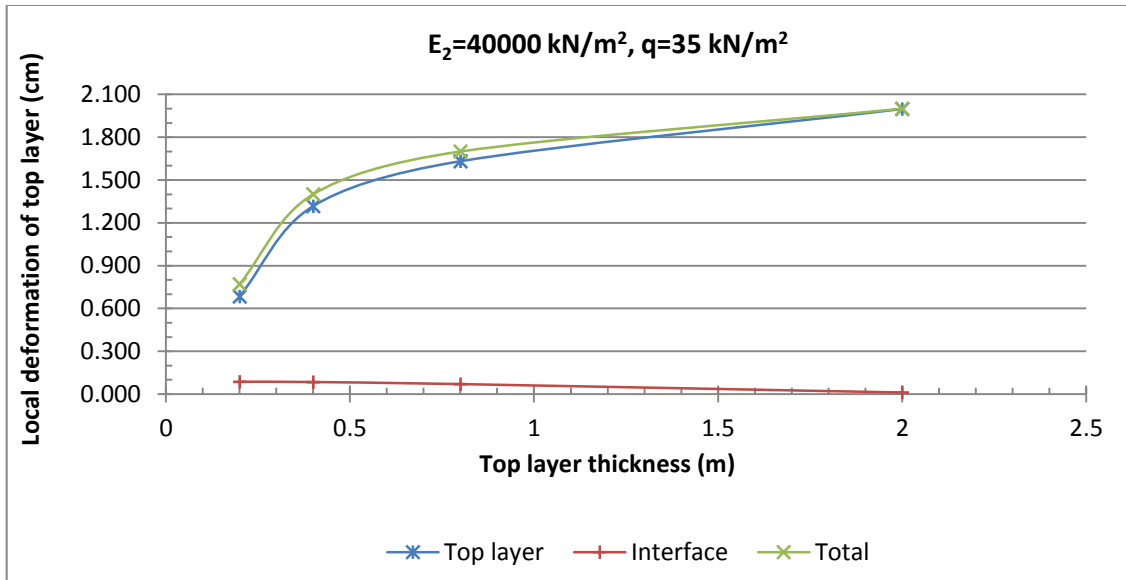
Figure 4.5: Results for increasing top layer thickness (lower layer stiffness of 40000 kN/m^2 and load of 35kN/m^2)

4.5 Effect of Increasing Load and Lower Layer Stiffness Simultaneously

This section shows the results when the top layer thickness is constant and both the load and lower layer stiffness are increased. As it can be seen in figures below (4.6-4.10), as both the load and lower layer stiffness, for specific top layer thickness, are increased then the associated compression is also increased. We can also see from figures that when comparing specific points on each curve the compressions tend to increase as the top layer thickness increases. It is also evident that as the stiffness of lower layer is increasing less compression is seen at the interface. This effect is magnified by incorporating the effect of increase in thickness of the top layer, because as the top layer thickness increases the stresses diminish with depth and thus the interface experiences less compression.
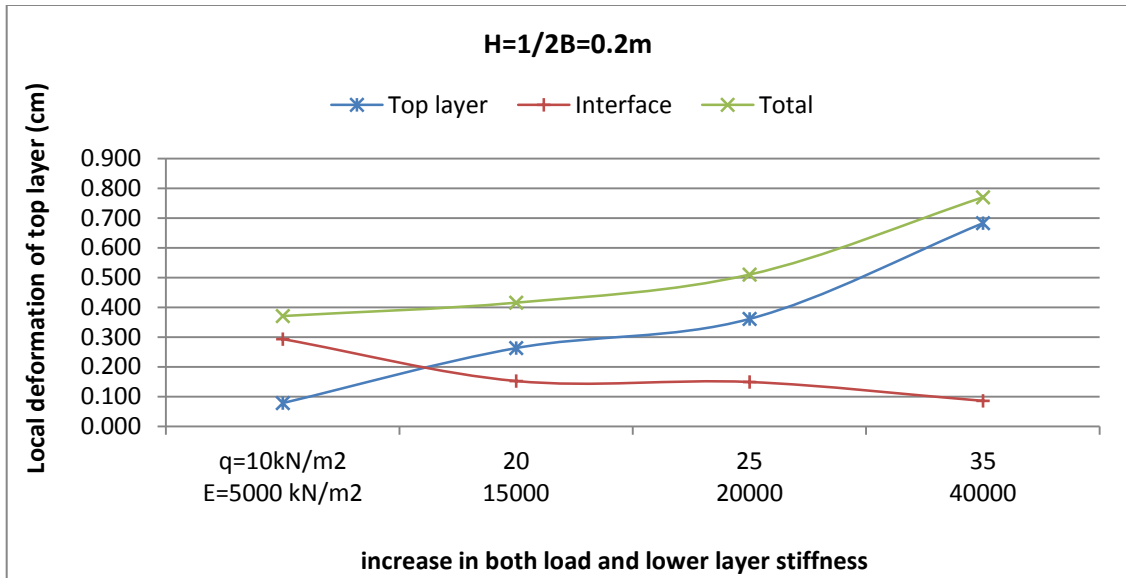
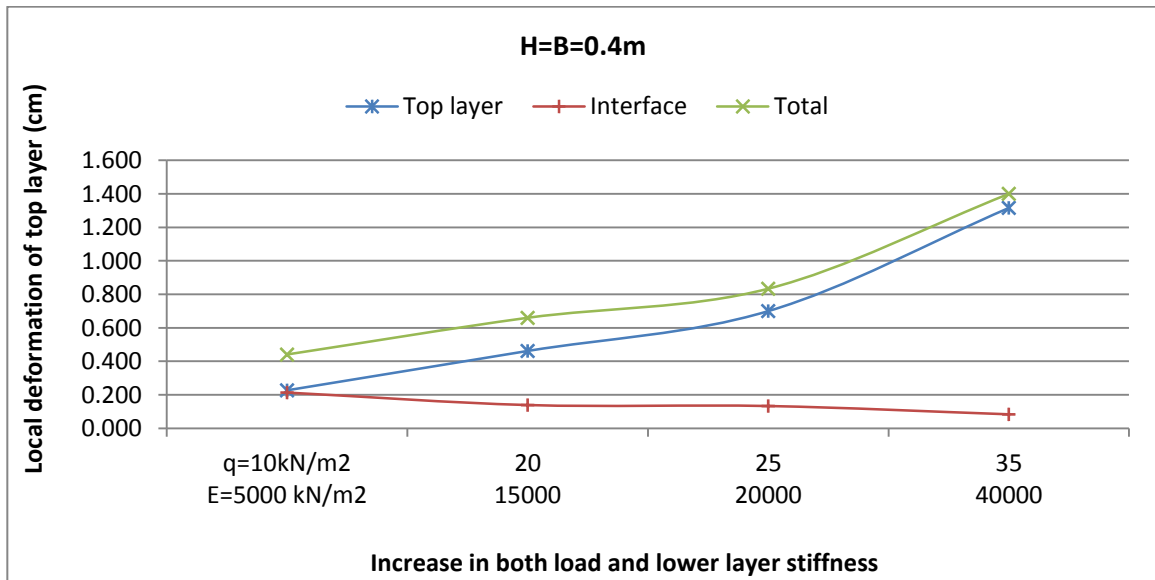Figure 4.6: Results for constant top layer thickness (top layer thickness of 0.2m)

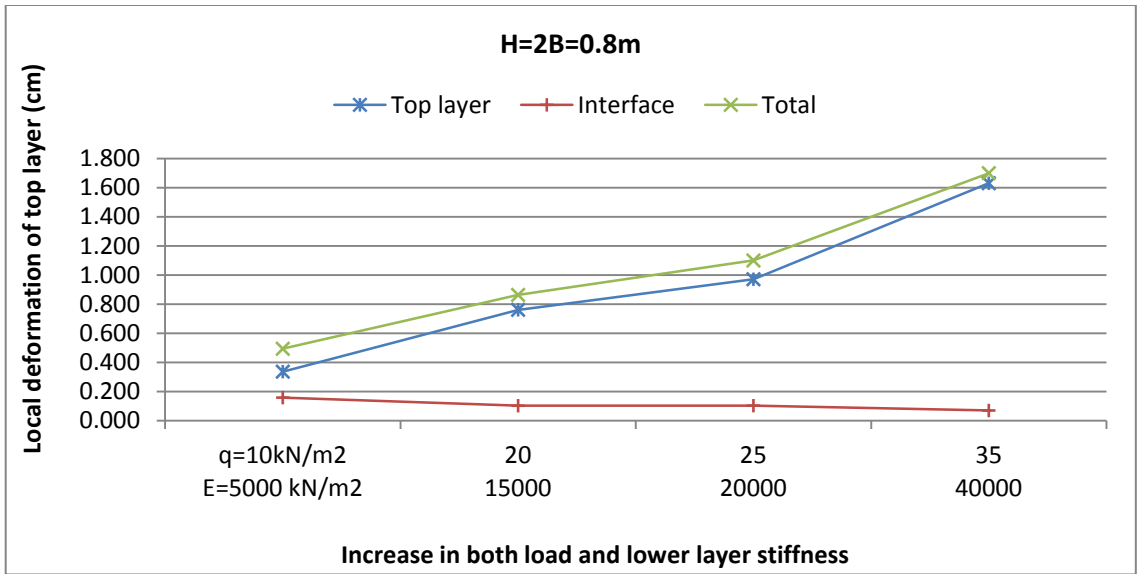Figure 4.7: Results for constant top layer thickness (top layer thickness of 0.4m)

Figure 4.8: Results for constant top layer thickness (top layer thickness of 0.8m)
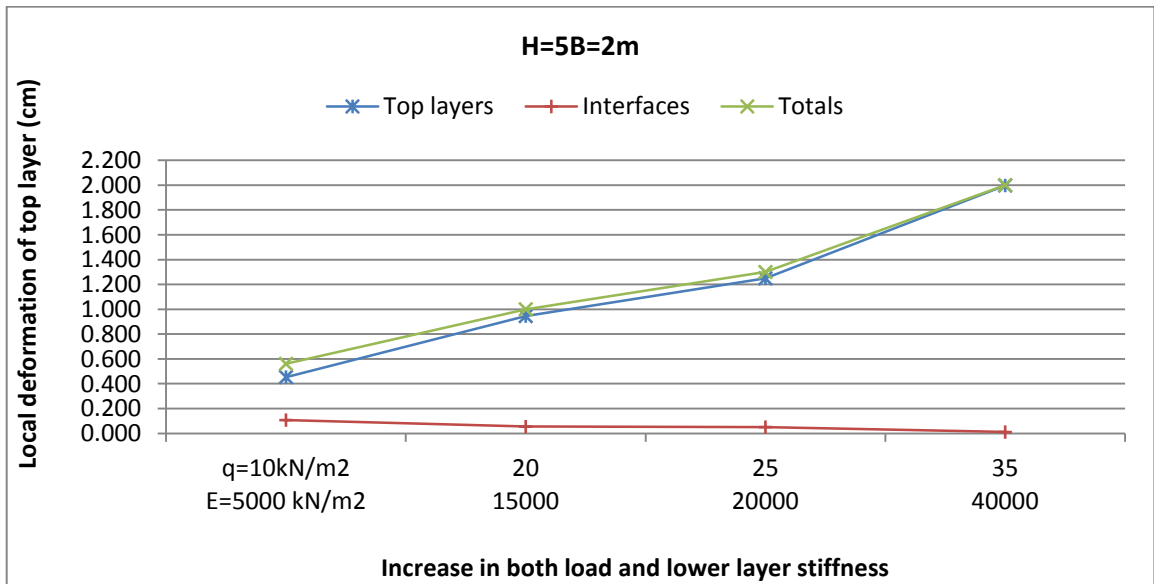
Figure 4.9: Results for constant top layer thickness (top layer thickness of 2m)

4.6 Representation of Increasing Load, Thickness and Lower Layer Stiffness

Figure 4.10 is an illustration of the effects of varying underlying layer stiffness, applied load and top layer thickness all together on the local compression of the top layer

Figure 4.10: representation of compression as top layer thickness, applied load, and lower layer stiffness are increased.

It is marked that compression of top layer is increasing as per increase in top layer thickness for each case. Furthermore it can be noted that for each top layer thickness, the compression of top layer increases as the stiffness of lower layer and the applied load are increased simultaneously.

4.7   Effect of Applied Load

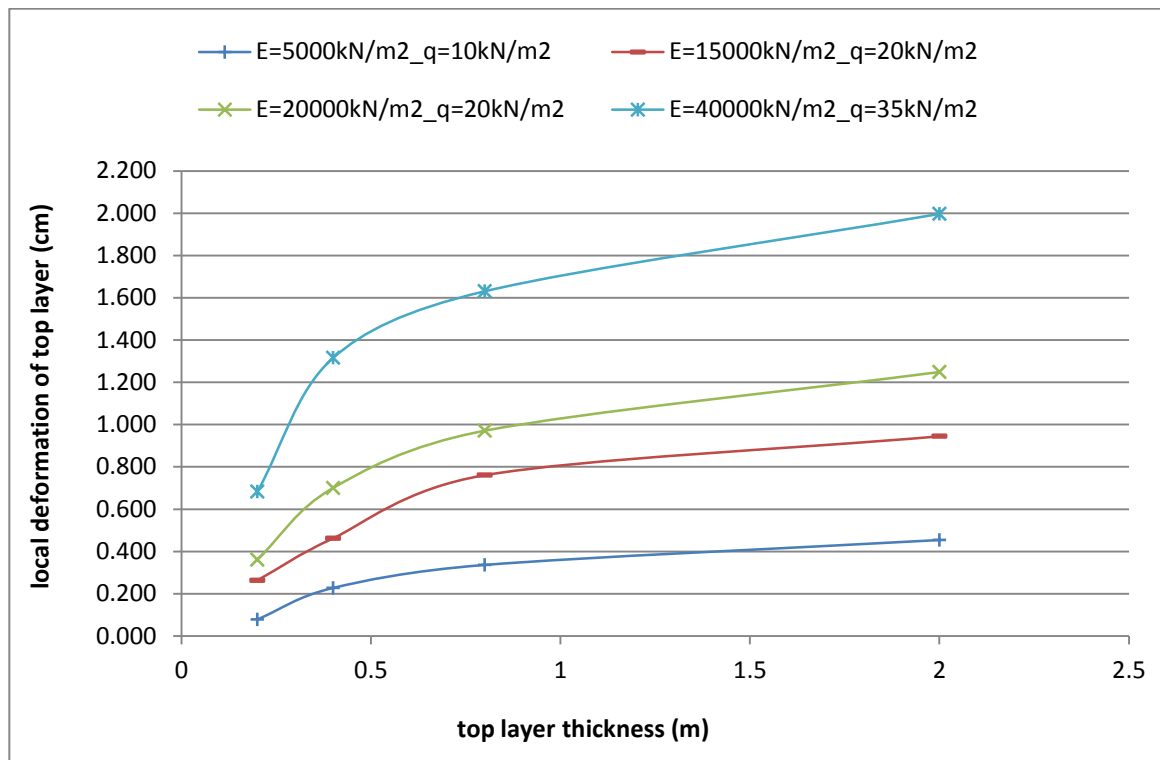The effect of load on the results is presented in the form of curves shown in the following figures. It can be seen that as the load is increased the associated compression is also increased. The effect of each type of loading is shown against increase of both top layer thickness and lower layer stiffness. This is done to show also how would different combinations of top layer thickness together with lower layer stiffness, in an increasing manner, effect the local compression of top layer.

Figures 4.11 to 4.14 show the isolated effect of load increase on the results. The results show an increasing trend of compression for all cases of top layer thickness and lower layer stiffness.

Figure 4.11: Effect of increase in applied load (lower layer stiffness of 5000kN/m^2 and top layer thickness of 0.2m)

Figure 4.12: Effect of increase in applied load (lower layer stiffness of 15000kN/m^2 and top layer thickness of 0.4m)
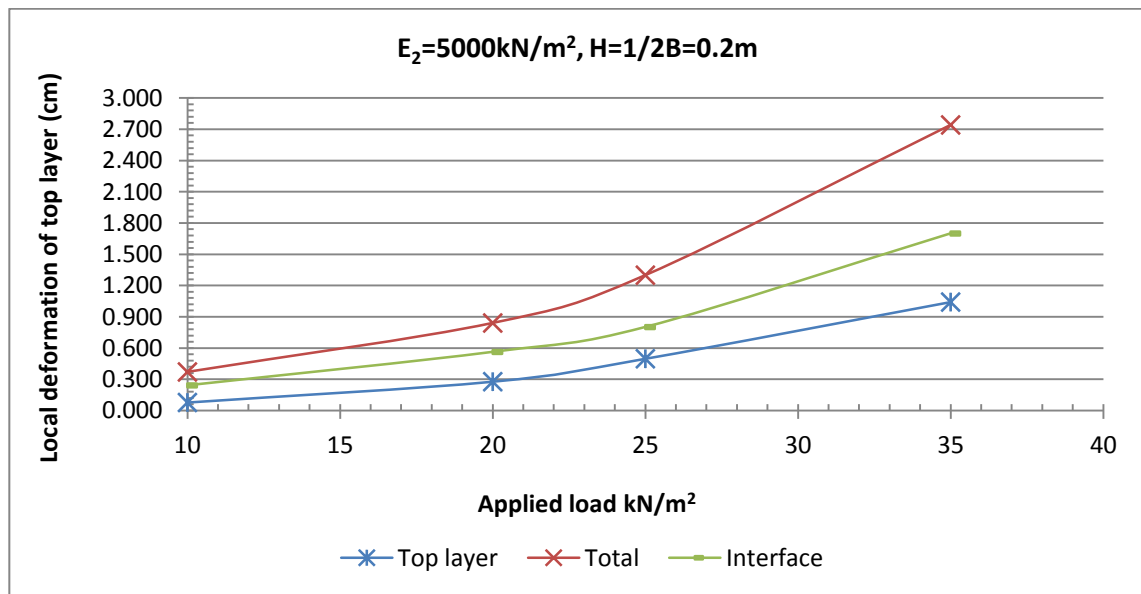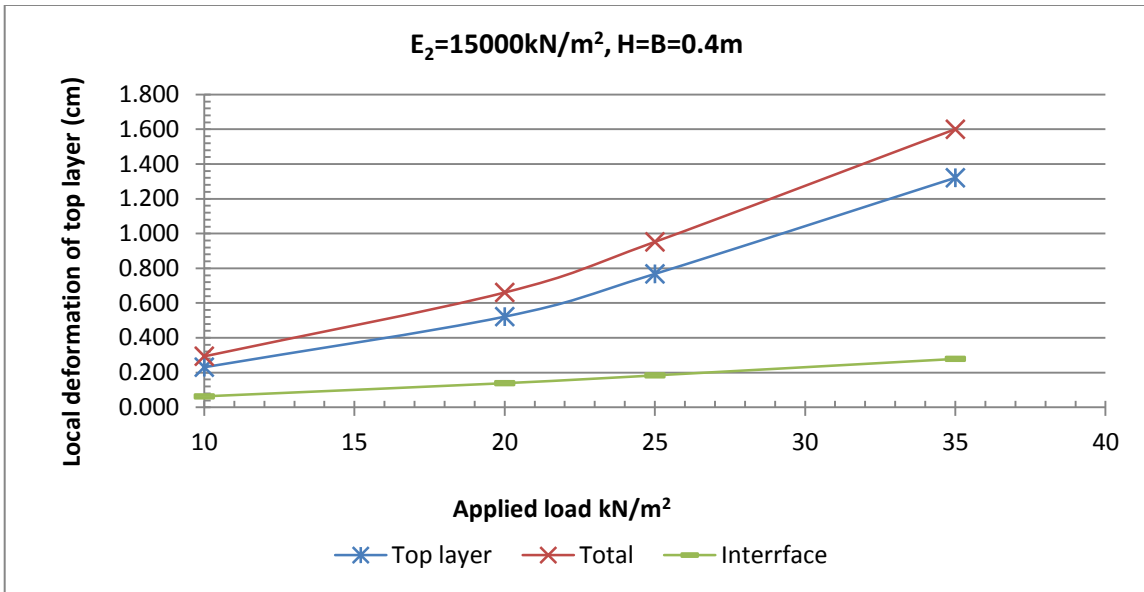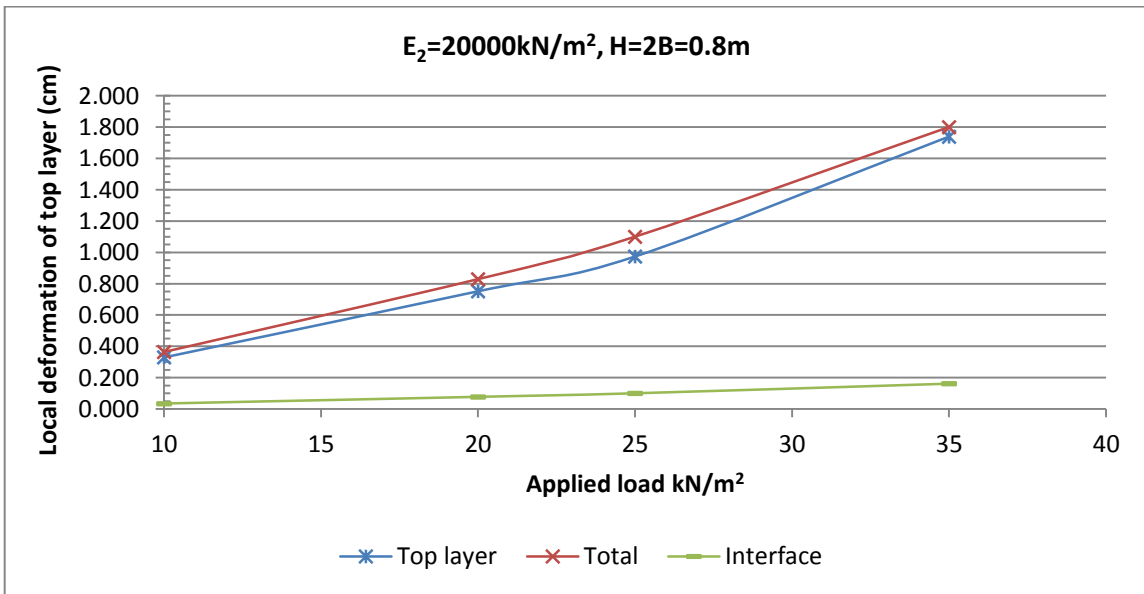

Figure 4.13: Effect of increase in applied load (lower layer stiffness of 20000kN/m^2 and top layer thickness of 0.8m)
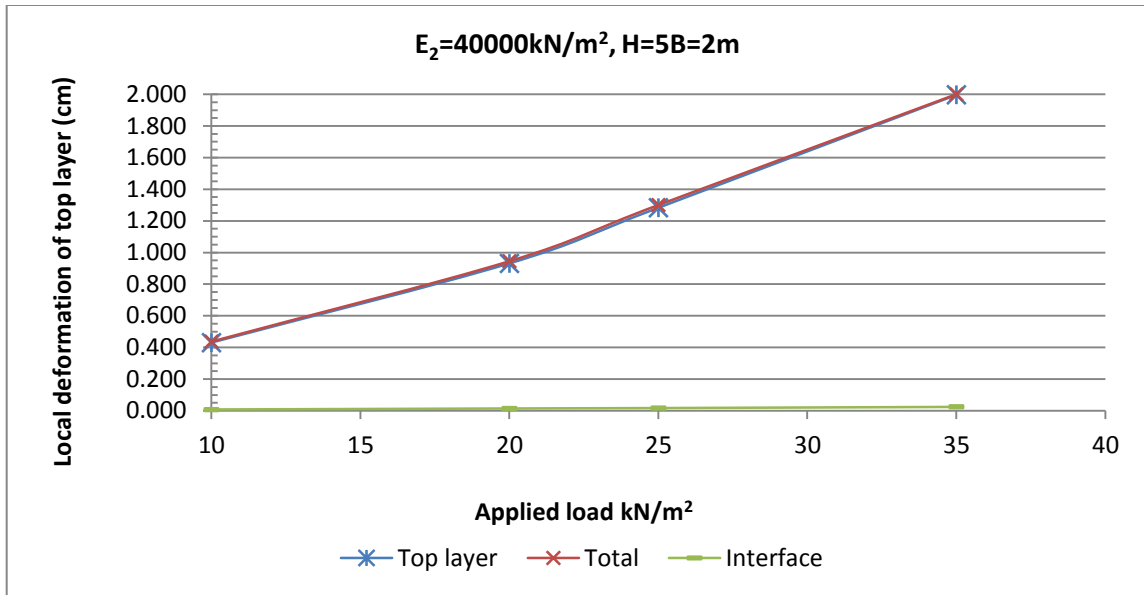
Figure 4.14: Effect of increase in applied load (lower layer stiffness of 40000kN/m^2 and top layer thickness of 2m)

4.8 Effect of Increasing Top Layer Thickness and Lower Layer Stiffness

The following figures 4.15 to 4.18 show for each amount of applied load the effect of increase in both the top layer thickness and lower stiffness simultaneously on the compression of top layer. It can be observed that in all the cases there is a transition phase (from decrease in compaction to increase in compaction) in the total compression rate when the top layer thickness, and lower layer stiffness reach beyond 0.4m and 15000 kN/m^2, respectively. As it can be seen at the beginning of the curve the lower layer stiffness is well below the stiffness of top layer, and the top layer thickness is shallow enough to let the stresses penetrate to the lower layer and hence having more compression than the next point where the lower layer stiffness and top layer thickness have both increased. This trend can be seen with all the loading applications, and its intensity increases as the load increases.
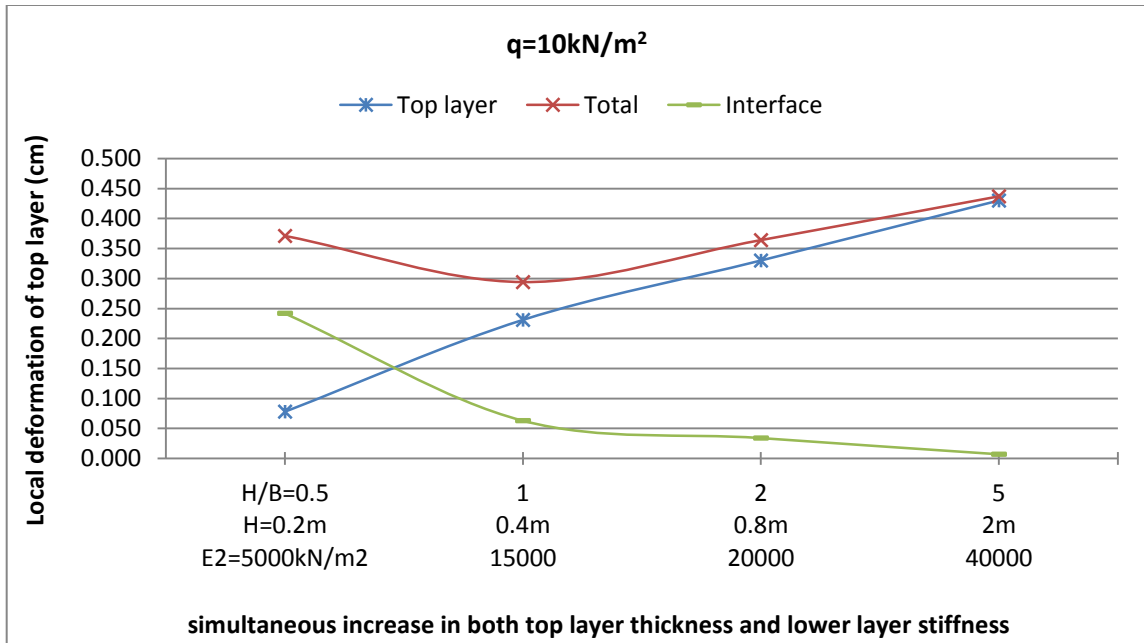
Figure 4.15: Compression against increase of top layer thickness and lower layer stiffness (applied laod of 10kN/m^2)
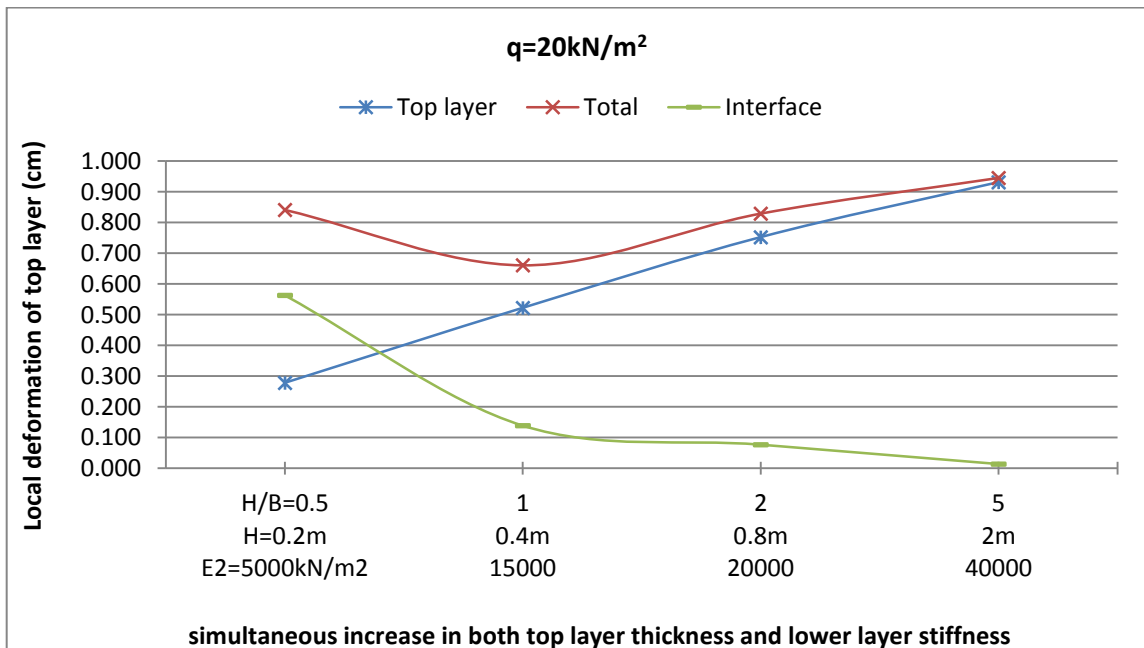
Figure 4.16: Compression against increase of top layer thickness and lower layer stiffness (applied load of 20kN/m^2)
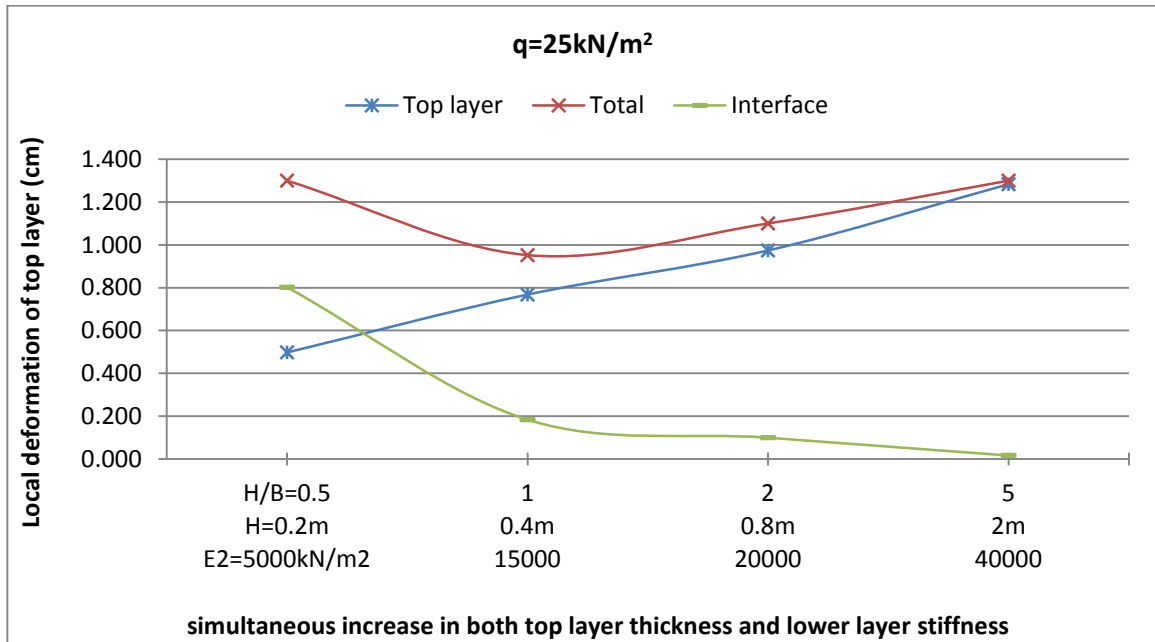
Figure 4.17: Compression against increase of top layer thickness and lower layer stiffness (applied load of 25kN/m^2)
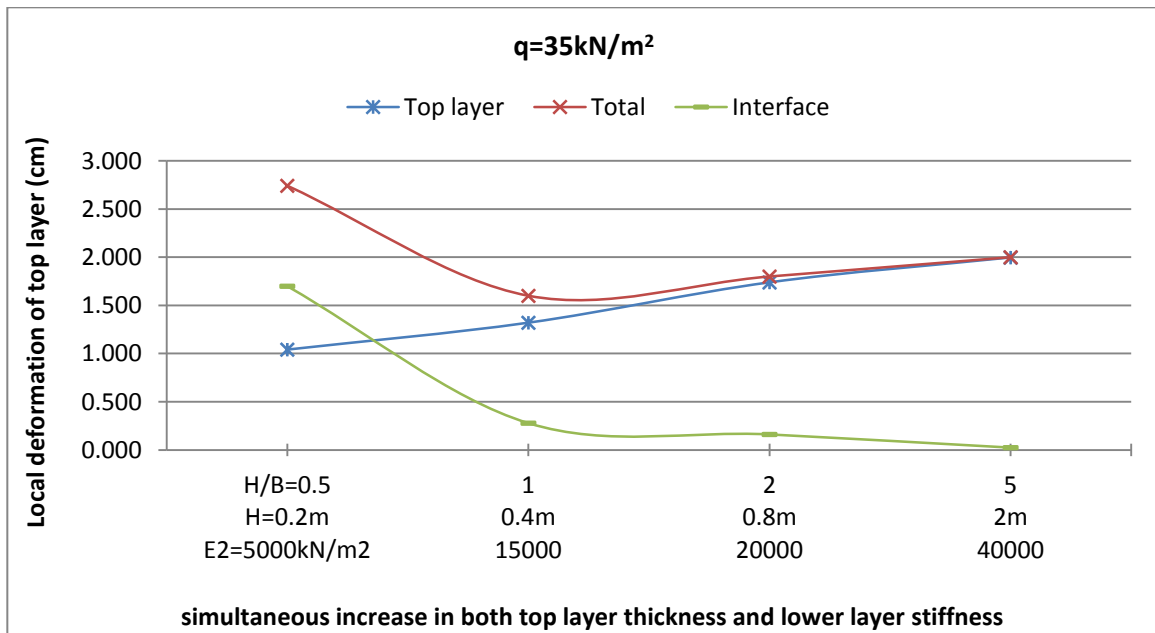
Figure 4.18: Compression against increase of top layer thickness and lower layer stiffness (applied load of 35kN/m^2)

4.9 Increasing Load for Different Thickness and Lower Layer Stiffness

Following figure 4.19 shows the trend of results for each case (with different top layer thickness and lower layer stiffness) for increasing applied load. It can be seen that as the load is increased so does the compression of the top layer, and as the top layer thickness and lower layer stiffness are both increased the compression is also increased.
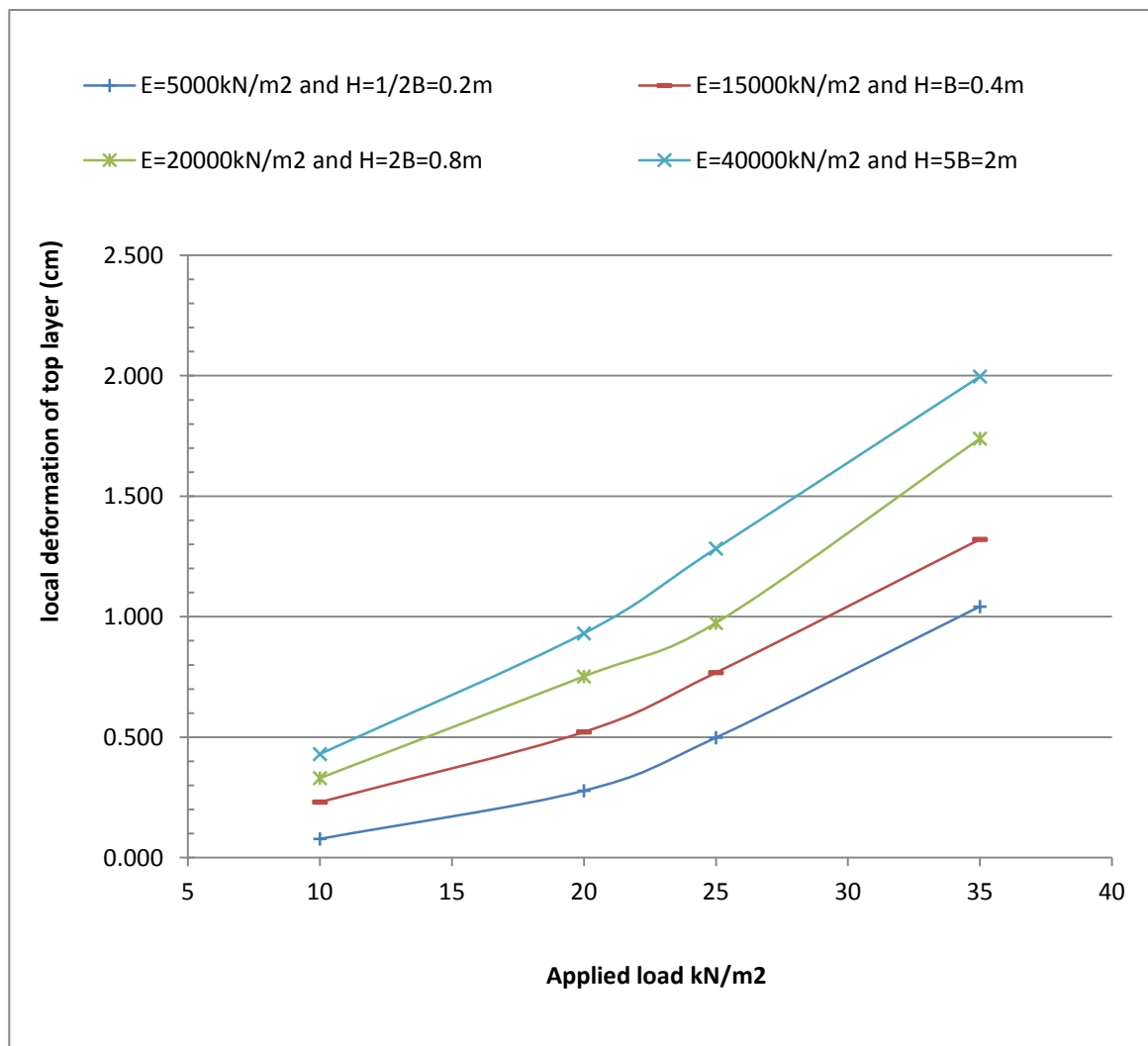
Figure 4.19: Increasing Load for Different Thickness and Lower Layer Stiffness

4.10 Effect of Number of Load Cycles

The following figures 4.20-4.23 illustrate the influence of load cycles on the compression characteristics of different cases. In some cases it is clearly evident that the top layer is reaching equilibrium after certain number of load cycles. The general trend is that the soil keeps on compressing with a rate which decreases by increase in load cycles. This is because of the nature of the granular soils where they get denser after each application of load and thus they become more reluctant towards further compression. And this behavior is represented by the Hardening Soil constitutive model in Plaxis.
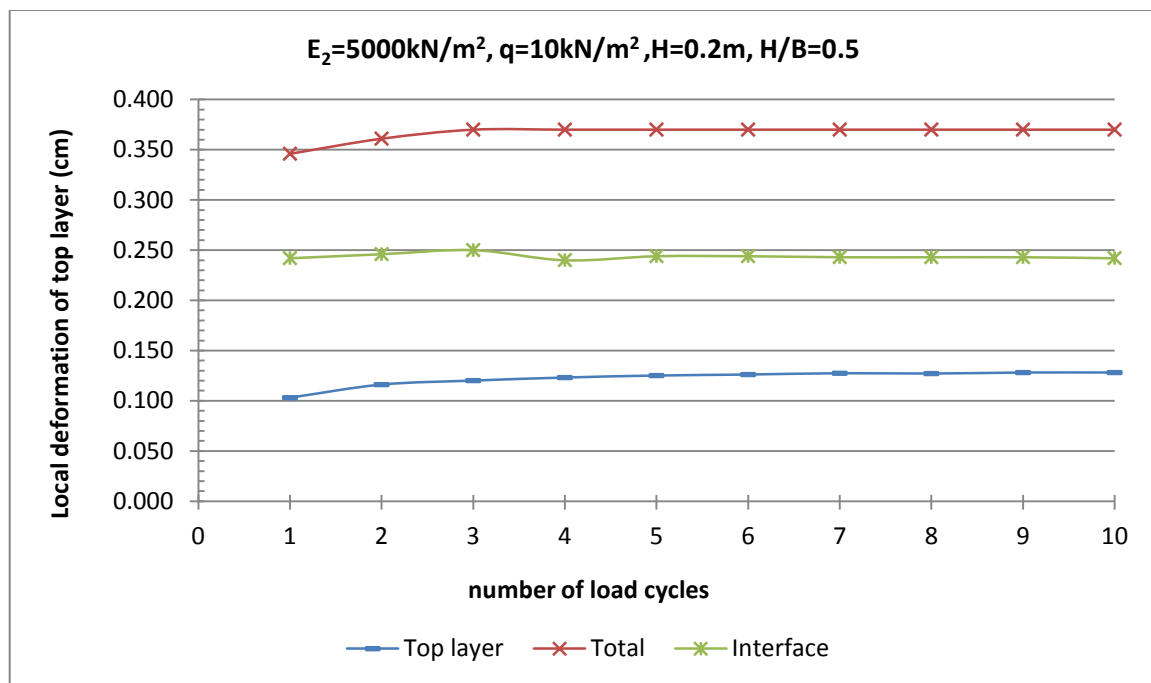
Figure 4.20: Compression against load cycles (lower layer stiffness of 5000kN/m^2, applied load of 10kN/m^2, top layer thickness of 0.2m)
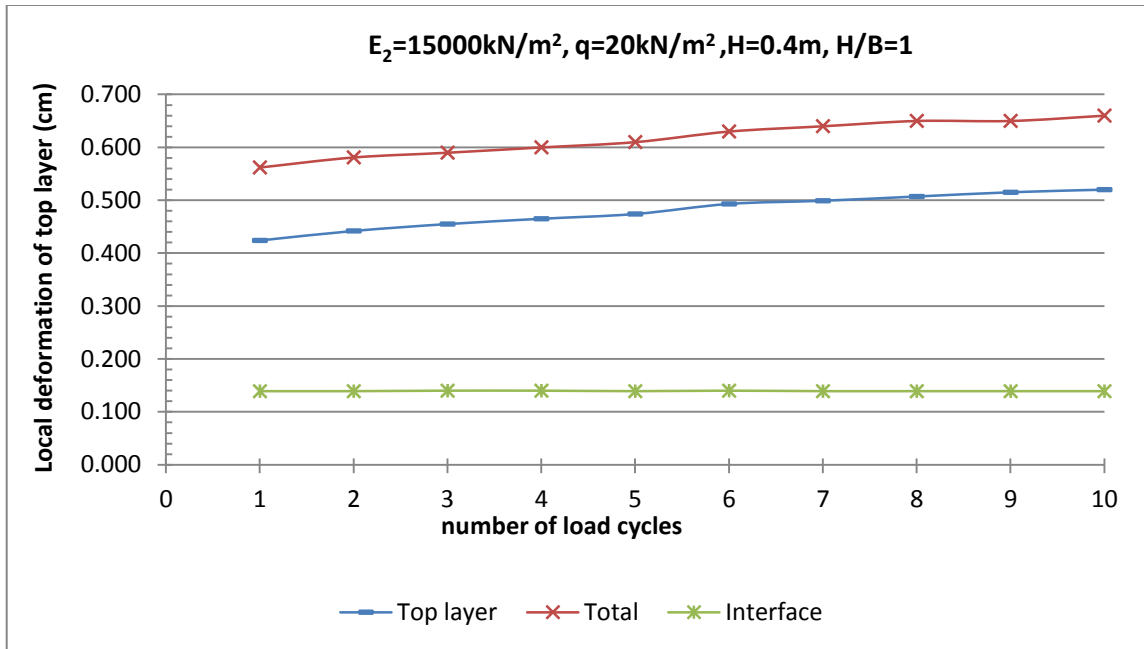
Figure 4.21: Compression against load cycles (lower layer stiffness of 15000kN/m^2, applied load of 20kN/m^2, top layer thickness of 0.4m)
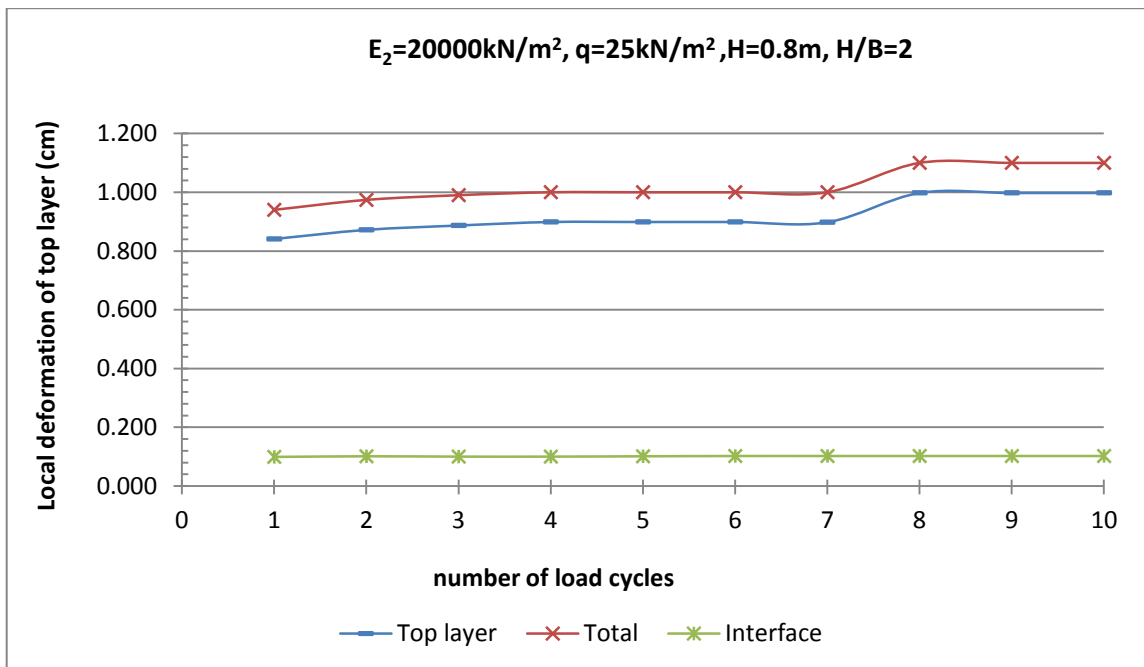
Figure 4.22: Compression against load cycles (lower layer stiffness of 20000kN/m^2, applied load of 25kN/m^2, top layer thickness of 0.8m)
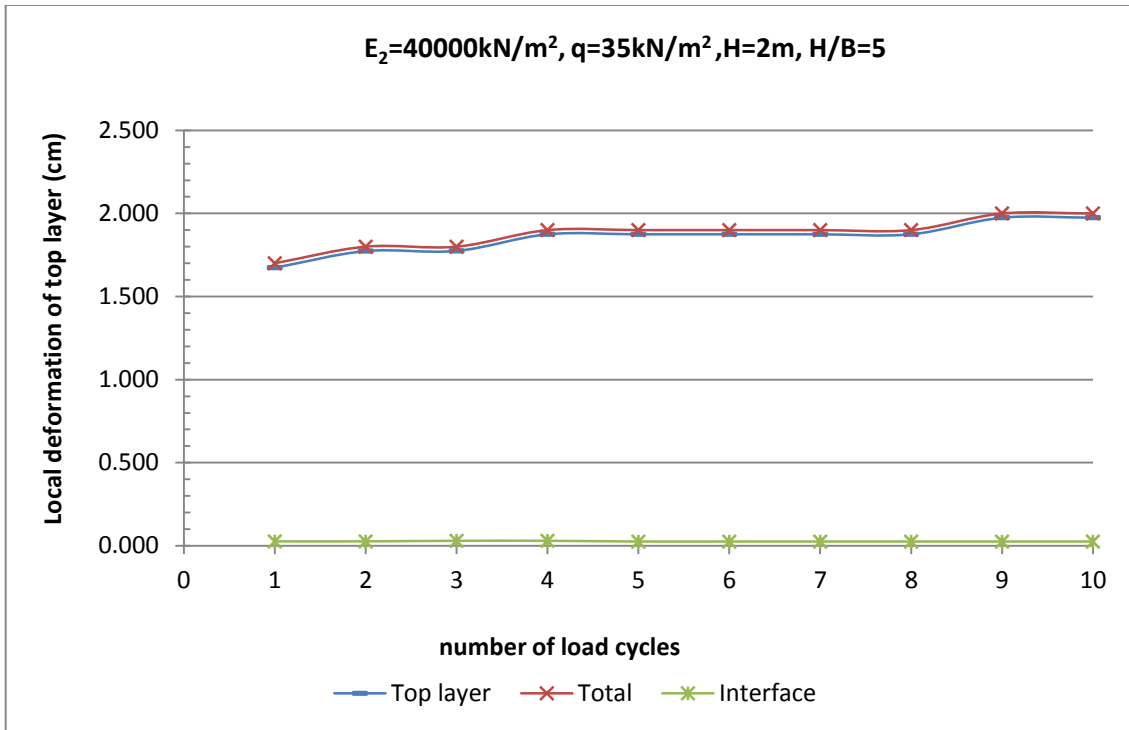
Figure 4.23: Compression against load cycles (lower layer stiffness of 40000kN/m^2, applied load of 35kN/m^2, top layer thickness of 2m)

4.11 Effect of Underlying Layer

Following figures 4.24-4.27 illustrate the influence of underlying layer, as they get stronger, on the behavior of the system. In these figures the total compression, compression at interface and consequently the local compression of top layer are shown. It can be seen from the curves that as the lower layer is getting stronger its compression is decreasing, and thus more energy is gained by the top layer achieving more compaction. This can be seen from the space between line of Top layer and Interface getting more and more, which is an indication of less waste of energy to lower layer.
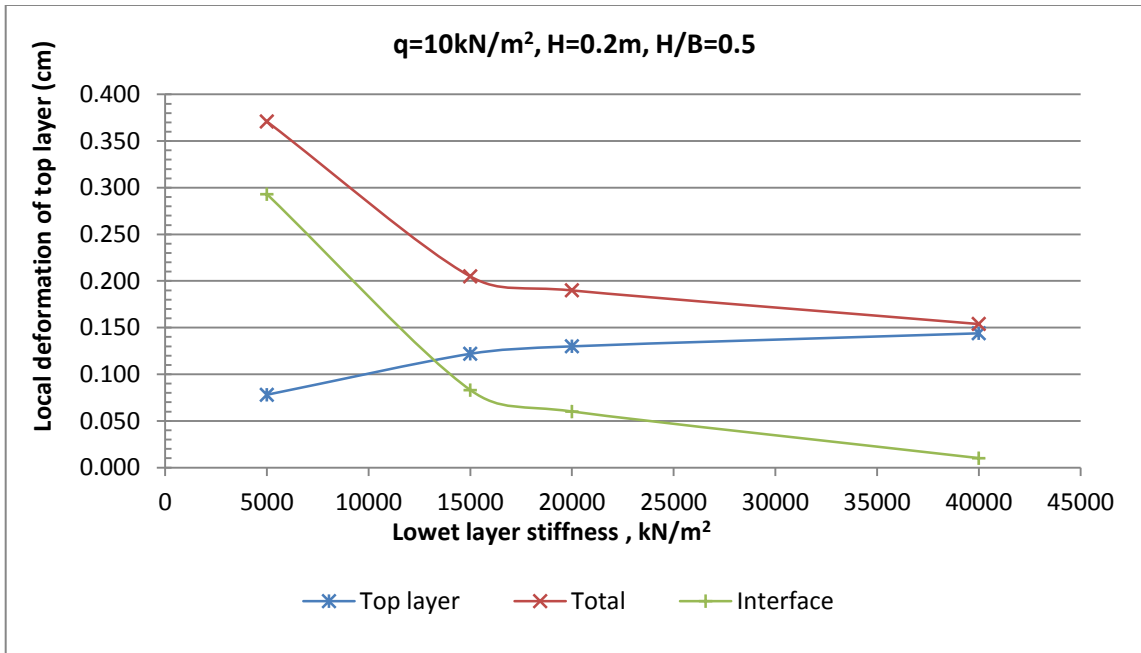
Figure 4.24: Compression against variation of lower layer stiffness (applied load of 10kN/m^2 and top layer thickness of 0.2m)
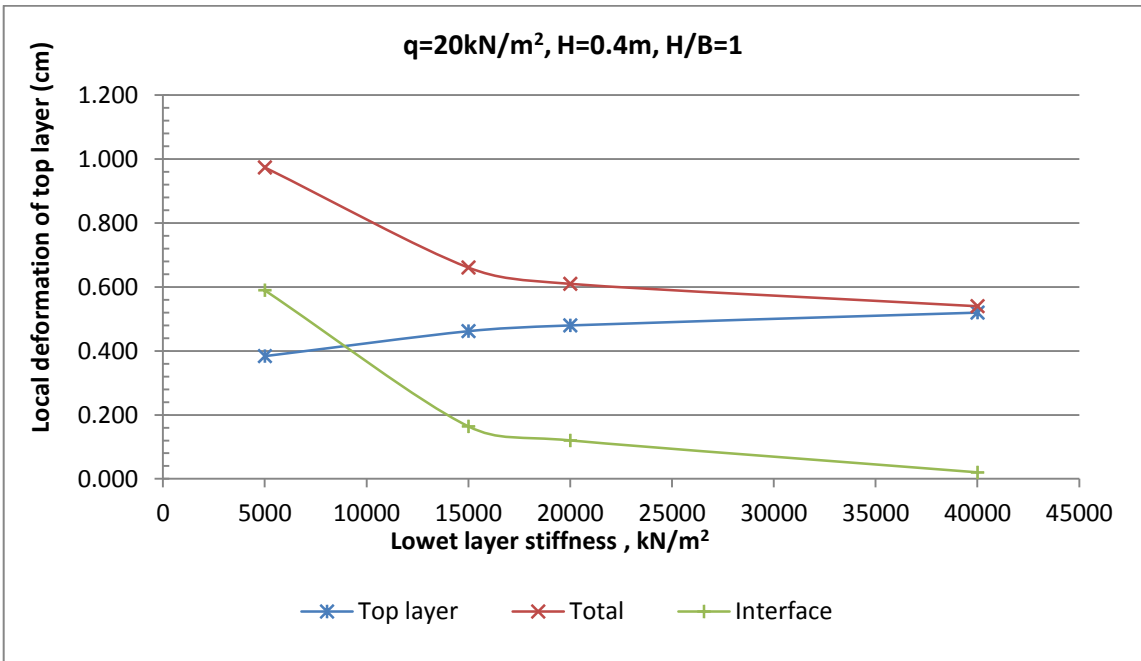
Figure 4.25: Compression against variation of lower layer stiffness (applied load of 20kN/m^2 and top layer thickness of 0.4m)
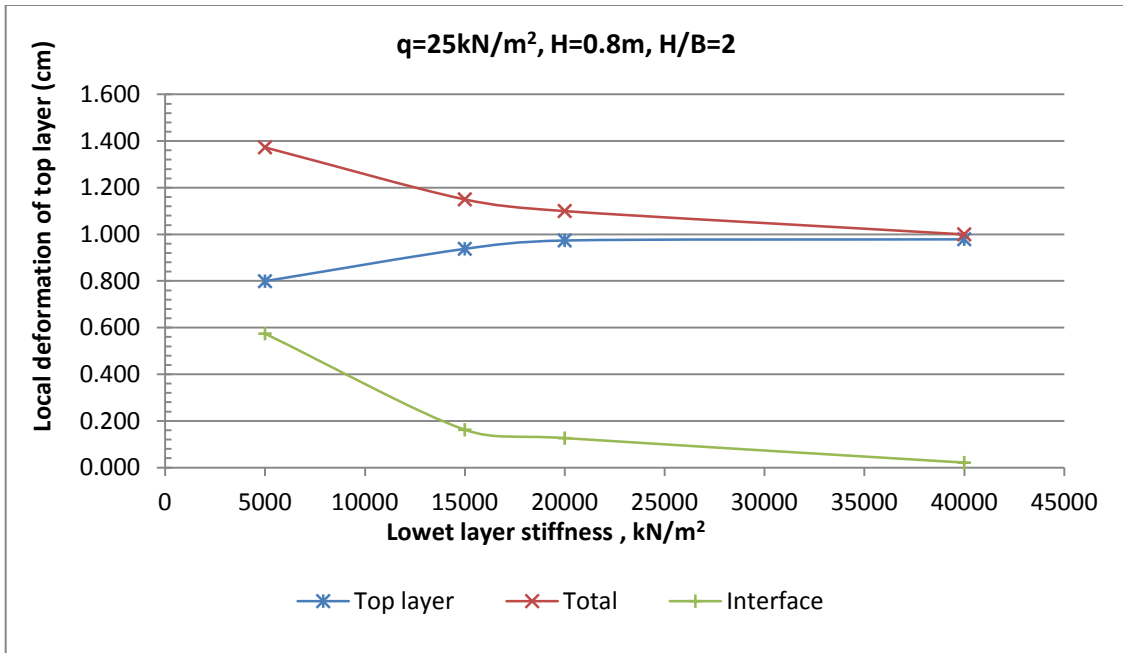
Figure 4.26: Compression against variation of lower layer stiffness (applied load of 25kN/m^2 and top layer thickness of 0.8m)
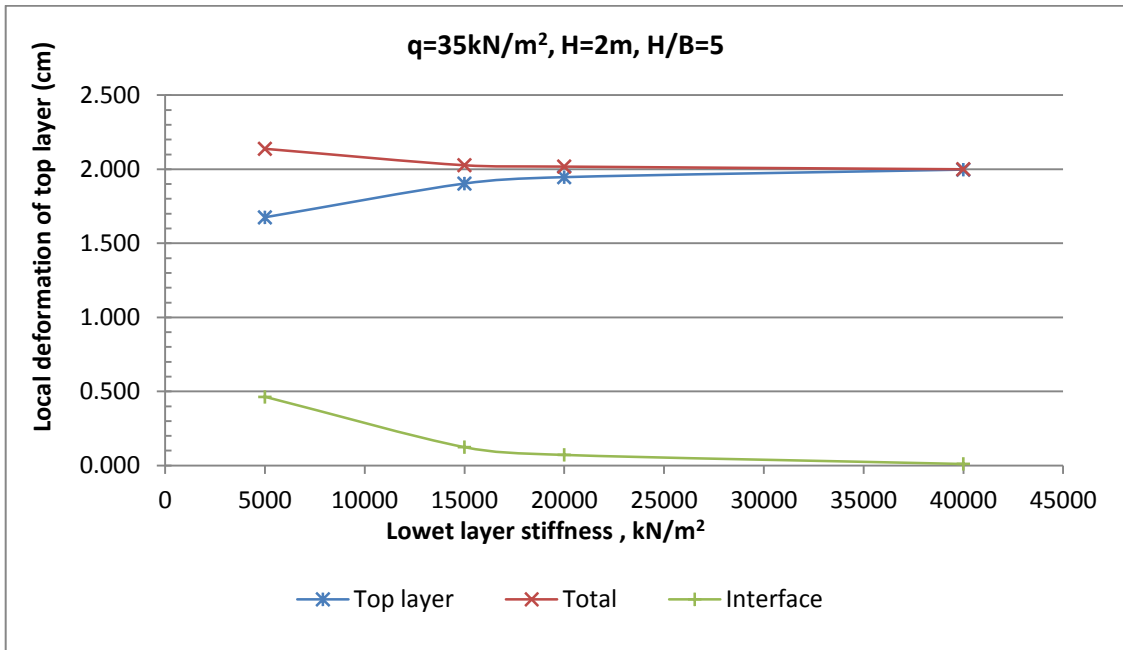
Figure 4.27: Compression against variation of lower layer stiffness (applied load of 35kN/m^2 and top layer thickness of 2m)

4.12 Effect of Increasing Load and Top Layer Thickness Simultaneously for Different Lower Layers

The following figures 4.28-4.31 represent the effect of lower layer stiffness on the behavior of the system. In each figure the total compression, compression at interface and local compression of top layer are shown. In each curve the lower layer stiffness is constant and the top layer thickness and the applied load are increased simultaneously. As the lower layer stiffness is increased we can see that the space between line of total compression and local compression of top layer is decreasing, indicating that the more the lower layer is resistive to compression the more compaction is attributed to the top layer only.
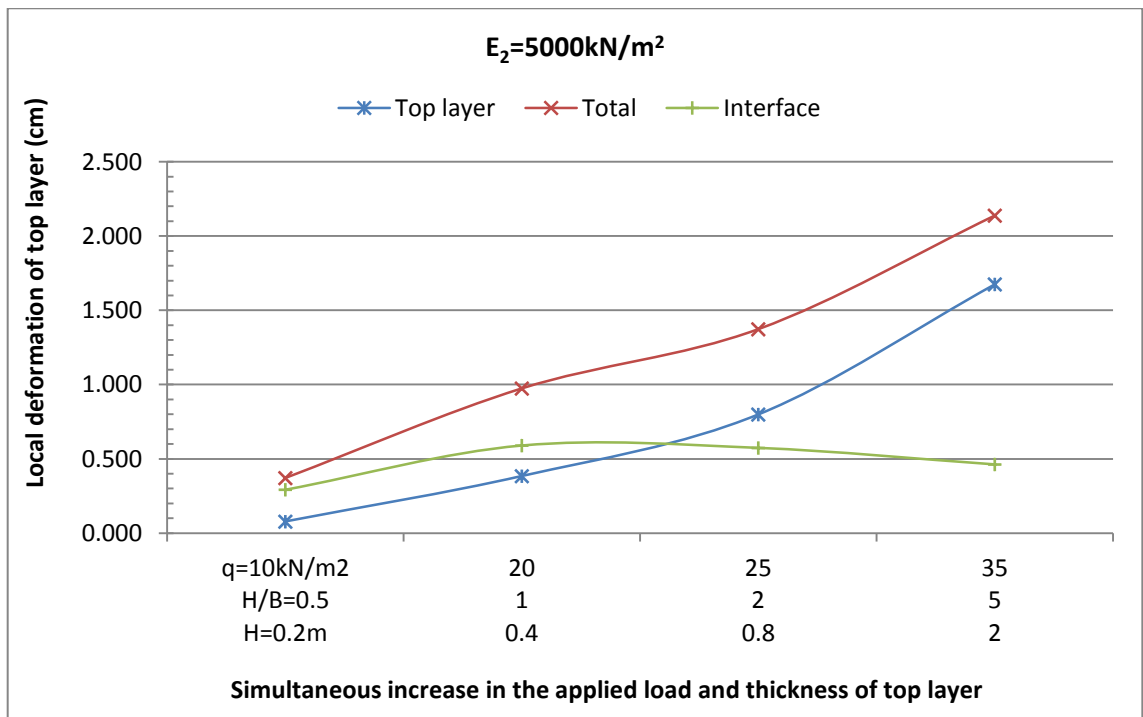
Figure 4.28: Compression against increase of applied load and top layer thickness (lower layer stiffness of 5000kN/m^2)
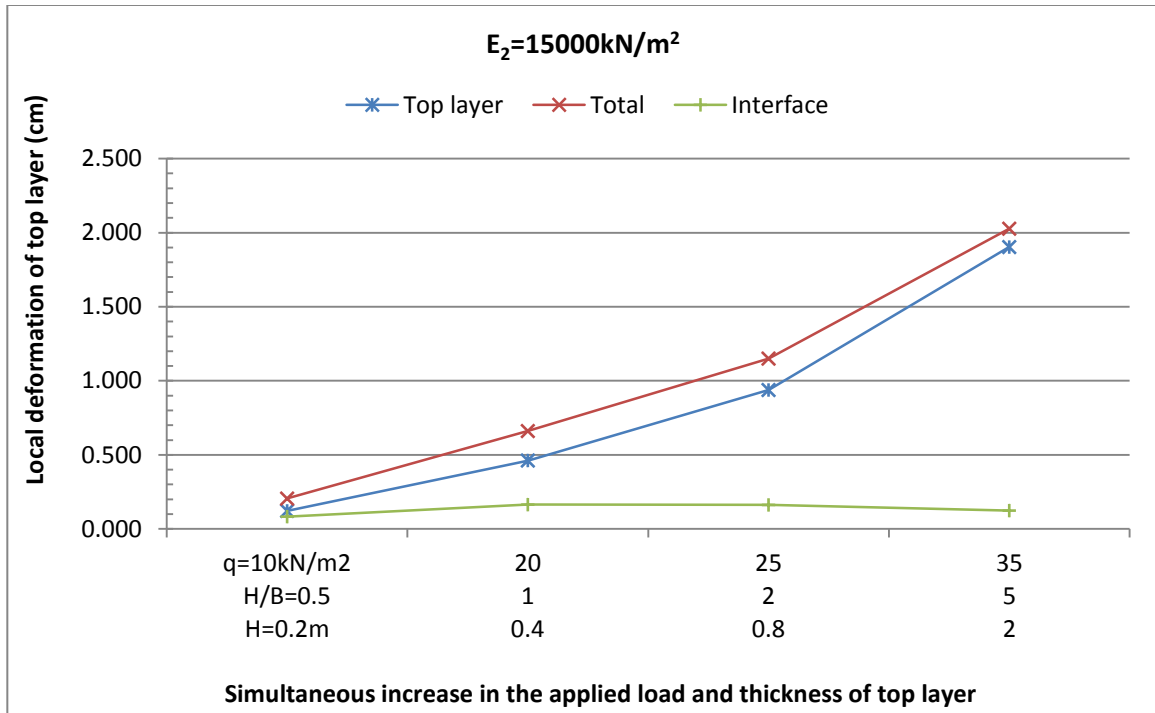
Figure 4.29: Compression against increase of applied load and top layer thickness (lower layer stiffness of 15000kN/m^2)
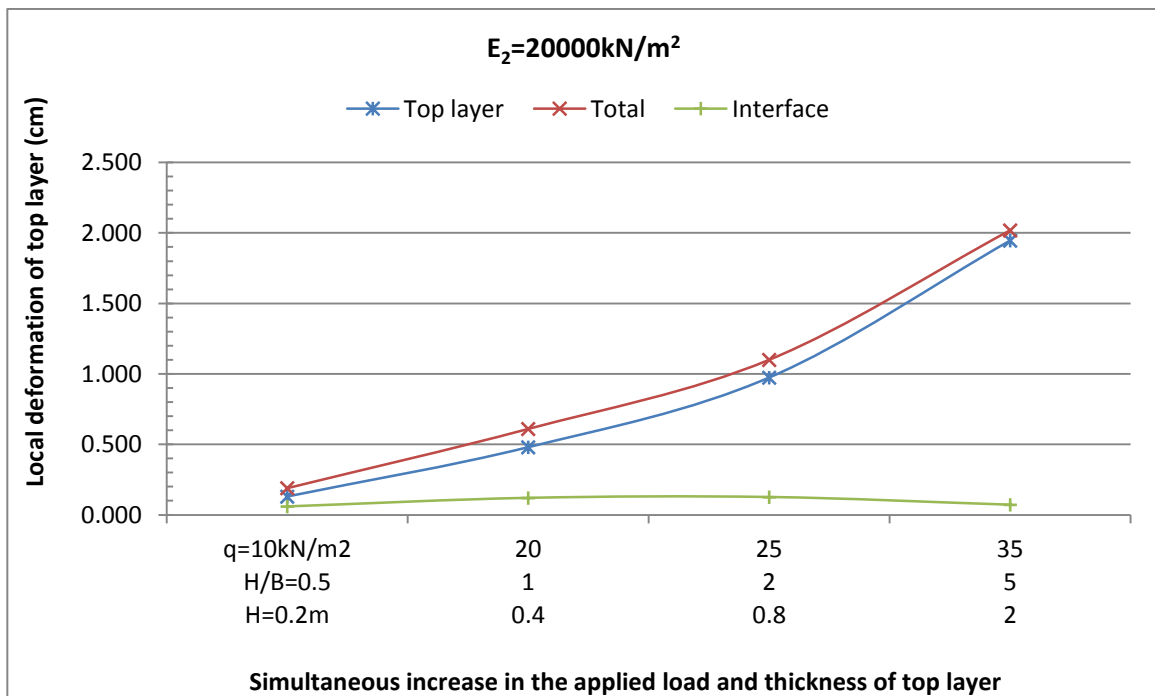
Figure 4.30: Compression against increase of applied load and top layer thickness (lower layer stiffness of 20000kN/m^2)
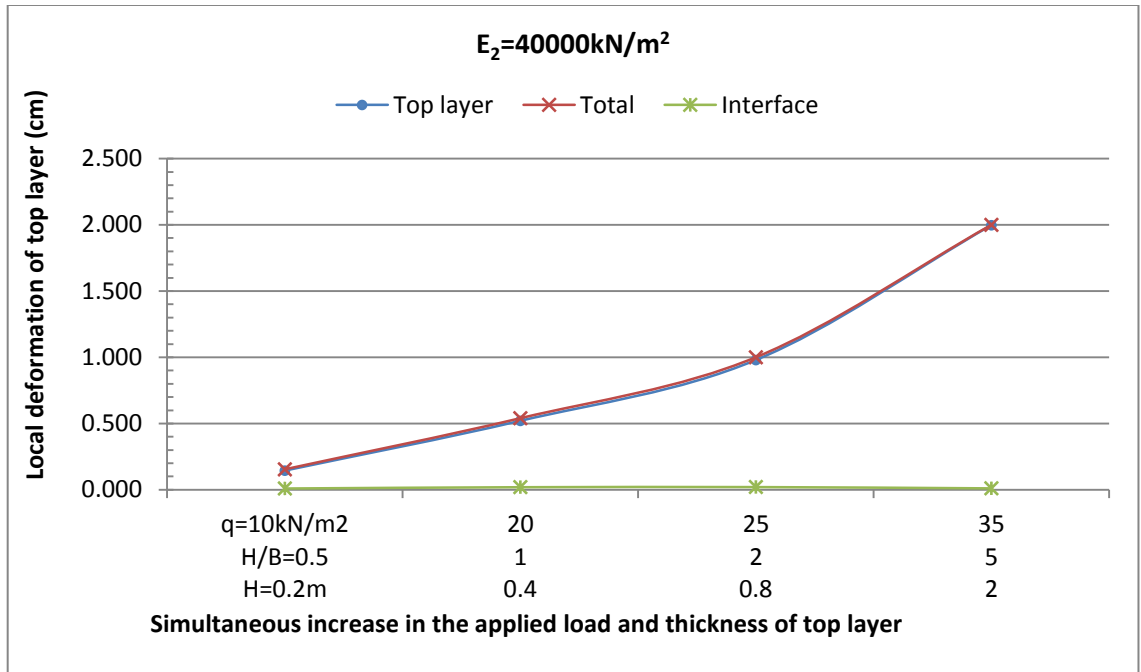
Figure 4.31: Compression against increase of applied load and top layer thickness (lower layer stiffness of 40000kN/m^2)

4.13 Increasing stiffness of lower layer for Different Thickness and applied load

Following figure 4.32 shows the trend of results for each case (with different top layer thickness and applied load) for increasing stiffness of lower layer. It can be seen that as the stiffness is increased so does the compression of the top layer, and as the top layer thickness and load are both increased simultaneously, for a constant lower layer stiffness, the compression of top layer is increased. This is because when the thickness is more than the applied load is locked-in more comparing to when the thickness is shallow causing the load to penetrate to the lower layer and resulting in lost in compaction.
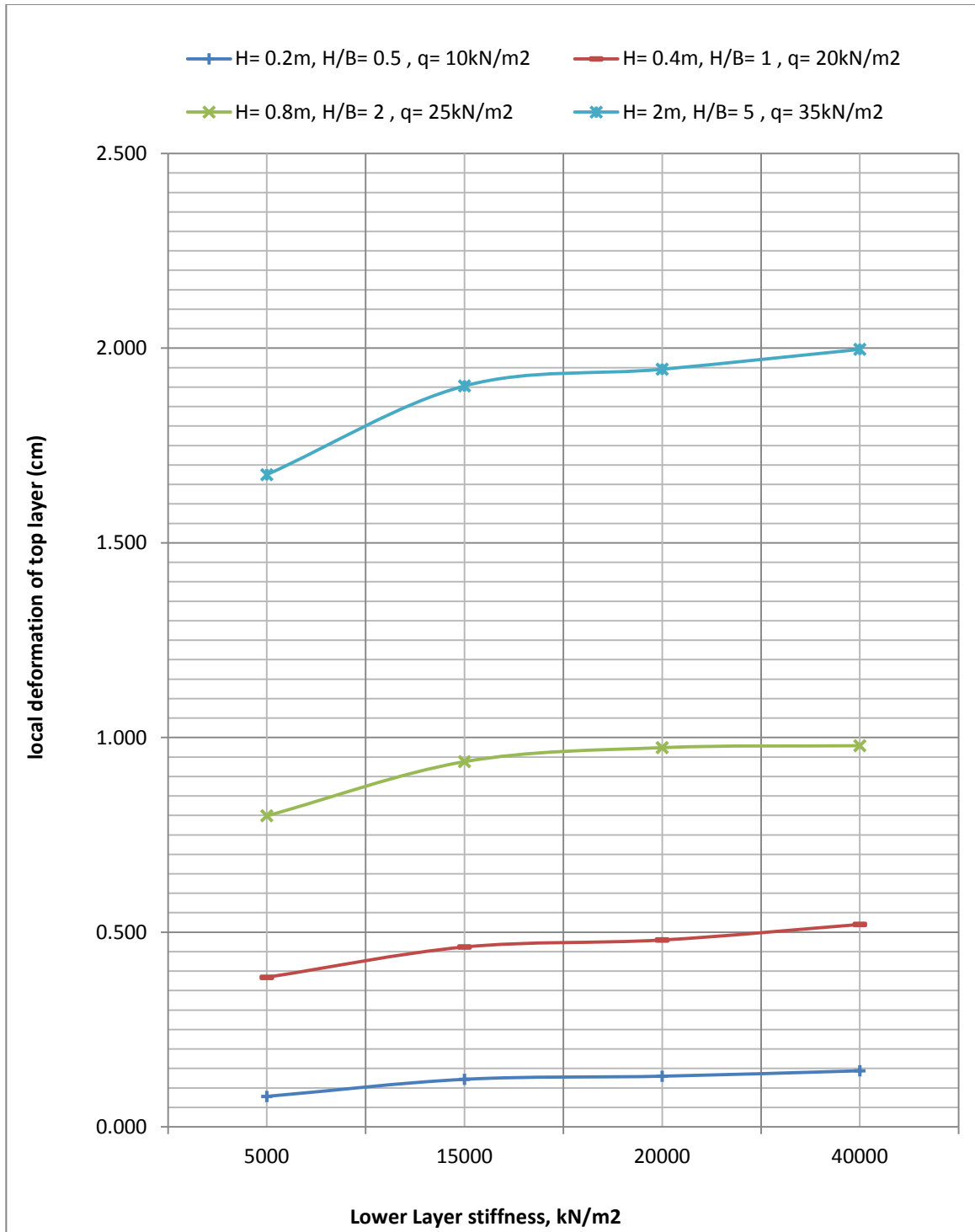
Figure 4.32: Increasing Stiffness of lower layer for Different Thickness and applied load

4.14 Analysis of Test Results

Two trends can be observed by looking at figures plotted with the resulting data of cases with upper layer thickness ranging from 0.2 to 5 m. First, from figures 4.2-4.18 it is observed that as the top layer thickness and applied load increases its associated compression increases, and therefore its compaction increases. Second, it can be seen from figures 4.24-4.32 that the compaction of the top layer increases with increasing of the stiffness of the lower layer. Since it is the subject of this research to see whether or not the lower layer has any influence on the compaction of top layer, it is necessary to determine the actual compression of the top layer, presented in tables 4.1-4.4. The compressions of the top layer in different cases are tabulated in tables 4.5 to 4.7.

Table 4.5: Present test results for varying top layer thickness for different lower layer stiffness and load combinations

H/B	H(m)	layer	E=5000 kN/m^2	15000	20000	40000
			q=10kN/m^2	20	25	35
0.5	0.2	Total	0.371	0.416	0.510	0.770
		Interface	0.242	0.152	0.149	0.086
		Top	0.078	0.263	0.361	0.683
1	0.4	Total	0.440	0.660	0.833	1.400
		Interface	0.214	0.139	0.133	0.084
		Top	0.227	0.522	0.700	1.316
2	0.8	Total	0.493	0.863	1.100	1.700
		Interface	0.158	0.102	0.102	0.069
		Top	0.336	0.761	0.974	1.631
5	2.0	Total	0.561	1.000	1.300	2.000
		Interface	0.107	0.055	0.051	0.011
		Top	0.454	0.945	1.249	1.997

Table 4.6: Present test results for varying load for different lower layer stiffness and top layer thickness combinations

Applied load (kN/m^2)	layer	E$_2$=5000kN/m^2	15000	20000	40000
		H=0.2m	0.4m	0.8m	2m
		H/B=0.5	1	2	5
10	Total	0.371	0.294	0.364	0.437
	Interface	0.242	0.063	0.034	0.007
	Top	0.078	0.231	0.330	0.430
20	Total	0.841	0.661	0.829	0.945
	Interface	0.563	0.139	0.077	0.014
	Top	0.278	0.522	0.752	0.931
25	Total	1.300	0.952	1.100	1.300
	Interface	0.802	0.184	0.100	0.017
	Top	0.498	0.768	0.974	1.283
35	Total	2.742	1.600	1.900	2.000
	Interface	1.700	0.279	0.162	0.025
	Top	1.042	1.321	1.739	1.997

Table 4.7: Present test results for varying lower layer stiffness for different top layer thickness and load combinations

lower layer stiffness (kN/m^2)	layer	H=0.2m	0.4	0.8	2
		H/B=0.5	1	2	5
		q=10kN/m^2	20	25	35
5000	Total	0.371	0.974	1.373	2.138
	Interface	0.293	0.590	0.574	0.463
	Top layer	0.078	0.384	0.799	1.675
15000	Total	0.205	0.661	1.150	2.027
	Interface	0.083	0.164	0.162	0.124
	Top layer	0.122	0.462	0.938	1.903
20000	Total	0.190	0.610	1.100	2.018
	Interface	0.060	0.120	0.126	0.072
	Top layer	0.130	0.480	0.974	1.946
40000	Total	0.154	0.540	1.000	2.000
	Interface	0.010	0.020	0.021	0.011
	Top layer	0.144	0.520	0.979	1.997

In order to obtain meaningful percentage differences, it is necessary to simulate a case with single homogenous layer subjected to same amount of loads with same width of load. And the soil material would have to be the same as that of the top layer in other Plaxis simulations, which are modeled with Hardening Soil model and are cohesionless granular soil, namely sand. The geometry of this homogenous model is 25m in width and depth, and its results are summarized in the table 4.8 below:

Table 4.8: Compression results of homogenous case subjected to similar loads.

Load (kN/m2)	Compression (cm)
10	0.5622
20	1.3
25	1.7
35	2.8

It is necessary to obtain these compression results in order to be able to compare the two layer system to these values and to see if having a stiffer lower layer instead of same material would have any influence. The percentage comparison is employed to have a meaningful numerical comparisons rather than curves and pure numbers.

The following tables 4.9 and 4.10 shows the percentage difference from compression results of simulations with two layer soil system and that of a single homogenous layer. As the percentage difference is getting a higher negative value it indicates more compactive energy has been lost to the lower layer. On the other hand as

the percentage shifts towards zero it is an indication that more compaction has been attributed to the top layer, which is a result of less compaction being lost to the lower layer.

Table 4.9: Compression of top layer in terms of percentage differences for varying lower layer stiffness for different load and thickness combinations

H/B	q (kN/m^2)	E$_2$=5000	E$_2$=15000	E$_2$=20000	E$_2$=40000
0.5	10	-86.13%	-78.30%	-76.88%	-74.39%
1	20	-70.46%	-64.46%	-63.08%	-60.00%
2	25	-53.00%	-44.82%	-42.71%	-42.41%
5	35	-40.18%	-32.04%	-30.50%	-28.68%

The percentage differences in table 4.9 indicate that as the lower layer gets stronger and more resistive to compressions, the compaction of the top layer increases.

Table 4.10: Compression of top layer in terms of percentage differences for varying top layer thickness for different stiffness and load combinations

q (kN/m^2)	E$_2$ (kN/m^2)	H/B			
		0.5	1	2	5
10	5000	-86.13%	-59.62%	-40.23%	-19.25%
20	15000	-79.77%	-64.46%	-41.46%	-27.31%
25	20000	-78.76%	-58.82%	-42.88%	-26.53%
35	40000	-75.61%	-53.00%	-41.75%	-28.68%

The results from tables 4.9 and 4.10 are illustrated graphically in the following figures 4.33 and 4.34. Figure 4.33 presents graphically the percentage difference against increase

of top layer thickness for different loading and lower layer stiffness. Figure 4.34 shows the percentage difference against increase in lower layer stiffness for different loading and top layer thickness.
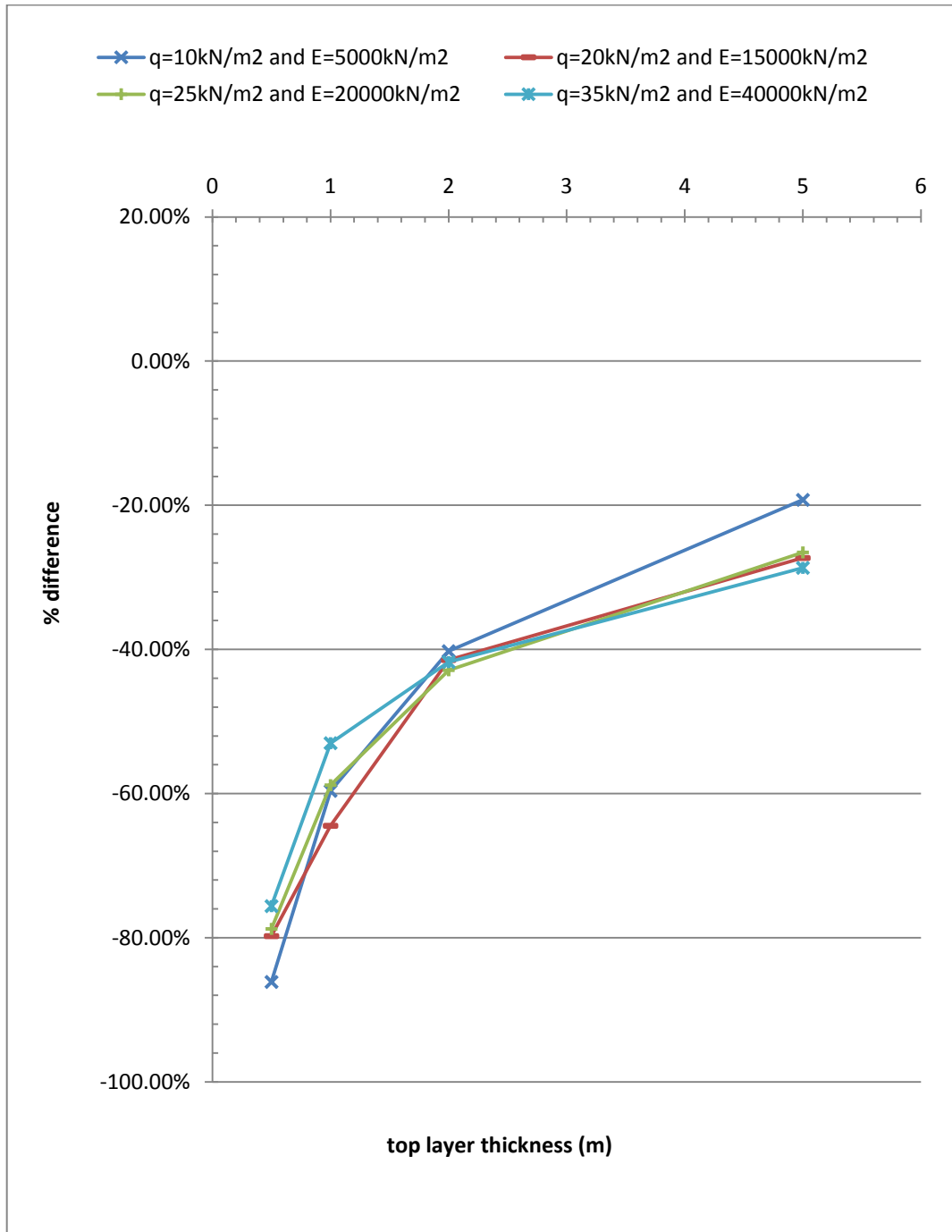

Figure 4.33: Percentage difference against increase of top layer thickness.
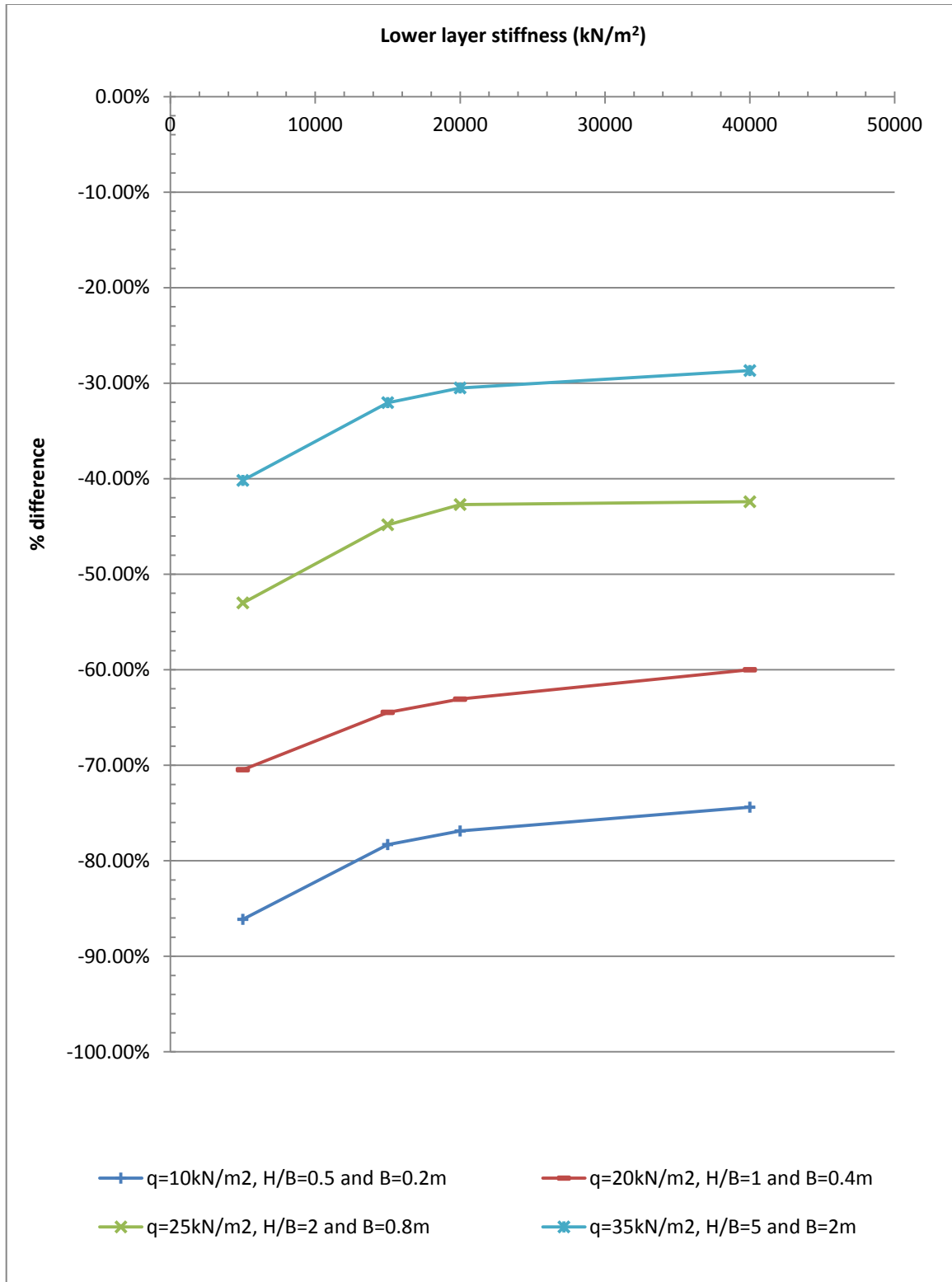
Figure 4.34: Percentage difference against lower layer stiffness.

It can be seen from figure 4.33 that as the thickness of the top layer is increasing, the percentage difference decreases, which is an indication of decrease in lost in compaction. It is expected that up to a certain thickness of top layer the system will still show decrease in percentage difference, beyond this point the system is expected to behave like a homogenous case and any further increase in the top layer thickness should not have any influence on the percentage difference. Figure 4.34 shows the influence of lower layer stiffness on the percentage difference in compaction. A general trend of decrease in compaction lost as per increase in lower layer stiffness can be seen.

4.15   Design Guidelines

The following design charts are generated in order to predict the level of compaction, in terms of vertical compressions, for a given lower layer soil, load and top layer thickness configuration. Given the initial stiffness of the lower layer and the thickness of top layer together with the applied load the maximum compaction of the top layer can be obtained.

From figure 4.35 it is possible to obtain the local compression of top layer if the applied load, top layer thickness and lower layer stiffness are given. Simply the correct curve corresponding to a specific case with a given applied and top layer thickness needs to be chosen, and then the top layer compression can be determined against any given underlying soil stiffness. In the end it is shown how to convert the compression of top layer into change in density.
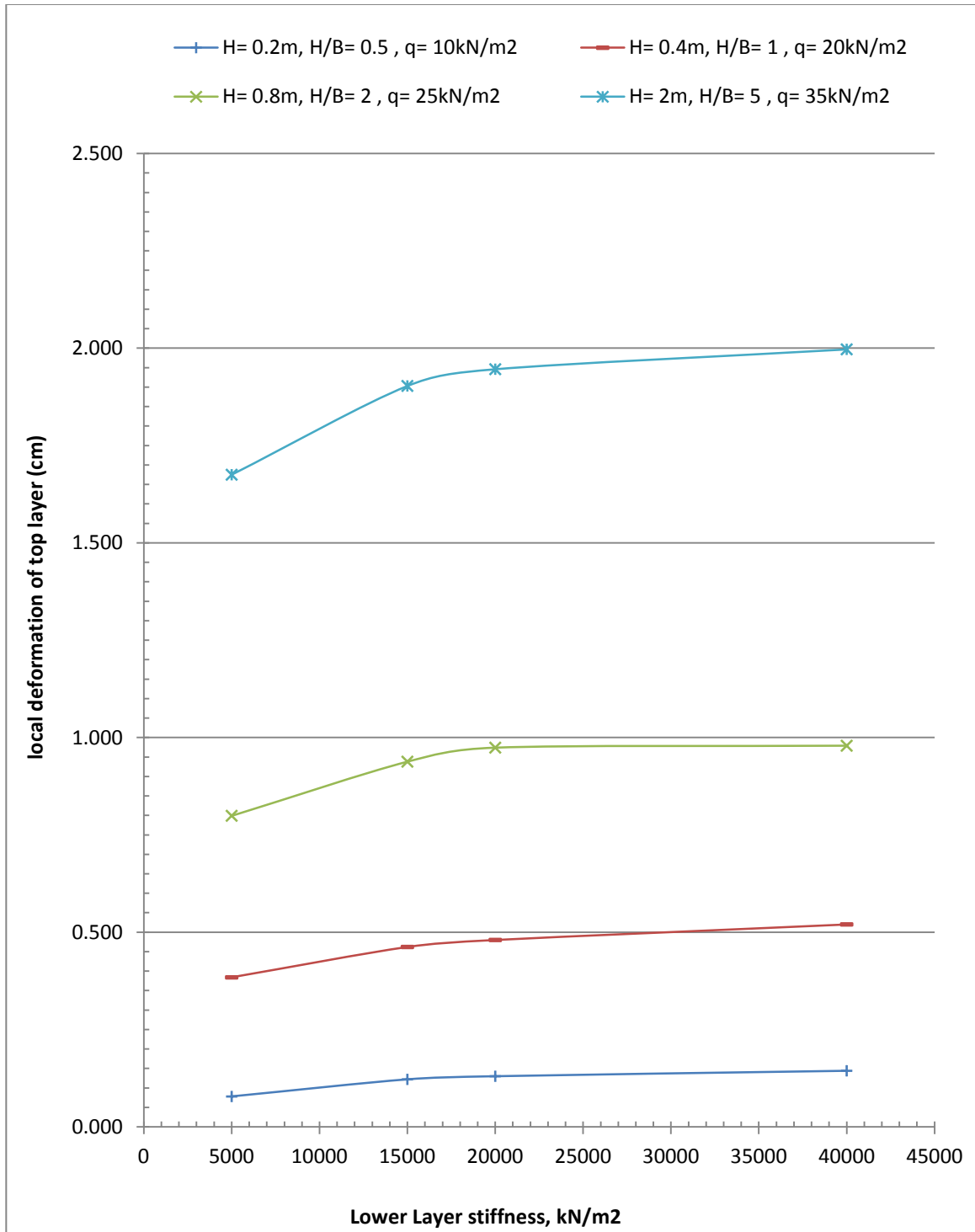
Figure 4.35: Determining top layer compression based on lower layer stiffness.

The following example illustrates the procedures explained in the above paragraph. Let us assume there is a case where we have a top layer with thickness of 2.0m and subjected to 10 cycles of static load with magnitude of $35kN/m^2$. It is required to see the compression of the top layer for different lower layer stiffness. We look at the chart and choose the curve with the closest traits of the given data. Then we simply chose different lower layer stiffness values on x-axis and draw a vertical line to intersect the chosen curve, and then a horizontal line is drawn to intersect the y-axis and the point of intersection marks the value of top layer compression corresponding to the given data and specific lower layer stiffness. This is clearly shown in figure 4.36 below. For instance for the given data, the top layer compression is 1.95cm if the lower layer stiffness is taken to be $21000kN/m^2$.
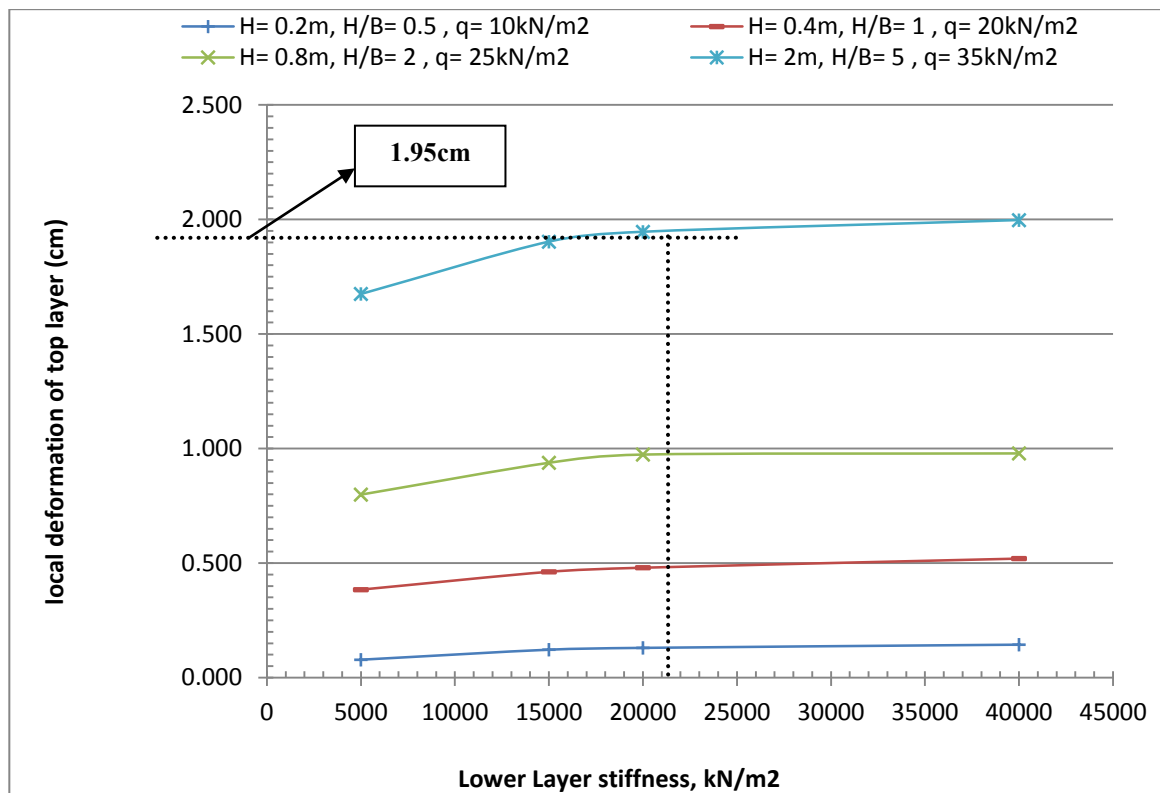
Figure 4.36: Obtaining compression for different lower layer stiffness.

The same procedures can be followed if there is site with specific characteristics. This means if we know the applied load and also the lower layer stiffness we can find out the corresponding top layer compressions regarding different top layer thickness. As seen in the following figure 4.37, for example we have a lower layer soil stiffness of $18000 kN/m^2$ and applied load of around $25 kN/m^2$, and we want to know the top layer compression against top layer thickness of 0.6m. we simply draw a vertical line from x-axis at point 0.6, to intersect the chosen curve, then we make a horizontal line to intersect the y-axis where the top layer compression of approx. 0.86cm)

Figure 4.37: Determining top layer compression based on top layer thickness.

Again the same procedures can be followed if there is site with specific characteristics. This means if we know the top layer thickness and also the lower layer stiffness we can find out the corresponding top layer compressions regarding different applied loads. As seen in the following figure 4.38, for example we have a lower layer soil stiffness of 18000kN/m^2 and top layer thickness of 0.8m, and we want to know the top layer compression against applied load of 22kN/m^2. We can draw a vertical line from x-axis at point 22, to intersect the chosen curve, then we make a horizontal line to intersect the y-axis where the top layer compression of approx. 0.83cm).
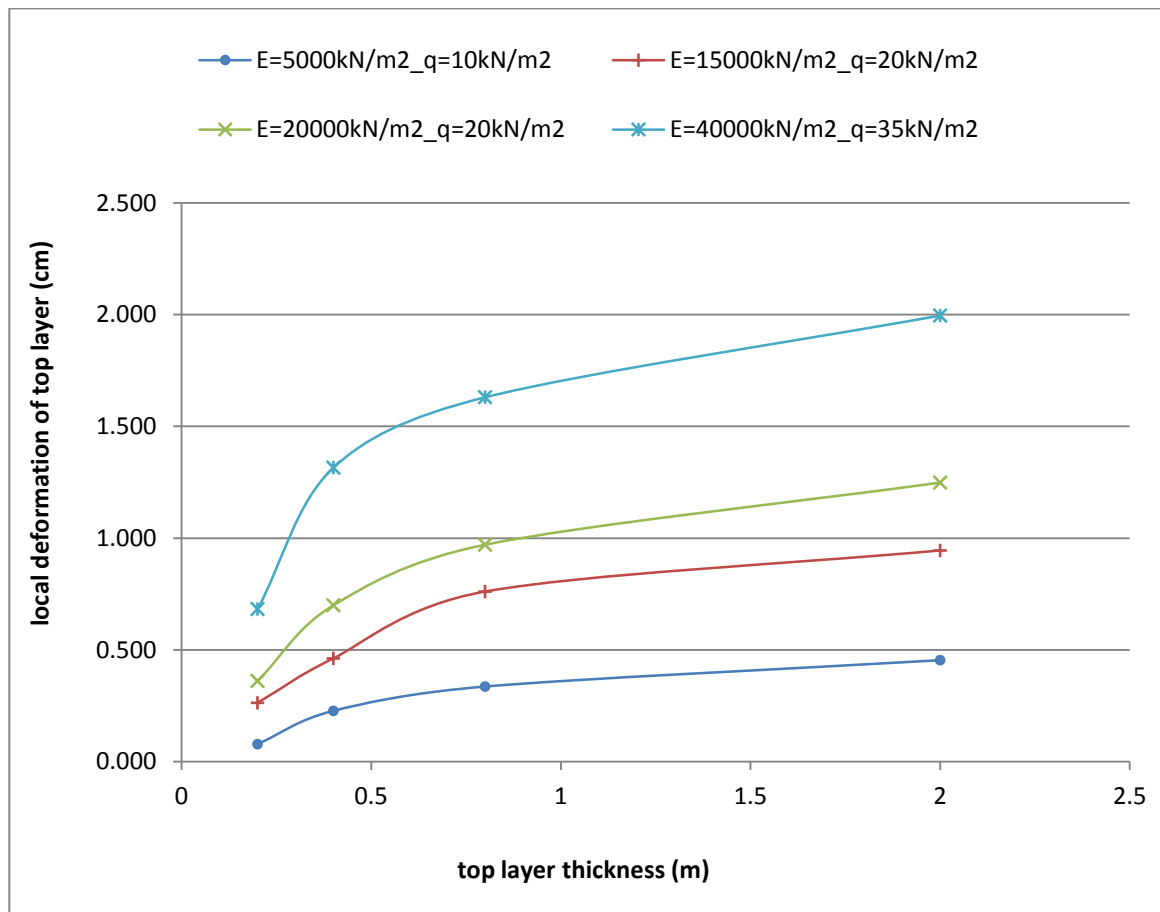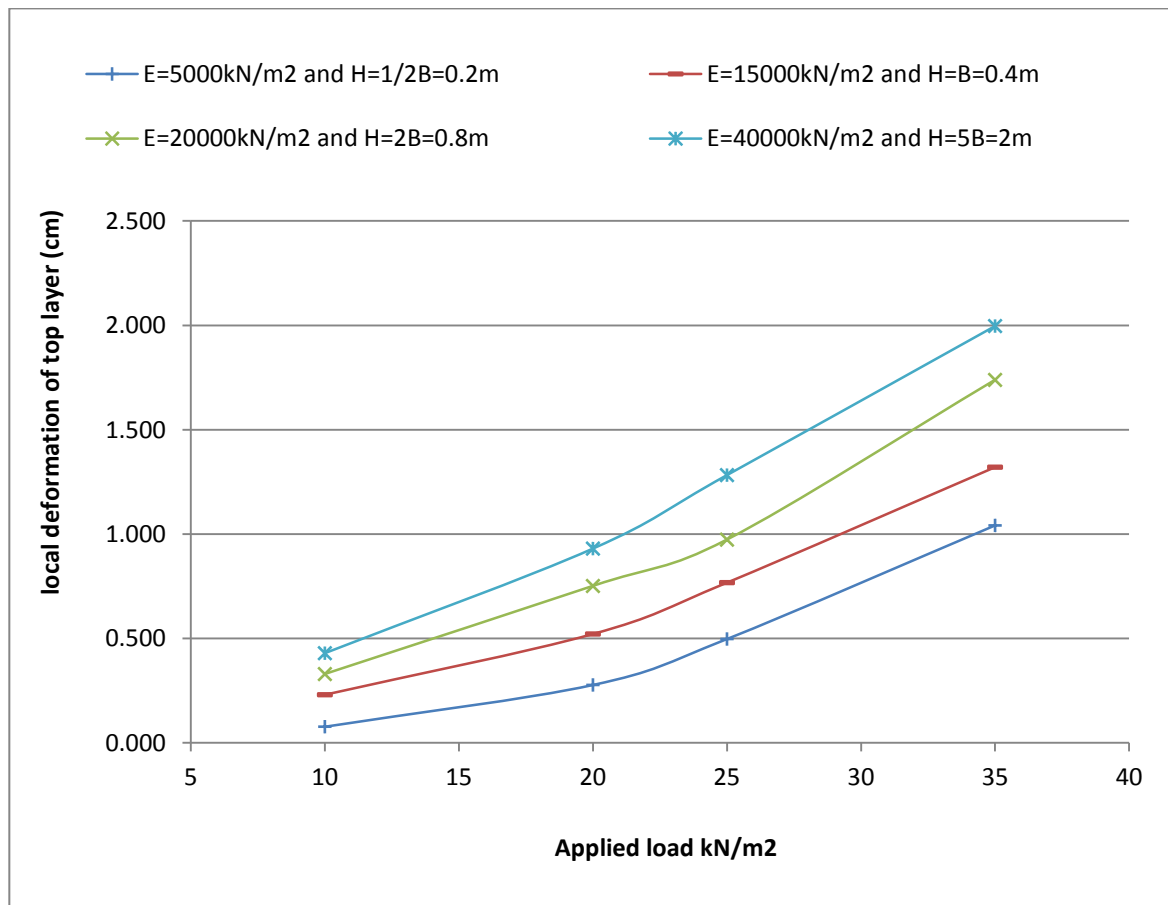

Figure 4.38: Determining top layer thickness based on the applied load.

The procedures above illustrate how to predict the compression of a top layer for some cases with known parameters. The compression values can further be converted into density changes. When a soil mass ,in a given volume, becomes compressed then simply its particulate aggregates become closer to each other and the density of soil mass increases. So for each cases considered, the post compaction density change of the top layer soil can be obtained depending on the soil's initial pre-compaction density and thickness, and post compaction thickness change.

In a case where the top layer thickness is 2m, its initial density is 17.5kN/m^2, and the associated compression of the top layer is 1.95cm the post compaction density of the top layer soil can be obtained as following:

Top layer soil post compaction density γ is the initial density multiplied by a ratio, C, that is a product of the initial thickness divided by the compressed thickness.

$$\gamma = \gamma_{initial} \times C \text{, where } C = \frac{H_{initial}}{H_{compressed}}$$

So in the example above $C = \frac{200}{200-1.95} = 1.1$

And $\gamma = 17.5 \times 1.1 = 19.25$

CHAPTER 5

Conclusion and Recommendations

5.1   Conclusion

Pertinent literature to compaction of soil was reviewed, and it is realized that there is lack of research on the influence of surrounding soil, particularly lower layer soil, on the compaction of subgrade on top of a deep deposit soil.

A plain strain numerical model was developed using the finite element software to simulate shallow compaction of a subgrade on top of a deep deposit. Static analysis of the two layer system were carried out with on and off mode of loading to represent the repeated loading method of shallow compaction similar to that of static roller compaction. Parametric study is carried out on the result to show the sensitivity of compaction to each of the parameters considered.

The following objectives are achieved throughout this research:

1. The factors dictating the compaction of the top layer are stiffness of the lower layer deposit, magnitude of the load applied, number of load applications, and thickness of the top layer.

2. As observed from the analysis, the stiffness of the lower layer provides more compaction to the subgrade layer when the lower layer has stiffness higher than the subgrade. On the other hand, when the lower layer has lower stiffness than the subgrade the compaction is lost and thus less compaction is achieved.

3. The results obtained from laboratory Proctor test cannot always be useful for field compaction predictions. This is because of the incompatibility of the boundary conditions between Proctor and field compaction. The soil surrounding the subgrade is not as stiff as the Proctor Test boundaries (the radial wall and the bottom plate).

4. Design charts are provided for practitioners. The design procedures will enable engineers to predict the appropriate compaction level of top layer on a deep deposit with a known stiffness.

5. Many times the soil encountered in lower levels is very weak to serve as foundation for subgrade layers. If the lower layer is relatively weak, it is better to improve this layer by employing various methods depending on the nature of the soil. Methods such as Vibro-floatation, Injecting cement, placing stone columns, and deep dynamic compaction may be used to improve the state of weak layers.

5.2   Future Work

- Modeling the presented model in the laboratory or field to further validate the current findings.
- Expanding the type of soils to be encountered in such problem
- Take into account the effect of width of the applied load
- Simulate a moving load
- Including the effect of vibration to the load

REFERENCES

Amick, H., et al. (1999). Frequency-dependent soil propagation model. *Optomechanical Engineering and Vibration Control.* July 20, Web. [2]

Assimaki, D., Kausel, E., & Whittle, A. (2000). Model for dynamic shear modulus and damping for granular soils. *Journal of Geotechnical and Geoenvironmental Engineering,* 126(10): October, Paper No. 21230.

AASHTO T99, Standard Method of Test for the Moisture-Density Relations of Soils

Athanasopoulos, G. A. (1995). Empirical correlations VSO-NSPT for soils of Greece: A comparative study of reliability. In: A. S. Cakmak, & C. A. Brebbia (eds). Proceedings of Seventh International Conference on Soil Dynamics and Earthquake Engineering. Chania, Crete, Greece, CMP, p. 19-26.

Athanasopoulos, G. A., Pelekis, P. C., & Anagnostopoulos, G. A. (2000). Effects of soil stiffness in the attenuation of Rayleigh-wave motion from field measurements. *Soil Dynamics and Earthquake Engineering,* 19, pp. 277-288.

Aversa S., Maiorano, R. M. S., & Tamagnini, C. (2007). Influence of damping and soil model on the computed seismic response of flexible retaining structures. In: Geotechnical Aspects of EC8. Madrid, 25 September, Bologna: Patron Editor.

Bergado, D. T. (1996). Chapter 2, Surface compaction. Soft ground improvement. In Lowland and Other Environments. New York, N.Y.: ASCE Press, Web. [1]

Bilotta, E., Lanzano, G., Russo, G., Santucci de Magistris, F., & Silvestri, F. (2007). Methods for the seismic analysis of transverse section of circular tunnels in soft ground. In: Proceedings of the ISSMGE-ERTC 12 workshop at XIV ECSMGE geotechnical aspects of EC8. Madrid, Spain, Chapter 22.

Bolt, B. A. (1988). Earthquakes, Freeman, New York.

Bornitz, G. (1931). Über die Ausbreiting der von Groszkolbenmaschinen erzengten Bondenschwingungen in die Tiefe Springer, Berlin.

Briaud, J. L., & Seo, J. (2003). Intelligent compaction: Overview and research needs, Texas A&M University.

Crabb, G. I., Hiller, D. M., & Wilson, P. E. (1998). Measurement and prediction of ground-borne vibration due to construction operations. In *Ground Dynamics and Man-made Processes* (skip B. O. (ed.)). Thomas Telford, London.

Crabb, G. I., et al. (2002). Prediction of groundborne vibration from vibrating rollers.

Das, B. M. (1983). Fundamentals of Soil Dynamics, Elsevier.

Department of the Navy, NAVFAC DM-7.3 (April 1983). Soil dynamics. Available from Naval Facilities Engineering Command, 200 Stovall Street, Alexandria, VA 22332.

Edil, T. B., Luh, G. F. (1978). Dynamic modulus and damping relationships for sands, Proceedings of the ASCE Geotechnical Engineering Division Specialty Conference, Earthquake Engineering and Soil Dynamics, Pasadena, CA, pp. 394-409.

Elisa Daniela Martinez Aviles (2008). Boundary condition in laboratory and field compaction.

Hanna, A.M. (2003). Laboratory Compaction of a Subgrade Layer Overlying a Deep Soil Deposit. Journal of Ground Improvement, England 7 (1), 1-8. 23.

Henrich, H. (1987). Compaction with vibratory rollers, Aspects of construction, Die Sivile Ingenieur, South Africa.

Hertz, H. (1895). Über die Berührung Fester Elastischer Körper: Gesammelte Werke. Bd. 1. Leipzig.

Hiller, D. M., & Bowers, K. H. (1997). Ground-borne vibration from mechanized construction works. *Proceedings of Tunneling'97,* pp.721-735.

Howeedy, M. F., & Bazaraa, A. R. (1975). Factors influencing vibratory compaction of cohesionless soils, 548(88).

Ishihara, K. (1996). Soil behaviour in earthquake geotechnics. Oxford University Press.

Ishibashi, I., & Zhang, X. J. (1993). Unified dynamic shear moduli and damping ratios of sand and clay. *Soils Found.*, 33(1), pp. 182-191.

Kim, D. S., & Lee, J. S. (1998). Source and attenuation characteristics of various ground vibrations. In: P. Dakoulas, M. Yegian, & B. Holtz (eds). Geotechnical earthquake engineering and soil dynamics III. ASCE, Geotechnical special publication No. 75, 2, p. 1507-17.

Kim, D. S., & Lee, J. S. (2000). Propagation and attenuation characteristics of various ground vibrations, *Soil Dyn Earthquake Eng 19*, pp. 115-126.

Ko, H. Y., & Scott, R. F. (1967). Compression of sand in hydrostatic compression. *Journal of the Soil Mechanics and foundations Division,* ASCE, 93(SM3), Proc. paper 5245, Mall, pp. 137-156.

Lanzo, G., Pagliaroli, A., & D'Elia, B. (2004). Influenza della modellazione di Rayleigh dello smorzamento viscoso nelle analisi di risposta sismica locale. Proc. XI Conf. L'Ingegneria Sismica in Italia.

Massarsch, K. R. Deep compaction of granular soils, Presented at Zhejiang University on January 21, 1999 "International Lecture Series on Geotechnical Engineering and Its Development in the 21st Century" Copyright Zhejiang University, Hangzhou, PR China.

Massarsch, K. R., Madshus, C., & Bodare, A. (1995). Engineering vibrations and solutions. In: S. Prakash (ed). Proceedings: Third International Conference on Recent Advances in Geotechnical Earthquake Engineering and Soil Dynamics. St. Louis, MO, 3, p. 1349-53.

Musimbi, O. M., Rinehart, R. V., & Mooney, M. A. (2010). Comparison of measured and BEM computed contact area between roller drum and layered soil, *Advances in Analysis, Modeling & Design.*

Parsons, A. W., & Transport Research Laboratory (Great Britain). (1992). Compaction of soils and granular materials: A review of research performed at the Transport Research Laboratory HMSO, London.

Ping, W. V., Yang, Z., Leonard, M., & Putcha, S. (2002). Laboratory simulation of field compaction characteristics on sandy soils, Transportation Research Record 1808, paper No.02-3164.

Richart, Jr., F. E., Hall, J. R., & Woods, R. D. (1970). In: Vibrations of soils and foundations, Prentice Hall, Englewood Cliffs, NJ, p. 414.

Sandström, Å. (1994). Numerical simulation of a vibratory roller on cohesionless soil, Internal Report, Geodynamik, Stockholm, Sweden.

Sanejouand, R., et al., (1980). Discussion of dynamic of vibratory-roller compaction, *Journal of the Geotechnical Engineering Division,* ASCE.

Seed, H. B., & Idriss, I. M. (1970). Soil moduli and damping factors for dynamic response analysis, *Earthquake Engineering Research Center*, Report No. EERC 70-10, College of Engineering, University of California, Berkeley, California.

Selig, E. T., & Yoo, T. S. (1977). Fundamentals of vibratory roller behavior. Proc., 9th International Conference on Soil Mechanics and Foundation Engineering, 2, Tokyo, Japan, pp. 375-380.

Selig, E. T. (1982). Compaction procedures, specifications and control considerations, Earthwork Compaction, Transportation Research Record 897, Washington D.C.

Sutherland, A. J., & Cenek, P. D. (2007). Vibration assessment, Central Laboratories Report 07-5C1124.06 100CL.

Tiedemann, D. A. (1970). Ground motions from vibratory compaction of cohesive soil. U.S. Department of the Interior, Denver, Interior Report REC-0CE-70-28.

Tika, T., Kallioglou, P., Papadopoulou, A. & Pitilakis, K. (2004). Advances in geotechnical engineering: The Skempton Conference, R.J. Jardine, D.M. Potts, & K.G. Higgins (eds). Thomas Telford, London.

Woods, R. D. (1997). Dynamic effects of pile installations on adjacent structures. NCHRP 253. Transportation Research Board. National Academy Press, Washington, DC, p. 86.

Woods, R. D. (1986). In-situ tests for foundation vibrations. In: S.P. Clemence, (ed). Proceedings of: Use of In-Situ Tests in Geotechnical Engineering. ASCE Geotechnical special publication No. 6, p. 336-75.

Wu, S., Gray, D.H., Richart Jr., F. H. (1984). Capilary effects on dynamic modulus of sands and silts, *Journal of Geotechnical Engineering*, 110(9), ASCE, pp. 1188-1203.

Wu, S., Gray, D. H., Richart Jr., F. H. (1985). Capillary effects on shear modulus at high strains, Proceedings of the 11th International Conference on Soil Mechanics and Foundation Engineering, 12-16 August, San Francisco, Balkema Rotterdam.

Wu, S. (1983). Capillary effects on dynamic modulus of fine-grained cohesionless soils, Ph.D. dissertation, University of Michigan, at Ann Arbor, Mich.

Yoo, T. S., & Selig, E. T. (1979). Dynamics of vibratory-roller compaction, *Journal of the Geotechnical Engineering Division,* ASCE, 105, GT10, Proc. Paper 14907, Oct., pp. 1211-1231.

Yulek, Mustafa (2006). Energy consumption in compaction of a thin layer overlying a deep deposit.